



**European volcanological supersite in Iceland:
a monitoring system and network for the future**

Report

**D8.5 - Statistical Assessment of Dispersion Model
Sensitivity**

Work Package:	<i>Distribution and Description of Eruptive Products</i>
Work Package number:	8
Deliverable:	<i>Statistical Assessment of Dispersion Model Sensitivity</i>
Deliverable number:	8.5
Type of Activity:	<i>RTD</i>
Responsible activity leader:	<i>Arve Kylling</i>
Responsible participant:	<i>Met Office</i>
Authors:	<i>Frances Beckett (MO), Claire Witham (MO), Ben Devenish (MO)</i>

Type of Deliverable:	<i>Report</i> <input checked="" type="checkbox"/> <i>Demonstrator</i> <input type="checkbox"/> <i>Prototype</i> <input type="checkbox"/> <i>Other</i> <input type="checkbox"/>
Dissemination level:	<i>Public</i> <input checked="" type="checkbox"/> <i>Restricted Designated Group</i> <input type="checkbox"/> <i>Prog. Participants (FP7)</i> <input type="checkbox"/> <i>Confidential (consortium)</i> <input type="checkbox"/>

Seventh Framework Programme

EC project number: 308377



Abstract

Atmospheric dispersion models are used to forecast the transport and dispersion of ash and gas from volcanic eruptions. This report aims to improve our understanding of the behavior of dispersion models and the uncertainties associated with their forecasts. To do this we assess the sensitivity of dispersion model forecasts to the forecast meteorology and the source parameters used in the dispersion model. Considering the source parameters which have been identified as critical for initialising dispersion models we then assess the usefulness of the analytical and field-based techniques developed through the FUTUREVOLC project for modelling volcanic ash clouds.

Dispersion models use forecast meteorological data from Numerical Weather Prediction (NWP) models to represent the weather that is expected to occur during an event. Of particular importance are the wind vectors, which vary both with altitude and time. We show that dispersion model forecasts are sensitive to the NWP model configuration used to produce the meteorological data, and that the choice of meteorological dataset depends on the scenario being modelled. The London VAAC uses the atmospheric **dispersion model NAME with meteorological data produced by the Met Office's NWP model, the Unified Model (UM)**. In common with most National Meteorological Services the Met Office run several NWP model configurations which can be broadly characterised by their different horizontal resolutions (~1 km to 10s km), extents (local to global) and intended focus/purpose. Volcanic ash clouds typically reside at heights > 2 km asl in the atmosphere, and the prediction of their spread is therefore critically dependent on the accuracy of the upper air (free troposphere and stratosphere) winds. We show that the **UM's Global model** is the most skilful model configuration at representing upper air wind speeds and wind direction. Higher resolution Limited Area Models (LAMs) have been developed primarily to improve forecasts of surface meteorology and are more capable of representing the local topography, which can significantly affect the local surface wind vectors. **We show that the UM's LAM, the Euro4, is more appropriate for forecasting the transport of near-surface gas plumes from effusive eruptions.**

It is known that forecasts of mass loadings of volcanic ash in the atmosphere are particularly sensitive to the Mass Eruption Rate (MER) and plume height used to initialise the dispersion model. Here we explore the sensitivity of the forecasts to the physical characteristics applied to the model particles: particle size, density and shape. We show that the forecasts are also highly sensitive to the Particle Size Distribution (PSD) applied. The density and shape assigned to the model particles have a lesser but still significant impact on the calculated fall velocity and hence forecast mass loadings. Focusing efforts on determining the Total Grain Size Distribution (TGSD) of the erupted tephra during an explosive eruption could therefore have significant benefits for VAACs. Ascertaining the TGSD in near real time is challenging, but the Tephra Samplers which have been developed through the FUTUREVOLC project have the potential to provide this critical information.

The MER and plume height are also difficult to measure in near real time. Near vent buoyant plume models offer the ability to estimate MERs given information on the plume height. Using the plume-rise model developed at the Met Office we show that the total estimated mass from the eruption of Eyjafjallajökull in 2010 agrees well with observations of the total mass of tephra. Further, the multi-parameter system REFIR which combines both field observations and estimates from buoyant plume models has the potential to provide a 'best guess' MER and the associated uncertainty on that estimate.

Buoyant plume models and empirical relationships require information on the plume height to estimate MERs. Atmospheric dispersion modellers also need to know the height to determine where to release ash into the atmosphere. Errors in the plume height used to initialise the atmospheric dispersion model can result in significant errors in the

forecast location of the ash cloud. We assess the use of radar data from the eruption of Grímsvötn in 2011 and show that it cannot be relied upon for accurate height information on ash emission for this eruption. Volcanic Ash Radar Retrieval (VARR) algorithms developed through the FUTUREVOLC project have the potential to discriminate ash particles from the gas phase, and height measurements from cameras may also be useful for improving height estimates during future eruptions.

Contents

1. Introduction	4
2. The sensitivity of dispersion model forecasts of volcanic ash cloud transport to meteorological data resolution.....	5
3. The sensitivity of dispersion model forecasts to NWP model topography.....	25
4. The sensitivity of dispersion model forecasts to the physical characteristics of the particles.....	40
5. Using buoyant plume models to estimate mass eruption rates for dispersion modelling.....	43
6. Assessment of the impact of radar height data on model forecasts for Grimsvötn 2011.....	48
7. Assessment of critical observations and measurements for dispersion modelling.....	54
8. Conclusions.....	58

Acknowledgements

References

Appendices

1. Introduction

This report outlines the findings of work carried out under WP8, deliverable D8.5, of the FP7 FUTUREVOLC project. The objective of WP8 is to provide quantitative information about volcanic eruptive products, including volcanic ash clouds, both in the near and far-field following volcanic eruptions.

Atmospheric dispersion models represent useful tools for forecasting and analysing volcanic ash clouds. Deliverable D8.5, Task 8.3, aims to improve our understanding of dispersion models and their uncertainties, and to consider the impact of improved observations of volcanic ash clouds delivered under WP7 and WP8 on model predictions of ash cloud transport. In the FUTUREVOLC Description of Work (DOW) this deliverable and task are described in the following manner:

Deliverable 8.5. *Statistical assessment of dispersion model sensitivity: Report on dispersion model prediction of ash distribution considering the influence of meteorological data resolution and topographical resolution on dispersion model prediction of ash deposition and dispersion. Report on dispersion model prediction of ash distribution considering the influence of (i) improved observations, (ii) near-vent model on dispersion prediction of ash distribution.*

Task 8.3. *Dispersion model analysis: Atmospheric dispersion modelling provides a useful tool for forecasting and analysis of volcanic clouds. To increase our understanding of the behaviour of dispersion models and their uncertainties, the NAME model (Jones et al. (2007) will be used: (i) to investigate the influence of meteorological data resolution and topographical resolution on model prediction of ash distribution; (ii) to investigate the influence of improved observations (Leadbetter et al. 2012), as delivered by WP7 and WP8, on model prediction of ash distribution; (iii) and to investigate the influence of near-vent model outputs from WP7, on model prediction of ash distribution (Met Office).*

In this report we present results from five studies. The first examines the sensitivity of dispersion model forecasts to meteorological data and considers which Numerical Weather Prediction (NWP) model output should be used to drive the operational dispersion model NAME, which is used by the London VAAC. The second study considers the sensitivity of forecasts of the transport of volcanic pollutants to the topography used in the NWP model. We use the Holhraun effusive eruption as a case-study and consider the impact on the near-surface gas plume. The third study examines the sensitivity of dispersion model forecasts of ash cloud transport to the physical characteristics assigned to model particles and considers which parameters have a significant impact on the forecasts. The fourth study considers the use of a near-vent, buoyant plume model, for assessing mass eruption rates. Critical for the initialisation of both NAME and the buoyant plume model is knowledge of the plume height; in the final study we assess the usefulness of radar height data, using the eruption of Grímsvötn in 2011 as a case-study. Finally, we identify which measurement techniques developed under WP7 and WP8 can potentially provide information on the critical source parameters which are required to initialise dispersion models.

2. The sensitivity of dispersion model forecasts of volcanic ash cloud transport to meteorological data

Authors: F.M. Beckett, C.S. Witham, R. Crocker, M. Bush, M.C. Hort, K. Mylne

2.1 Introduction

Volcanic Ash Advisory Centres (VAACs) are responsible for monitoring and forecasting the movement of volcanic ash clouds and issuing volcanic ash advisory messages. There are currently 9 VAACs worldwide, each with a designated geographical area of responsibility. In the event of an ash cloud the VAACs issue Volcanic Ash Advisories (VAAs) and Volcanic Ash Graphics (VAGs) to indicate the forecast location of the ash. The forecasts are produced to the standards and tolerances set by the regulator, the International Civil Aviation Organisation (ICAO), and support decision-making by aviation authorities as to whether it is safe for aircraft to fly.

The London VAAC based at the Met Office in the UK is responsible for the area covering the UK, Scandinavia, the north eastern part of the North Atlantic, and the volcanically active island of Iceland. In the event of a volcanic eruption producing an ash cloud in this area of responsibility they issue the standard advisories (VAAs and VAGs), providing guidance at T+0, T+6, T+12 and T+18, and over three flight levels: FL000 - FL200, FL200 - FL350, FL350 - FL550 (where FL is flight level in hundreds of feet). Forecasts are produced using the Lagrangian atmospheric dispersion model NAME (Numerical Atmospheric-dispersion Modelling Environment, Jones et al. (2007)). NAME is driven by the Met Office's Numerical Weather Prediction (NWP) model, the Unified Model (UM) (Davies et al., 2005). To produce an accurate forecast of the location of the volcanic ash cloud, the meteorological data, specifically the wind vectors with height, used to drive the dispersion model must accurately represent the weather during the event. The UM has been shown to be a highly competitive NWP model compared to other models run by Met Services around the world. Figure 2.1 shows the ability of the UM's global model configuration to forecast upper air winds (250 hPa) at T+24 since January 2011, demonstrating that it is consistently one of the leading models in the world.

NWP models are used to model the state of the atmosphere over the Earth's surface and predict its future state. To initialise a forecast, observation data are blended with a previous forecast, through the process of data assimilation, to give a best prior estimate of the state of the atmosphere. NWP variables: exner pressure, density, potential temperature and wind vectors are then evolved through time by solving the dynamical equations of motion. The UM's dynamical core uses a semi-implicit semi-Lagrangian formulation to solve the non-hydrostatic, fully compressible, deep-atmosphere equations of motion (Davies et al., 2005; Wood et al., 2014). Physical processes such as convection, turbulent mixing and precipitation which occur on a sub-grid scale are instead parameterized.

There are several model configurations under the umbrella of the UM which produce output at different resolutions and for different purposes, see Table 2.1 for a description of all the model configurations considered in this study. The Global model configuration provides medium range weather forecasts for the whole globe. It is a grid-point model using a standard latitude/longitude coordinate system with a horizontal resolution ~17 km at mid-latitudes. It uses a 4-dimensional hybrid data assimilation system (Hybrid 4DVAR) which considers the spread of observations over time and space (4DVAR) and includes data from the Met Office's ensemble prediction system MOGREPS-G (Clayton et al., 2013). There are also Limited Area Models (LAMs), which have been developed to provide high resolution meteorological data over limited areas. The NAE produced

Table 1. The properties of the UM model configurations. The Global model configuration currently has a horizontal resolution of 17 km, prior to July 2014 it was 25 km. The NAE model configuration was retired in July 2014.

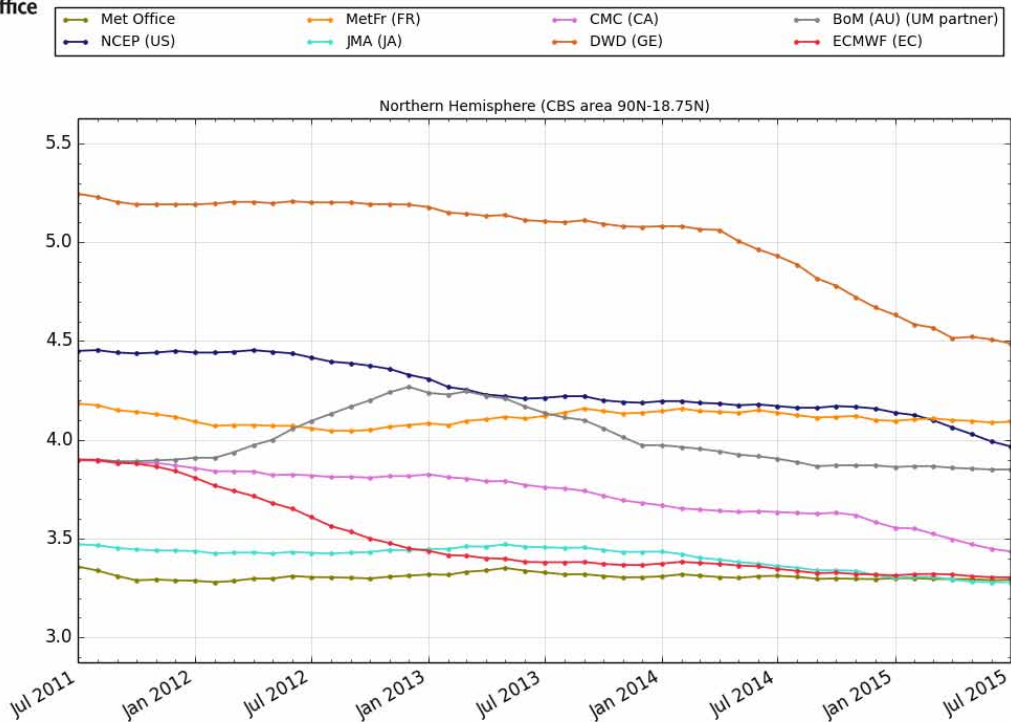
	Global	NAE (Retired)	Euro4	UKV
Horizontal resolution	Pre July 2014: 25 km Current: 17 km	12 km	4 km	1.5 km
Vertical top height	80 km	80 km	40 km	40 km
Forecast range	144 Hr	48 Hr	120 Hr	36 Hr
Data assimilation	Hybrid 4DVAR	4DVAR	None	3DVAR
Dynamical core	Pre July 2014: New Dynamics Current: ENDGame	New Dynamics	Pre February 2014: New Dynamics Current: ENDGame	Pre February 2014: New Dynamics Current: ENDGame

meteorological data over the North Atlantic and Europe (Figure 2.2) at a horizontal resolution of 12 km (Bush et al., 2006). It included data assimilation at T+0, using 4DVAR, and used many of the same physical parameterisations that are applied in the Global model configuration, the main exception being that it used a different cloud scheme. The Euro4 model was introduced as an operational LAM at the Met Office on the 16th January 2013, replacing the NAE. It produces meteorological data over Europe at a horizontal resolution of 4 km (Figure 2.2) and has no data assimilation; it is simply downscaled from the Global model configuration. The Euro4 uses many of the same physical parameterisations as the UKV, which produces meteorological data over the UK, but it also includes a convection scheme. The UKV has a variable resolution horizontal grid with a fixed resolution domain over the UK of 1.5 km. Prior to July 2014 all of the UM configurations **used a dynamical core known as 'New Dynamics'** (Davies et al., 2005). This **has recently been replaced by 'ENDGame'** which has improved accuracy and reduced damping. To solve the New Dynamics equations stably required artificial damping, which removed detail from the resulting forecasts. The introduction of ENDGame allows less artificial damping and more detailed forecasting of individual synoptic features such as cyclones, fronts, troughs, and jet stream winds (Walters et al., 2014).

One of the main drivers for the development of the Global model has been the requirement to provide global forecasts for aviation. The Met Office is a World Area Forecast Centre (WAFC) whose role is to provide forecasts of upper air winds and temperatures for flights around the world in order to optimise safety and fuel consumption. The 80 km vertical top height in the Global configuration means that observations of the upper atmosphere derived from satellite instruments are included in the data assimilation and that the interactions between the stratosphere and troposphere are captured in the model. This allows skillful forecasts of upper air winds and temperatures to be produced out to 144 hours, and prediction of turbulence and cumulonimbus clouds which are also important for aviation. The motivation for the development of LAMs is to improve forecasts of surface weather and to provide information at finer scales than can be supplied by the lower resolution Global model. The higher resolution NAE and Euro4 configurations therefore better represent processes influenced by the underlying surface such as orography, the land-sea mask and vegetation, and better resolve moist physical processes, such as clouds and precipitation (Davies, 2014), leading to improved forecasting skill of meteorology close to the surface, such as screen temperatures, near surface winds and precipitation.



Mean of the Daily Root Mean Square Vector Difference (Forecast - Analysis), T+24, Analysis



© Crown Copyright 2015. Source: Met Office

Figure 2.1 The performance of the Met Office's Unified Model for the Northern Hemisphere, compared to models run by other Met Services, at forecasting upper air wind speed (250 hPa) at T+24, presented as a running mean of the daily RMSE of forecast versus analysis data. This data is produced in accordance with the method recommended by the World Meteorological Organisation (WMO) Commission for Basic Systems (CBS).

Currently the highest resolution meteorological data available for the area of responsibility covered by the London VAAC is produced by the Euro4 model. However, it is not clear that using a LAM improves forecasting skill of upper air winds, knowledge of which is needed to model the dispersion of ash clouds which typically reside at altitudes > 2 km asl in the atmosphere (Mastin et al., 2009). Further, LAMs necessarily require Lateral Boundary Conditions (LBCs) and there can be degradation of the forecast at the domain edges. This is particularly relevant when considering forecast meteorology over Iceland as it is close to the model boundaries of both the NAE and Euro4 domains (Figure 2.2). During the eruption of Eyjafjallajökull in 2010 internal discussion at the Met Office between UM model developers and atmospheric dispersion scientists concluded that the Global data was the most appropriate meteorological dataset to use with NAME for forecasting the transport and dispersion of volcanic ash clouds, and this is now the default meteorological dataset used by the London VAAC.

In this study we re-visit this question and present a detailed statistical assessment of the forecast upper air wind vectors over Iceland, the north east North Atlantic, Scandinavia and the UK by comparing NWP model output to measurements of wind speed and wind direction with altitude from radiosondes. We assess the performance of the Global and the NAE model configurations during 2010, which includes the period when European air space was disrupted by the ash cloud from the eruption of Eyjafjallajökull (April-May 2010), and the performance of the current Global model configuration with ENDGame dynamics to the Euro4 model. We identify which dataset, the Global or LAM forecasts, is

the most appropriate to use with NAME when modelling the dispersion of volcanic ash clouds from Iceland. By comparing NAME forecasts using Global and LAM data for the same time period we show that the dispersion model forecasts are sensitive to the meteorological dataset used. Finally, we consider the impact of the uncertainty associated with the modelled winds on the forecast transport of volcanic ash clouds.

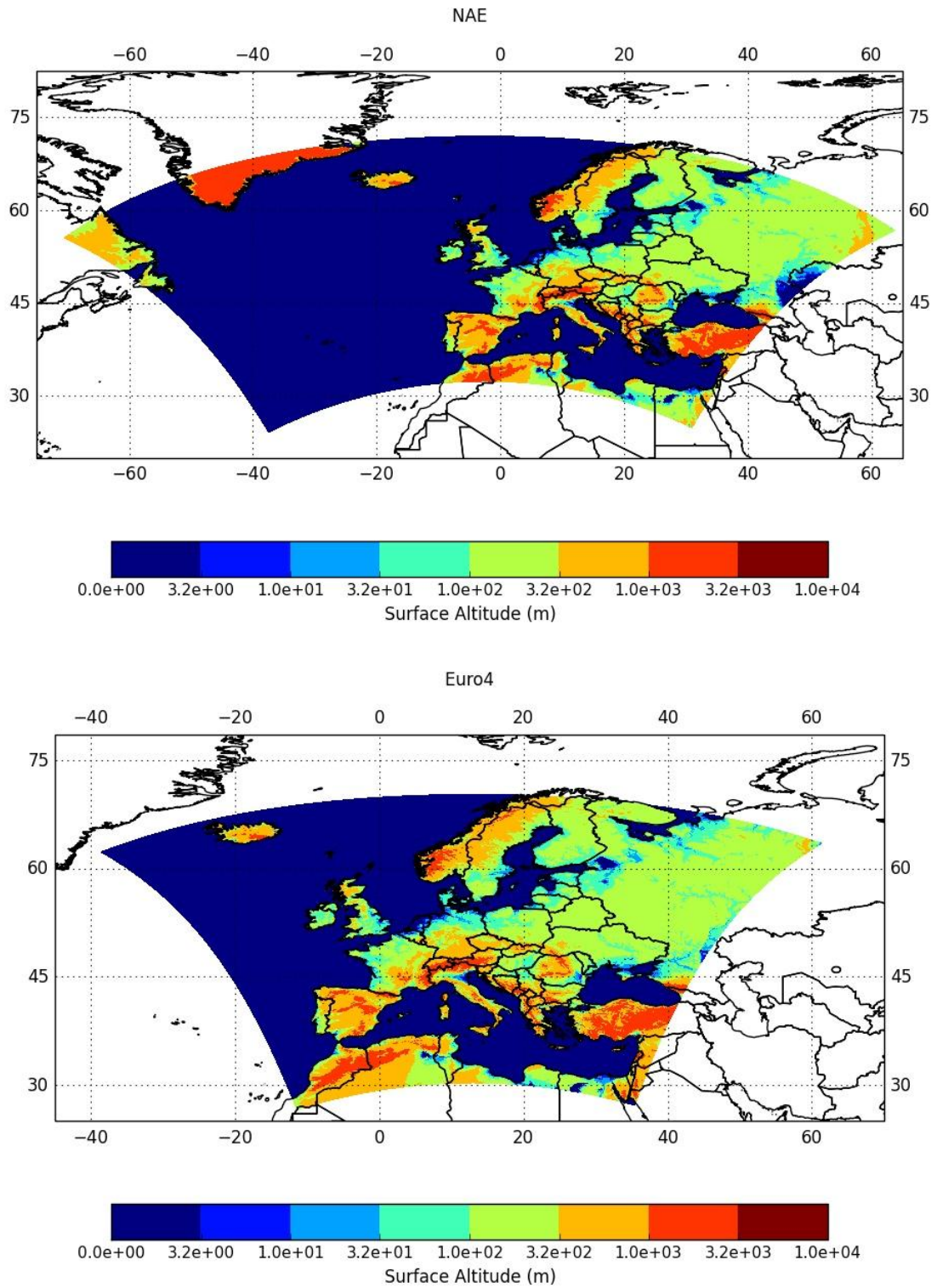


Figure 2.2. Surface topography represented in the Met Office's operational limited area model domains, the NAE (retired in July 2014) and the Euro4, to indicate the geographical extents of the two model configurations.

2.2 Statistical Assessment of Meteorological Data

To assess the performance of forecast upper air wind speed and wind direction from the Global, NAE and Euro4 model configurations we compare the model forecasts to radiosonde data collected at 0Z and 12Z from stations across the UK, Iceland, Scandinavia and from an oil rig in the North Sea, representing the area of responsibility covered by the London VAAC (see Figure 2.6 for a map of the radiosonde stations used). Data from radiosonde launches across the world are made available through the World Meteorological Organisation (WMO), observations are exchanged via the Global Telecommunications System (GTS) in various formats (WMO, 2011) and observing standards are coordinated via the WMO. As such this data is available at the Met Office. WMO (2010) describes station layout and the various instruments and processing used. We consider data from altitudes over 1000-100 hPa, which corresponds to the altitudes covered by the London VAAC forecasts (maximum 550FL). The radiosonde data are compared to model output at 0Z and 12Z, from T+6, T+12 and T+18 NWP forecasts (where, for example, T+6 is the forecast data 6 hours from the start of the NWP forecast). These correspond to the forecast times of volcanic ash advisories produced by the London VAAC. The forecast and observation data are equalised, such that if a observation is missing then the corresponding NWP model forecast data is also discarded.

Standard verification measures are used to assess the meteorological data, the Mean Absolute Error (MAE) and Root Mean Square Error (RMSE) (Jolliffe and Stephenson, 2011; Chai and Draxler, 2014):

$$MAE = \frac{1}{N} \sum_{i=1}^N |Forecast - Observation| \quad (1)$$

$$RMSE = \sqrt{\frac{1}{N} \sum_{i=1}^N (Forecast - Observation)^2} \quad (2)$$

Where the MAE is the average over the verification sample of the absolute differences between the forecast and the corresponding observation. The RMSE squares the error between the observation and forecast before they are averaged, and therefore gives a relatively high weight to large errors and penalises variance. We use traditional point verification of the forecast data to the observations: radiosonde data and modelled grid point data are matched by bi-linear interpolation (Mittermaier, 2014).

2.3 Results

2.3.1 Global versus NAE

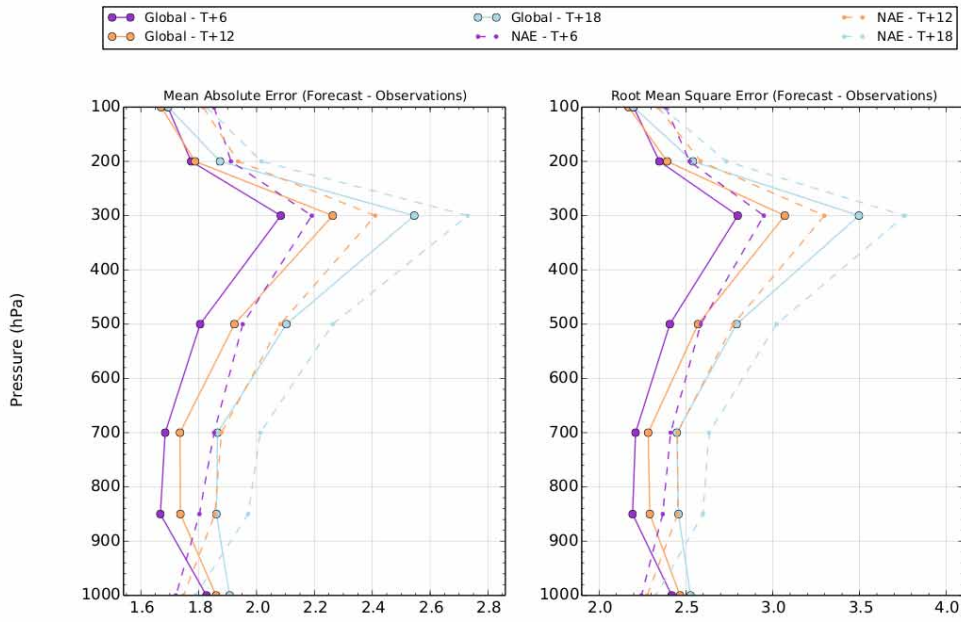
The ability of Global and NAE forecasts to predict upper air wind speed and wind direction during the period 01/01/2010-31/12/2010 is considered. Comparing forecast data to the individual 0Z and 12Z radiosonde data sets indicates that there were no significant differences in the model performance between midday and midnight and therefore both data sets are included in the following analysis (Appendix A.1, Figures A.1.1, A.1.2, A.1.3 and A.1.4). Time averaged vertical profiles of the MAE and RMSE for T+6, T+12 and T+18 forecast data are shown in Figure 2.3. The Global model forecasts better represent measured wind speed and wind direction than NAE forecast winds through much of the depth of the atmosphere (< 850 hPa), and particularly at upper levels. The increased skill of both the Global and NAE forecasts with decreasing forecast time are clear; forecast wind speed and wind direction for T+6 have lower MAEs and RMSEs than forecasts for T+18. For all data sets the most significant errors are found to occur at 300 hPa, which corresponds to the height of the jet stream.

Time-series of the MAE and RMSE of the forecast wind speeds and wind direction at 300 hPa (~10 km asl) for T+18 are shown in Figure 2.4. Global model forecasts consistently better represent the 300 hPa winds and there are no significant changes in model performance between summer and winter periods, suggesting the results are applicable across a wide range of synoptic conditions (Figure 2.4).

Error maps showing the average RMSEs at 300 hPa for the T+18 forecast data during 2010 at each of the individual radiosonde sites are shown in Figures 2.5 and 2.6. The NAE forecast wind speed and wind direction have slightly higher RMSEs than the Global forecast wind speed and direction across all of the radiosonde data sets. Considering the NAE forecast winds we also find that RMSEs are slightly higher at the Keflavik (Iceland) station. Time-series of the MAE and RMSE for each of the individual stations show that this observed increased error is consistent in time (Appendix B, Figure B.1). This could be due to the NAE model boundary being so close to Iceland.

(a)

Wind Speed (m/s), Combined stations,
Equalized and Meaned between 20100101 00:00 and 20101231 12:00, Sondes



(b)

Wind Direction (deg), Combined stations,
Equalized and Meaned between 20100101 00:00 and 20101231 12:00, Sondes

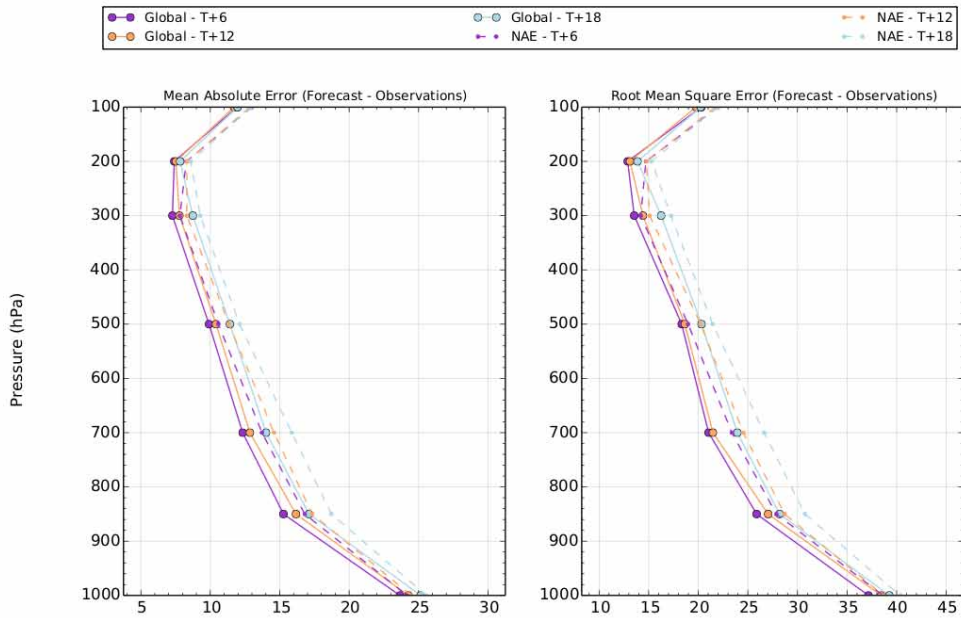
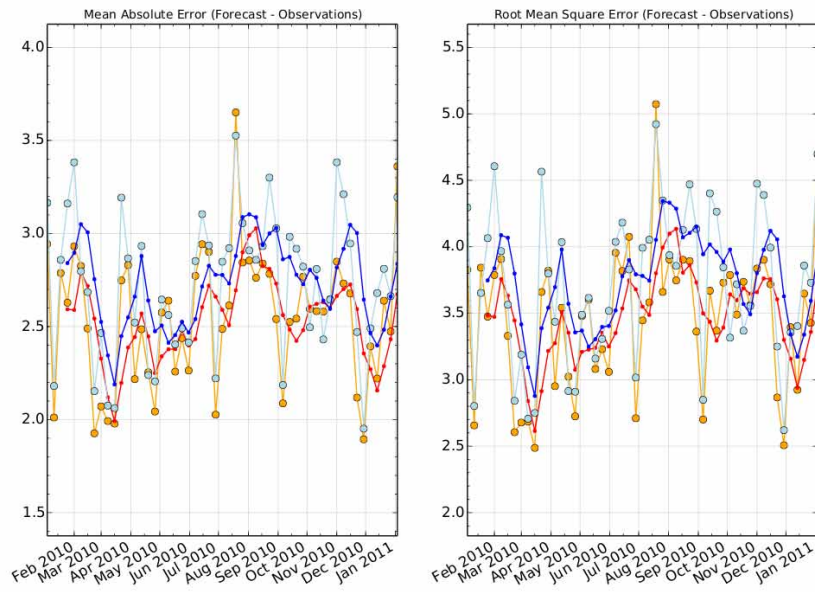


Figure 2.3. Vertical profiles of MAE and RMSE, comparing Global model and NAE model (a) forecast wind speed and (b) forecast wind direction to radiosonde data during 2010.

(a)

Wind Speed (m/s) @ 300hPa, Combined stations, T+18, Sondes, Equalized



(b)

Wind Direction (deg) @ 300hPa, Combined stations, T+18, Sondes, Equalized

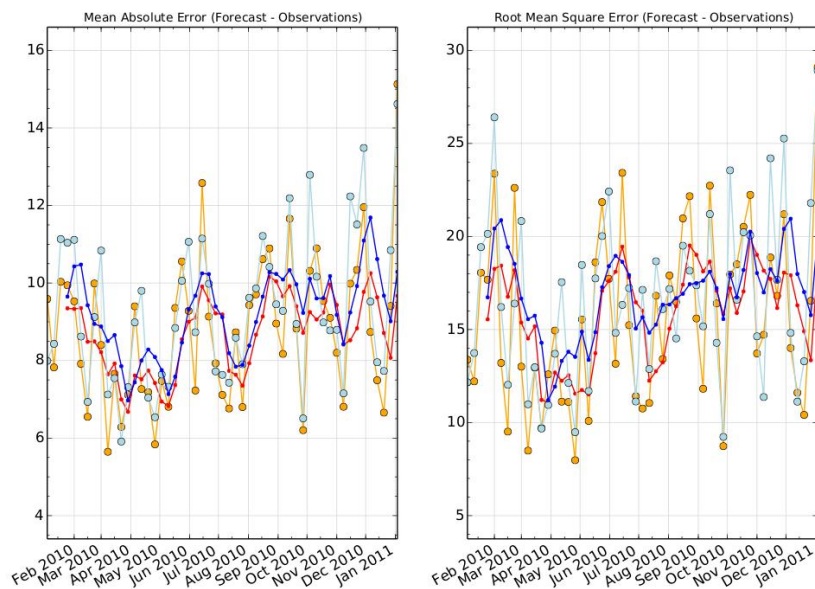
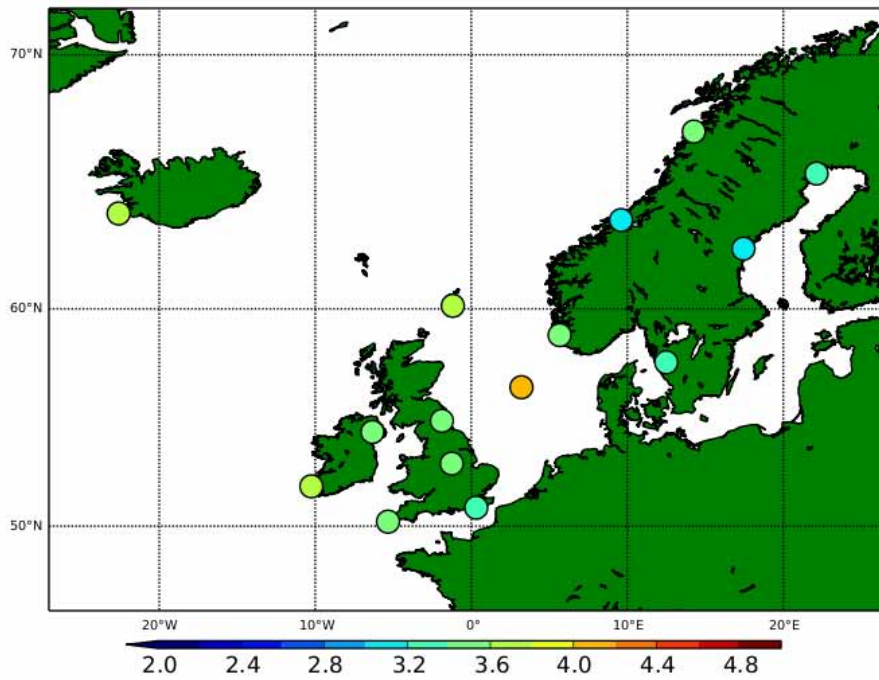


Figure 2.4. Time series of MAE and RMSE of the Global and NAE forecast (a) wind speed and (b) wind direction with respect to radiosonde data, at 300 hPa for T+18 during 2010. The orange and light blue lines show the weekly mean, using daily aggregated data, of the Global and NAE forecast meteorology respectively. The red and dark blue lines show the 4-weekly running mean using weekly aggregated data for the Global and NAE forecast meteorology respectively.

(a)



(b)

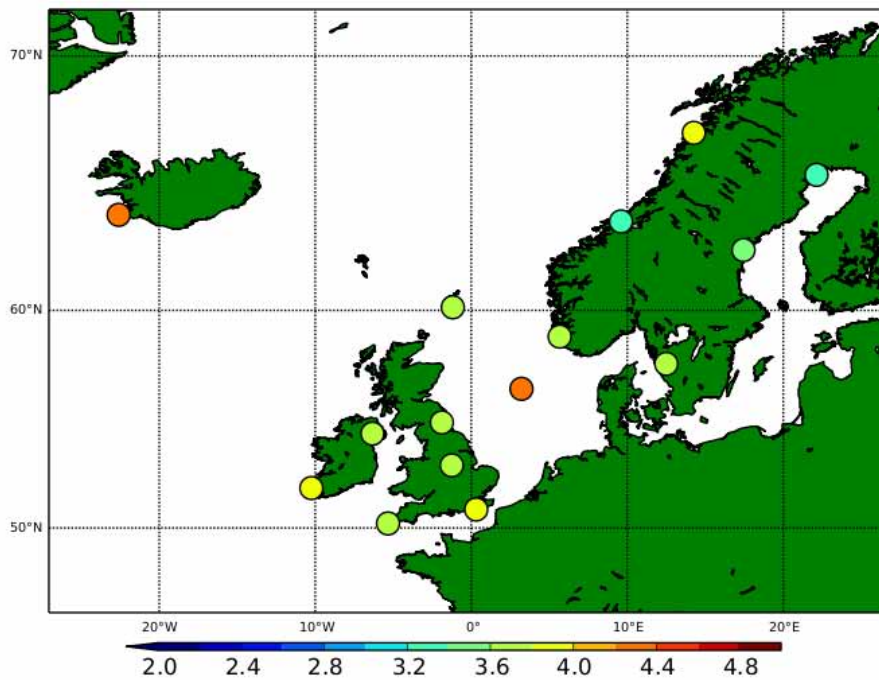
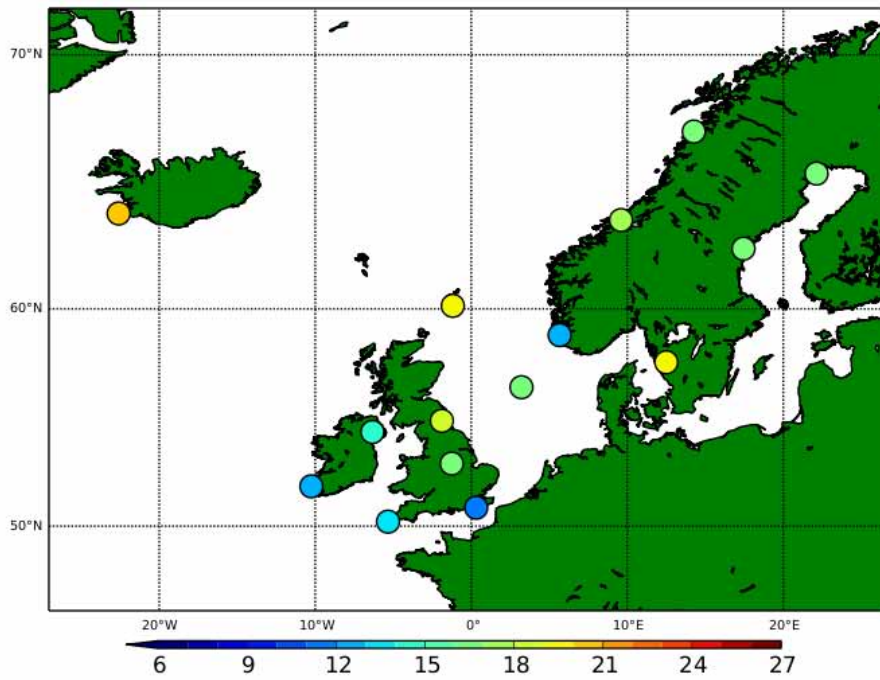


Figure 2.5. Error maps to show the time-averaged RMSE of (a) Global and (b) NAE forecast wind speed to radiosonde data during 2010.

(a)



(b)

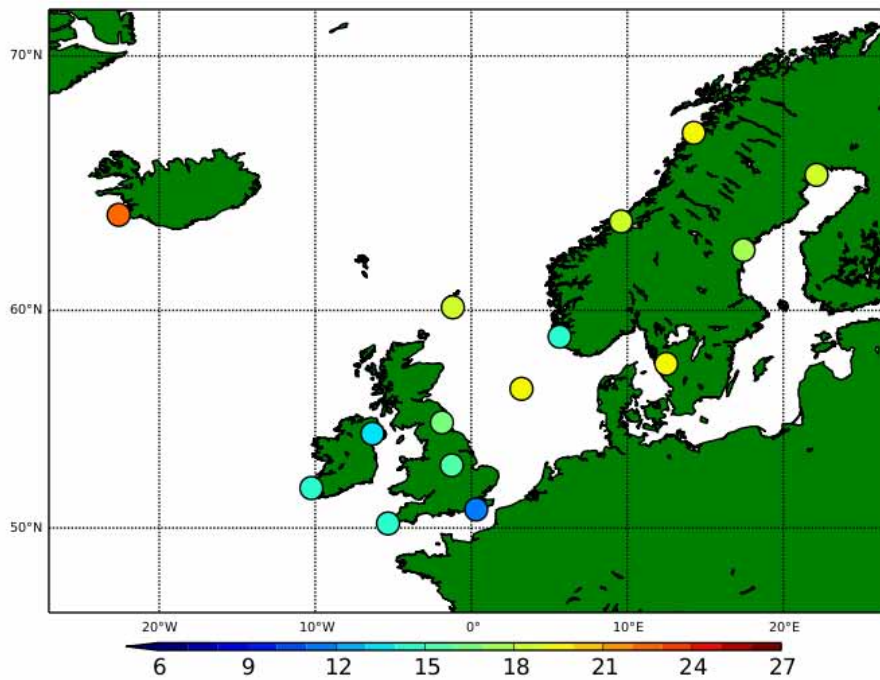


Figure 2.6. Error maps to show the time-averaged RMSE of (a) Global and (b) NAE forecast wind direction at 300 hPa, T+18, to radiosonde data during 2010.

2.3.2 Global with ENDGame Dynamics versus Euro4

The ability of the Global model configuration with ENDGame dynamics and the Euro4 model configuration with New Dynamics at predicting upper air wind speeds and wind direction during the period for which these configurations were operational, 16/07/2014-31/01/2015, are shown in Figures 2.7 and 2.8. Consideration of the individual 0Z and 12Z components indicated that there were no significant differences in the model performance between midday and midnight, therefore both were included in the analysis (Appendix A.2, Figures A.2.1, A.2.2, A.2.3 and A.2.4).

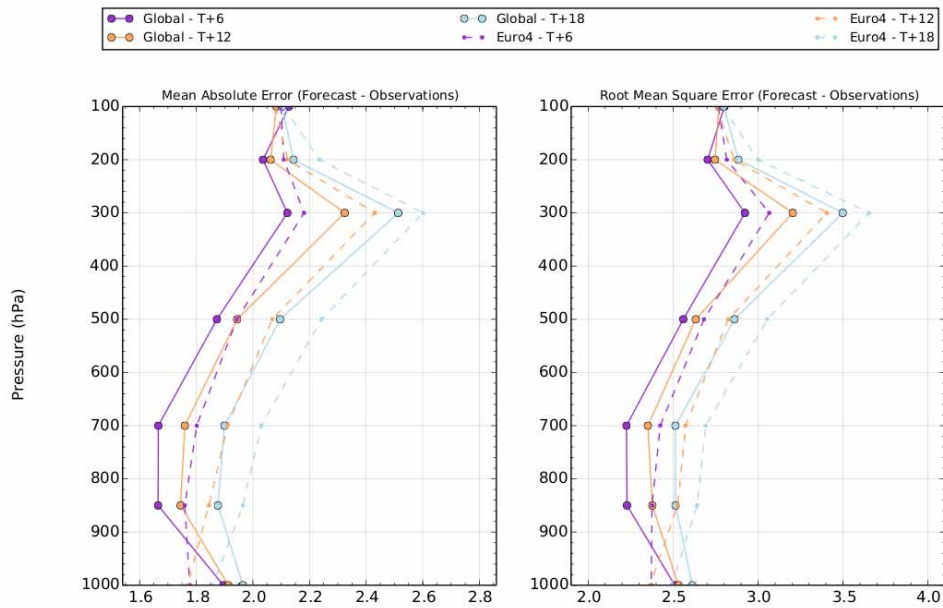
Figure 2.7 shows time-averaged vertical profiles of MAEs and RMSEs for T+6, T+12 and T+18 forecast data. The Global forecasts better represent measured wind speeds and wind direction than the Euro4 at upper levels in the atmosphere (< 850 hPa). The increased skill of both the Global and Euro4 model configurations in forecasting the wind vectors with decreasing forecast time is also observed; data at T+6 have lower MAEs and RMSEs than data at T+18. The most significant errors are again found to occur at 300 hPa, at the level of the jet stream.

Timeseries of MAEs and RMSEs for T+18 forecast data at 300 hPa are shown in Figure 2.8. The Global forecasts better represent the 300 hPa winds than the Euro4 forecasts. Using the Euro4 forecast wind speeds and wind direction over this period have lower errors than forecast winds using the NAE during 2010 (c.f. Figure 2.4). Some changes in model performance between the summer and winter periods are observed: the MAEs and RMSEs of the Global and Euro4 forecast wind speed over the winter period increase, while the calculated MAEs and RMSEs for wind direction decrease. As the dataset is limited, constrained to the time-period for which these particular model configurations were operational, we are unable to draw any conclusions as to whether the results are applicable to all synoptic conditions.

Error maps showing the time-averaged RMSEs at 300 hPa for T+18 forecast wind speeds and wind direction at individual stations are given in Figures 9 and 10. The Euro4 forecast wind speed and wind direction have slightly higher RMSEs than the Global forecasts across all the radiosonde datasets. Interestingly the calculated mean RMSEs for the Euro4 data at the Keflavik station which is close to the model boundary are not significantly higher than calculated RMSEs for other stations located further into the domain.

(a)

Wind Speed (m/s), Combined stations,
Equalized and Meaned between 20140716 00:00 and 20150131 12:00, Sondes



(b)

Wind Direction (deg), Combined stations,
Equalized and Meaned between 20140716 00:00 and 20150131 12:00, Sondes

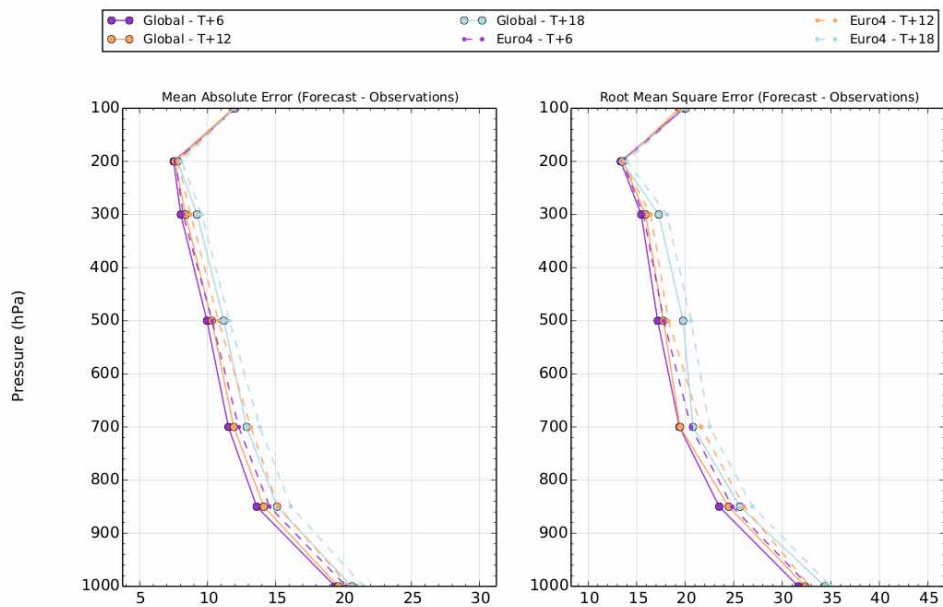
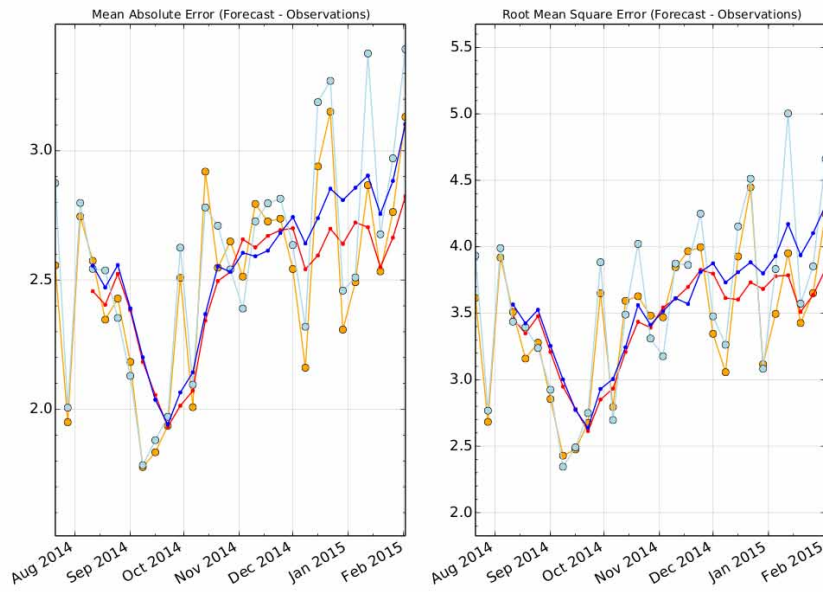


Figure 2.7. Vertical profiles of MAE and RMSE, comparing Global model with ENDGame dynamics and Euro4 forecast (a) wind speed and (b) wind direction to radiosonde data between July 2014 and January 2015, the period for which these model configurations were operational.

(a)

Wind Speed (m/s) @ 300hPa, Combined stations, T+18, Sondes, Equalized



(b)

Wind Direction (deg) @ 300hPa, Combined stations, T+18, Sondes, Equalized

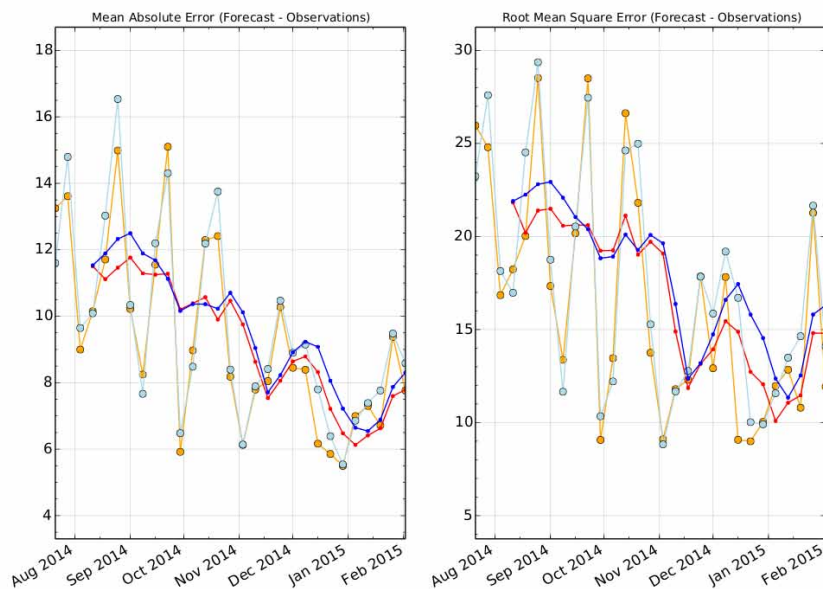
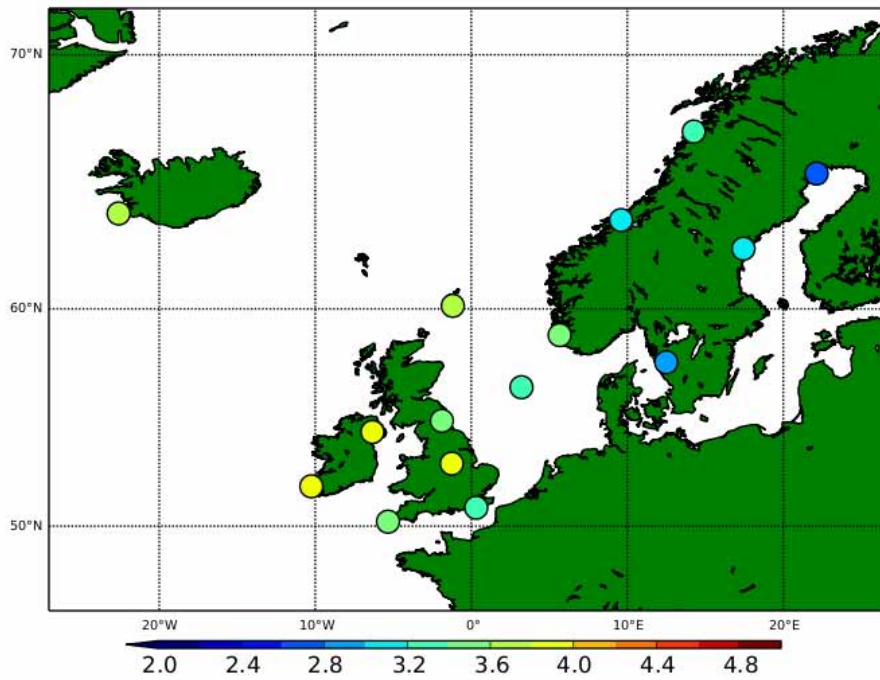


Figure 2.8. Timeseries of MAE and RMSE, comparing Global model with ENDGame dynamics and Euro4 forecast (a) wind speed and (b) wind direction to radiosonde data between July 2014 and January 2015 at forecast time T+18. The orange and light blue lines show the weekly mean, using daily aggregated data, of the Global and NAE forecast meteorology respectively. The red and dark blue lines show the 4-weekly running mean using weekly aggregated data for the Global and Euro4 forecast meteorology respectively.

(a)



(b)

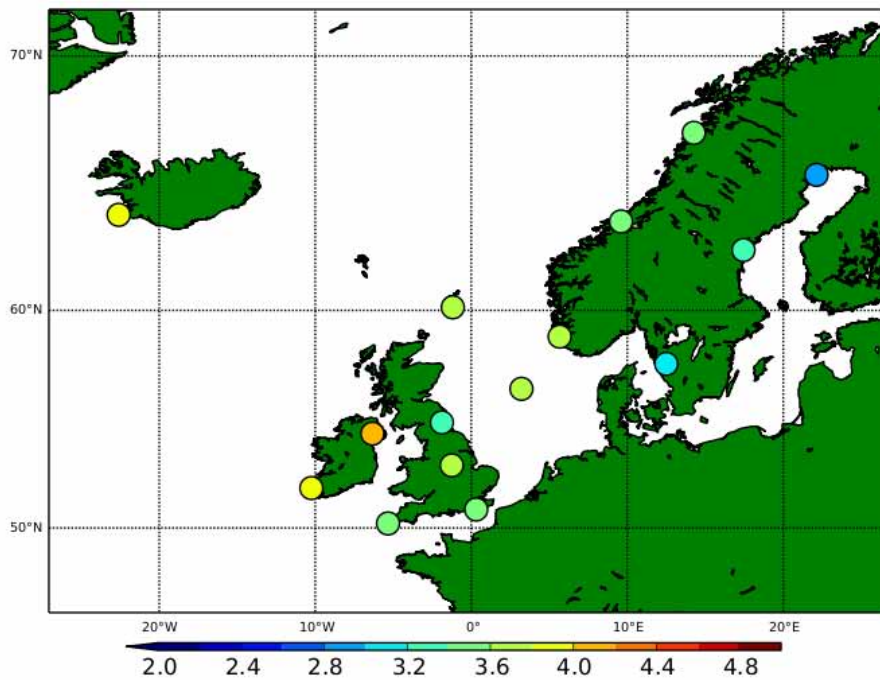
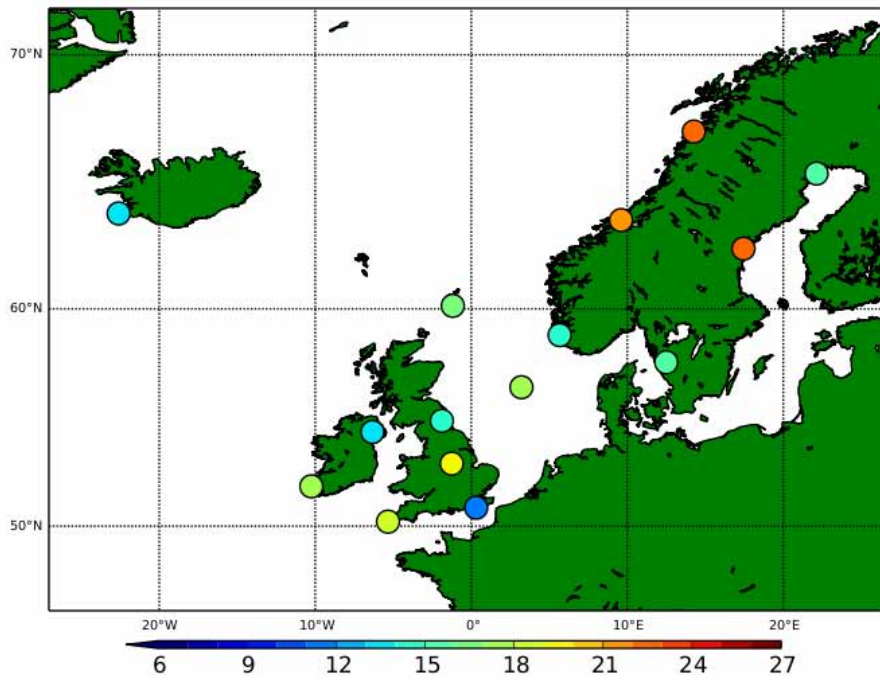


Figure 2.9. Error maps to show the time-averaged RMSE of (a) Global and (b) Euro4 forecast wind speed to radiosonde data between July 2014 and January 2015.

(a)



(b)

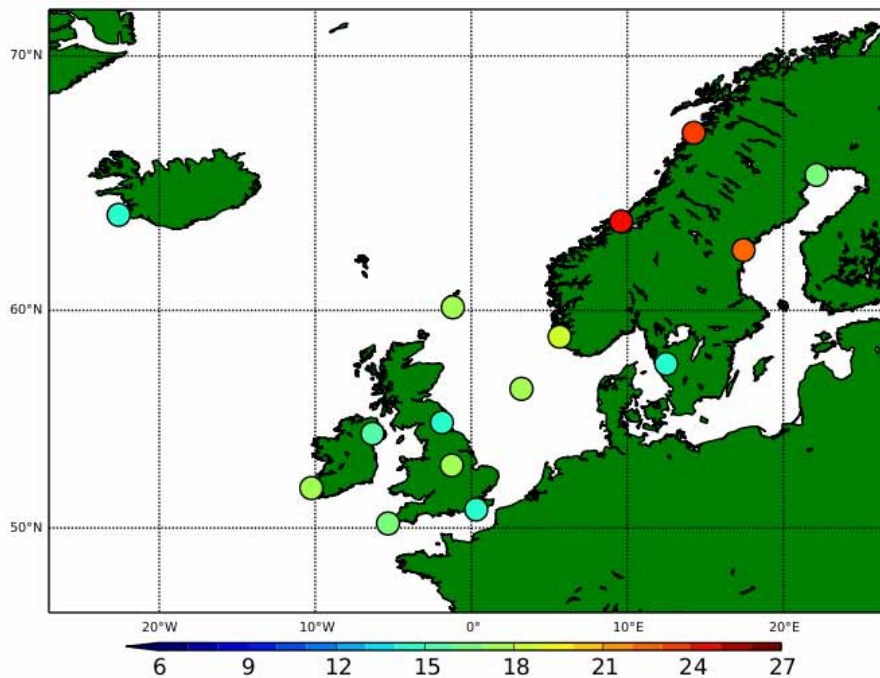


Figure 2.10. Error maps to show the time-averaged RMSE of (a) Global and (b) Euro4 forecast wind direction at 300 hPa, T+18, to radiosonde data between July 2014 and January 2015.

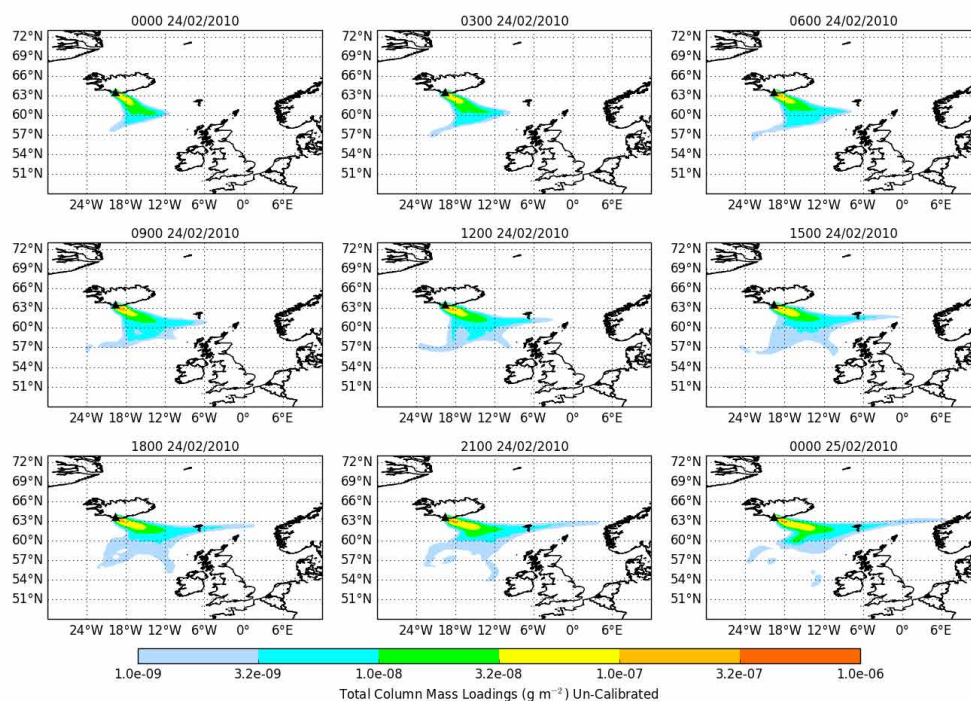
2.4 Impact on NAME simulations

To assess the sensitivity of NAME simulations to the meteorological dataset used we compare the simulated dispersion of a hypothetical volcanic ash cloud using forecast meteorological data from the different UM model configurations over the same time period. Particles are released at Eyjafjallajökull at 10 km asl throughout the NAME model run, we assume a mass eruption rate of 100 g hr^{-1} , as such calculated total column mass loadings are un-calibrated.

Using the calculated time-series of MAEs at T+18 and 300 hPa (~10 km asl) (Figure 2.4) we identify that on the 24/02/2015 the Global model configuration predicted significantly different winds to the NAE model configuration. Figure 2.11 shows the NAME simulated total column mass loadings (g m^{-2}) of the volcanic ash cloud on the 24th February 2010 using Global and NAE forecast meteorological data from the OZ UM run. The NAME runs were started on the 23rd February 2010 at 0Z and initially both use the same meteorological data (Global), before switching to use either the Global or NAE at 0Z on the 24th February 2010, this allowed the ash cloud to develop in the model and to be transported away from the vent before the comparisons were made. Initially the forecast plumes are very similar but differences develop as the forecast time increases.

By 18:00 UTC on the 24/02/2010 (T+18) the predicted ash cloud extends further to the west when the NAE is used. At 00:00 UTC on the 25/02/2010 (T+24) the forecast using the NAE predicts higher total column mass loadings to the east towards Scandinavia, whereas using the Global met data total column mass loadings are greater closer to the source. The Figure of Merit in Space (FMS) is a statistical coefficient which represents the percentage of overlap of data in space, see Appendix D for a discussion on the statistical measures used in this report. At 18:00 UTC on the 24/02/2010 (T+18) FMS=61, at 00:00 UTC on the 25/02/2010 FMS=54. The Pearson's Correlation Coefficient (PCC) represents the scatter between paired (i.e. at the same location) data points, and ranges in value between -1 and +1. A value of +1/-1 represents a perfect positive or negative linear association between the two variables. In our example this accounts for the difference in both the position of the plume and the given total column mass loading values at a grid point. At 18:00 UTC on the 24/02/2010 (T+18) PCC=0.70, at 00:00 UTC on the 25/02/2010 PCC=0.75.

(a)



(b)

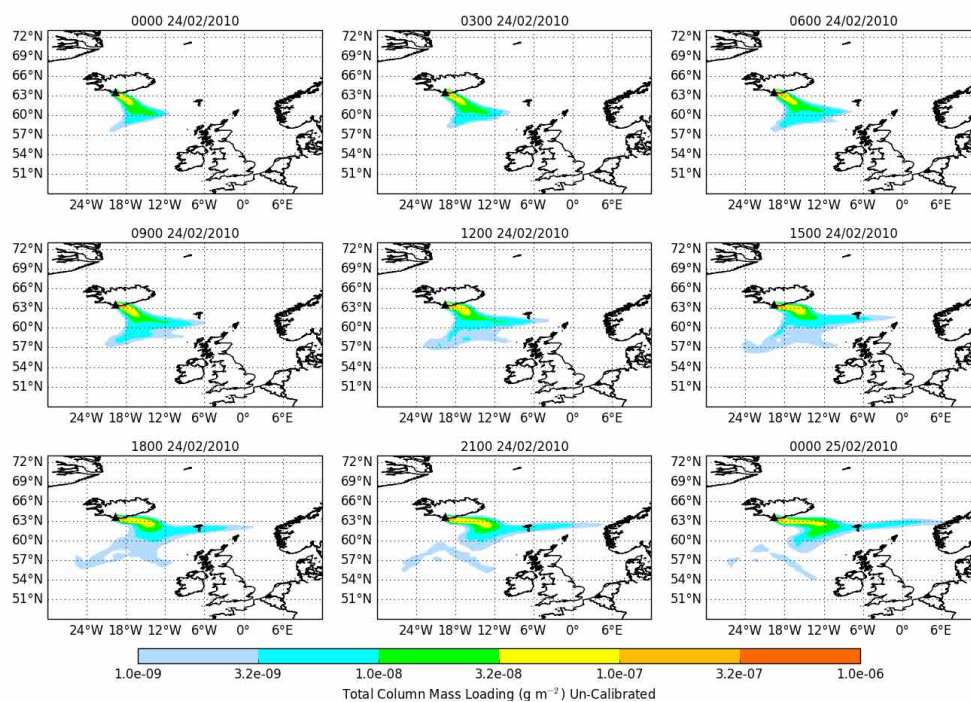


Figure 11: NAME forecasts of the transport of a hypothetical plume from Eyjafjallajökull during the 24th February 2010 using forecast (a) Global and (b) NAE meteorological data. Particles were released at a height of 10 km asl with a unit release rate of 100 g hr⁻¹ , as such modelled total column mass loadings are un-calibrated.

2.5 Discussion

Upper air wind data from the UM's Global model configuration have been shown to be consistently more accurate than LAM (NAE and Euro4) output at forecasting upper air winds over the area of responsibility covered by the London VAAC. It is clear that Global model output is currently the most appropriate dataset to use with NAME to simulate the transport and dispersion of volcanic ash clouds over Iceland, the north east North Atlantic, Scandinavia and the UK. The ability of the Global model to predict upper air winds is due to the model set-up: the higher vertical top height (80 km) means that observations derived from satellite retrievals of the upper atmosphere are included in the data assimilation and the interactions between the stratosphere and troposphere are captured. However, the affect of model resolution on upper air winds is not yet clear. As the resolution of a model increases small errors in the forecast can mean that the model is penalised more than a lower resolution model.

The Euro4 dataset was found to be more capable than the retired NAE at forecasting upper air winds. Whereas the NAE was 'allowed' to diverge from the Global forecasts, the Euro4 is a downscaler and is therefore constrained to the Global meteorological data, this has perhaps aided it in forecasting upper air winds. We have only considered Euro4 model data up to January 2015, after which ENDGame dynamics were introduced to its dynamical core. It is too soon to consider any statistical assessment of this model output, as the data set is too limited. However, it will be important to assess the capability of this model configuration in the future. The reduced damping in the ENDGame dynamics results in less diffusive output, increasing variability in forecast winds, and this may further improve the capability of the Euro4 to forecast upper air winds.

There are further advantages associated with using Global rather than LAM forecast meteorological datasets. Currently Global model output has smaller data sizes than LAM output, the larger data sizes associated with LAM data would mean that using NAE or Euro4 met data would increase NAME run times which is undesirable when the model is being used operationally by the London VAAC. Further, as the limited area domains of both the NAE and Euro4 have boundaries close to Iceland any NAME run to forecast the transport of volcanic ash clouds using LAM data would need to be used along side Global model data, in the event that the ash cloud was to leave the LAM domain.

Considering calculated MAEs of wind speed data at 300 hPa and T+18 the Global and NAE forecast wind speeds during 2010 had average errors of 2.5 m s^{-1} and 2.7 m s^{-1} respectively (Figure 2.3). Considering the MAE of wind speed data at 300 hPa and T+18 during 16/07/2014-31/01/2015 we find that the Global met data continued to have an average error of 2.5 m s^{-1} and the Euro4 an had an average error of 2.6 m s^{-1} (Figure 2.7). The average error in wind direction during 2010 and 16/07/2014 -- 31/01/2015 at T+18 and 300 hPa was 9° for all the model configurations (Figures 2.4 and 2.8). Calculated errors associated with both the forecast wind speed and wind direction are smaller at shorter forecast times (T+6 and T+12). To assess the errors between the radiosonde and forecast meteorological datasets we have used the MAE, as opposed to the Mean Error (ME). The MAE does not allow the average bias, either a negative or positive behavior, to be identified. However, using the ME to assess the forecast data often presents a 'null' result, this is due to the significant variability between positive and negative errors in the wind data, which cancel-out as they are averaged over time. Plots of MEs are given in Appendix C for the periods studied. Although the magnitudes of the calculated errors are not meaningful it is clear that during 2010 both the Global and NAE forecasts were under-estimating wind speed, whereas during 16/07/2014-31/01/2015 both positive and negative bias can be identified in the Global and Euro4 data. It should be remembered though that the ability of the Global vs. NAE and Global with ENDGame vs. Euro4 to forecast upper air winds varies on any given day (see Figures 2.4 and 2.8)

and as such the uncertainty associated with NAME forecasts of volcanic ash cloud dispersion must be assessed for the individual forecast produced.

The chaotic nature of our atmosphere means that small errors in temperature, winds or other NWP variables are amplified with time. Small errors in the model's initial state of the atmosphere can result in large errors in the forecast. The future state of the atmosphere therefore can not be completely described with a single model run and deterministic forecast, rather an ensemble of model runs are needed to fully predict all the possible variances. To completely describe the uncertainty associated with a forecast for volcanic ash cloud transport the dispersion model would need to use ensemble meteorological data.

Finally, it should be noted that when NAME is used for research projects to consider past events, analysis meteorological data sets are used which have been calibrated using available observations. Therefore forecasts produced for research purposes will not have the same errors associated with them.

2.6 Conclusions

We have shown that the Global model configuration of the UM is more skillful at forecasting upper air wind speeds and wind direction than the NAE and Euro4 model configurations. When forecasting the dispersion of volcanic ash clouds in the atmosphere, the London VAAC should use the Global forecast meteorology to drive NAME. The average error on the forecast wind speeds and wind directions, at T+18 and 300 hPa, using the Global model configuration is $\sim 2.5 \text{ m s}^{-1}$ and $\sim 9^\circ$, this can result in positional errors in the modelled transport of the volcanic ash cloud. When interpreting dispersion model forecasts of volcanic ash clouds the uncertainties associated with the forecast meteorology should always be assessed.

3. The sensitivity of dispersion model forecasts to NWP model topography

Authors: F.M. Beckett, C.S. Witham

3.1 Introduction

Orography can affect the weather in a number of ways, ranging from local effects such as enhanced precipitation and severe turbulence over mountains, to large-scale effects on global circulation through the generation of turbulent wakes behind hills, flow blocking at low levels upwind of large mountain ranges, and internal gravity wave motions aloft which can propagate large distances both downwind and above mountains (e.g. Smith, 1979). The relationship between terrain and wind speed at the surface is complex. Land surface area, and therefore surface friction, decreases with altitude. Surface roughness decreases with altitude as tall vegetation and buildings become sparse. These characteristics tend to lead to an increase in wind speed at the surface (e.g. Oke, 1987). However, surface area increases with ruggedness and wind speeds therefore tend to decrease over complex terrain (Nawri et al., 2012). Understanding and representing the effects of topography in Numerical Weather Prediction (NWP) models is therefore crucial for modelling surface winds.

Nawri et al. (2012) assessed the seasonal averages and temporal variability of surface winds over Iceland using the WRF model with ECMWF meteorological and topographical data at two different horizontal resolutions: a low resolution version with a grid spacing of 27.8 km in latitude and 23.5 km in longitude and a high resolution version with a grid spacing of 13.9 km in latitude and 11.7 km in longitude. They found that the highest wind speeds over Iceland occur over the highest model terrain and the lowest wind speeds occur over the most rugged terrain of the island. They show that during the winter the prevailing surface winds flow from low to high temperatures, down-slope in the interior of the island, and offshore along the coast. In summer, surface wind speeds are weaker due to weaker pressure gradients over the island, and land-sea temperature gradients result in prevailing on-shore winds in most places.

To forecast the transport and dispersion of pollutants in the atmosphere atmospheric dispersion models, such as NAME, use 3-dimensional meteorological fields from Numerical Weather Prediction (NWP) model output. In this study we assess the sensitivity of NAME forecasts of the dispersion of a volcanic gas plume, which is near to the surface, to the topography used in the NWP model and the associated meteorology **used. We assess two model configurations under the umbrella of the Met Office's NWP model, the Unified Model: the Global and the Euro4 (see Section 2 for an over-view of the model configurations).** We consider how the resolution of the topography used in each affects the forecast winds at the surface. The impact on NAME forecasts of the dispersion of the gas plume from the Holuhraun fissure eruption during September 2014 is then explored.

3.2 Topography and the Unified Model

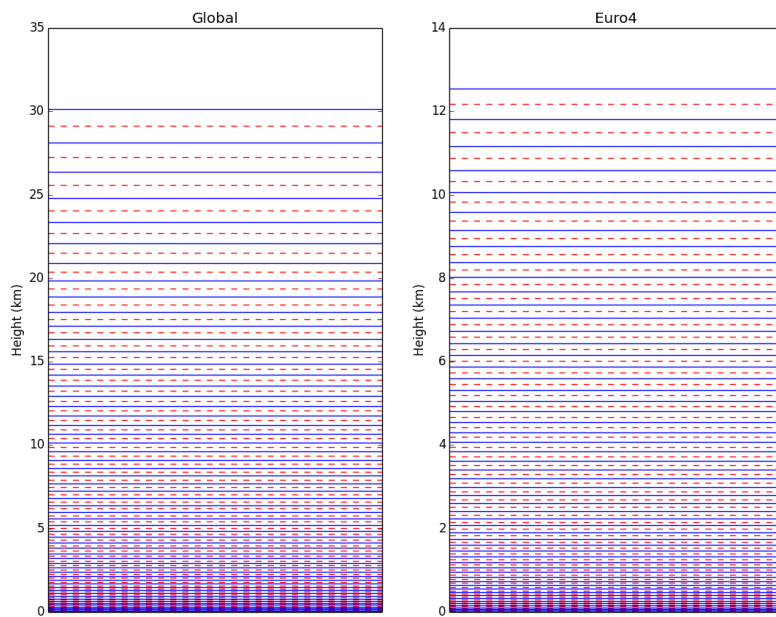
The Unified Model (UM) is the numerical modelling software developed by and used at the Met Office to describe the state of the atmosphere over the Earth's surface for both operational Numerical Weather Prediction (NWP) and atmospheric research (Davies et al., 2005). **The UM's dynamical core uses a semi-implicit semi-Lagrangian formulation** to solve the non-hydrostatic, fully compressible, deep-atmosphere equations of motion and resolve the three-dimensional wind components, potential temperature, Exner pressure,

density and components of moisture (vapour, cloud water and cloud ice) in the atmosphere (e.g. Walters et al., 2014). These prognostic fields are discretised onto a grid point scheme; in the horizontal a regular longitude–latitude grid with Arakawa C-grid staggering (Arakawa and Lamb, 1977) is used. In the vertical Charney–Phillips staggering (Charney and Phillips, 1953) is employed, with terrain following height coordinates which evolve to constant height surfaces higher up in the atmosphere (≥ 18 km asl). This simulates the fact that air motion is terrain following near the surface but becomes less so with increasing height in the atmosphere.

There are several model configurations under the umbrella of the UM which produce output at different resolutions, and for different purposes. The Global model produces meteorological data for the whole globe at a horizontal resolution of 17 km. The Euro4 has been developed to provide high resolution meteorological data over Europe, including Iceland, it has a horizontal grid of 4 km (see Section 2 for a comprehensive overview of all the model configurations). The Global and Euro4 have different vertical level sets; the Global model has a top height of 80 km and has 70 model levels, the Euro4 also has 70 model levels but has a lower lid, at 40 km, this means that the vertical resolution close to the surface is increased. When NAME uses the UM met data it uses limited vertical extent datasets, the Global met data has a top height of 30.1 km and the Euro4 12.5 km, this reduces file sizes and computational burden. Figure 3.1 shows the model levels used by NAME with the Global and Euro4 model configurations for zero topography i.e. over the sea. The wind (ρ) levels are vertically staggered with potential temperatures (θ levels).

Orography data used by the UM is derived from the GLOBE (The Global Land One-km Base Elevation) dataset (Walters et al., 2014). However, orography must be averaged to represent the surface elevation at the horizontal resolution of the model. The elevation of the model surface at a grid point is therefore equal to the mean height of the real surface over the area of the grid square. This smoothing process may result in fine-scale meteorological features being lost as sub-grid orographic affects are not explicitly resolved. Model surface heights tend to be most different from actual surface heights in mountainous areas, where the variability of elevation is most marked. Figure 3.2 shows the resolution of the topography used in the Global and Euro4 models, it is clear that the topography data used in the Global is coarser than the topography represented in the Euro4. For example in the Global model Askja volcano is not represented in the topography data-sets used, but can be identified in the Euro4 model topography. However, neither fully represent the complex topography of Iceland. The extent of the models land surface is limited by the land-sea mask applied, which again is a function of the horizontal resolution of the model. Figure 3.3 shows the land-sea masks applied for the Global and Euro4 model configurations.

(a)



(b)

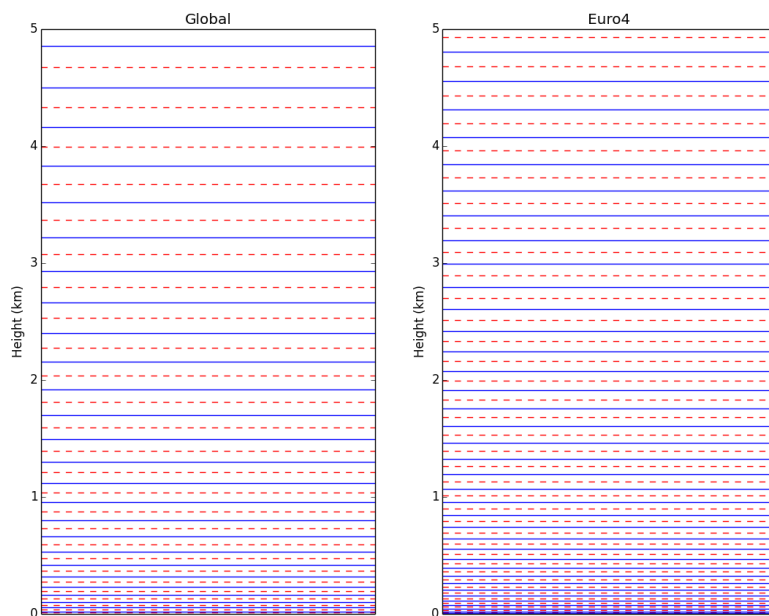


Figure 3.1. The vertical model level sets for the UM model configurations, as used by NAME. The **red solid lines represent the 'rho' levels** on which the wind vector data are stored, the **blue dashed lines represent the 'theta' levels** on which temperature data are stored. In (a) all of the model levels used in NAME simulations are represented, (b) shows the model levels over the lowest 5 km, the Euro4 has a finer vertical resolution than the Global close to the surface.

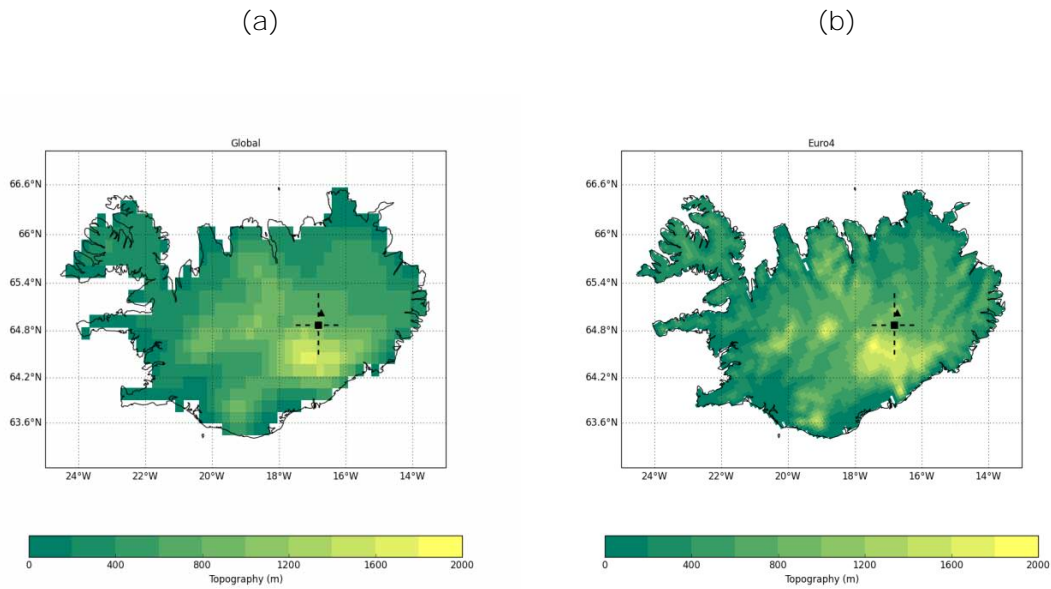


Figure 3.2. The resolution of the topography used in the different UM model configurations over Iceland (a) Global with a horizontal resolution of 17 km and (b) Euro4 with a horizontal resolution of 4km. The dashed cross-lines indicate the location of the cross-section topography plots (Figure 3.4). The Holuhraun area is indicated by the black square, the triangle indicates the location of Askja.

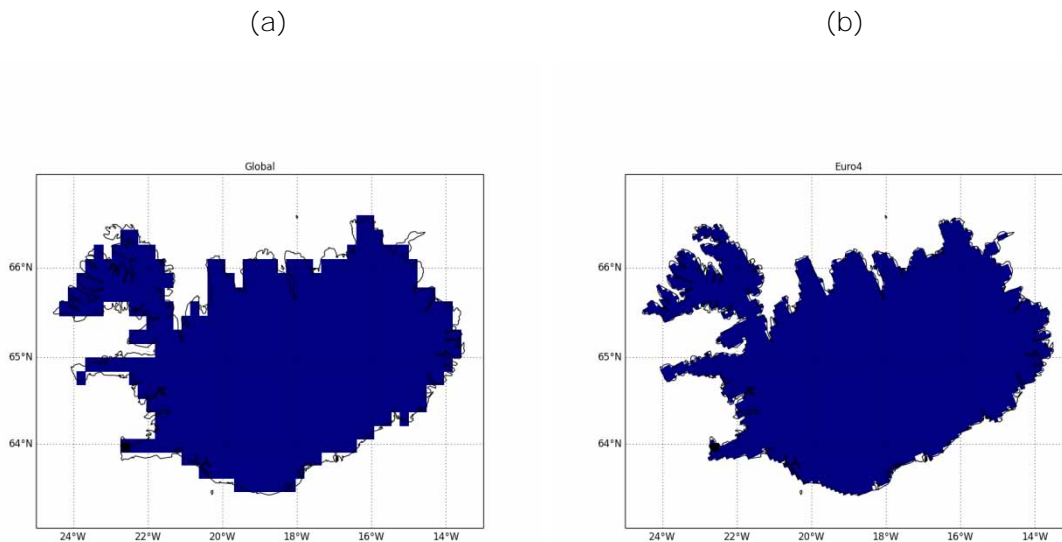


Figure 3.3. The (a) Global and (b) Euro4 Land Sea Masks for Iceland. The black square indicates the location of Keflavik, where the international airport is located. The coarser resolution of the NAE model configuration means that this land location is expected to be in the sea.

3.2 Sensitivity of NAME forecasts to topography

To assess the sensitivity of dispersion model forecasts to NWP model topography we compare the difference in forecasts of the gas plume from the Holuhraun fissure eruption in September 2014 using NAME with meteorological data from the Global versus Euro4 UM model configurations. We compare the modeled meteorology to the topography used in each of the models to assess its impact on the model wind speeds and wind directions and hence the forecast transport of the gas plume.

On the 16th August 2014 at 03:00 UTC an intense seismic swarm began at Barðarbunga, a subglacial basaltic volcano at the north-western corner of Vatnajökull ice cap in Iceland (Gudmundsson et al. 2007). GPS observations indicated simultaneous deflation of the caldera and dyke displacement to the north of the Vatnajökull ice-cap (Sigmundsson et al. 2015). The lengthening of the dyke ended on 27 August, around 10 km north of Vatnajökull and a minor fissure eruption in Holuhraun, lasting 4 hrs, occurred on the 29th August 2014 (Sigmundsson et al. 2015). On the 31st August the fissure eruption in Holuhraun re-started and continued for six months.

The topography surrounding the Holuhraun eruption site is complex. To the south is the Vatnajökull ice-cap under which are there several volcanoes, including Barðarbunga (summit height 2009 m) and Grímsvötn (summit height 1725 m) on the north-west edge of the glacier. To the north is the Askja caldera (summit height 1516 m). The Holuhraun lava field lies in a valley between these two volcanic complexes. Figure 3.4 shows cross-sections of the topography of this area (indicated by the cross-sections shown on the maps in Figure 3.2) represented in the Global and Euro4 model configurations. The distinction between the valley and higher lands of the volcanic complexes to the north and south of Holuhraun are clear in the Euro4 topography. However, the topography used by the Global model configuration does not recognise Askja and suggests a lower surface altitude in this area than over Holuhraun.

Differences in NAME forecasts using the Global versus Euro4 met data of the predicted location of the gas plume and surface air concentrations are considered. Gas, represented as a tracer in the model, is released in a uniform vertical line source from the surface to 1000 m agl at Holuhraun, no chemical reactions in the atmosphere are considered, and we assume a constant, un-calibrated, source strength of $1 \times 10^{10} \text{ g hr}^{-1}$. Thus modelled air concentrations are relative, indicating areas of high and low concentrations only and not actual mass loadings in the atmosphere. We use analysis met data, in which observations have been assimilated into the model to produce a best-guess forecast.

Forecast 1-hour averaged air concentrations over 0-100 m agl, 0-500 m agl and 0-1000 m agl, at 12:00 UTC for each day during September 2014 are given in Appendix E. From examination of Figures E1-E6 and using the statistical coefficients Figure of Merit in Space (FMS) and Pearson's Correlation Coefficient (PCC), several periods can be identified when there is a marked difference in the forecast location of the gas plume and predicted air concentrations when using the Global versus the Euro4 met data. See Appendix D for a description of the statistical measures used and Appendix F for calculated FMS and PCC values for each of the daily forecasts.

The calculated minimum PCC, indicating a significant difference in the predicted air concentrations between the NAME forecasts using the Global versus Euro4 met data, for the plume over 0-100 m agl occurs on the 02/09/2014. The minimum FMS is found to occur on the 30/09/2014 suggesting a significant difference in the predicted location of the plume on this day. When considering the forecast air concentrations over 0-500 m agl and 0-1000 m agl the calculated minimum PCC and FMS occur on the 30/09/2014. Examination of the forecasts also suggests significant differences in the predicted plume location and air concentrations on the 10/09/2014. We now present case-studies for

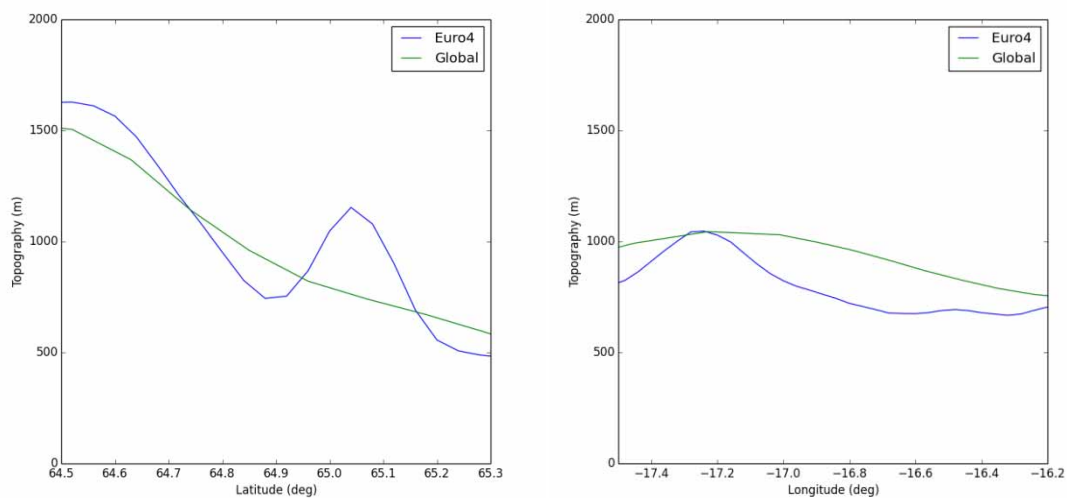


Figure 3.4. Cross-sections of the Global and Euro4 model topography over the Holuhraun area, (a) at -16.8313 deg longitude and (b) at 64.8725 degrees latitude, as indicated by the dashed cross-lines in Figure 3.2.

each of these dates in which we consider the influence of the model topography on the forecast gas plumes.

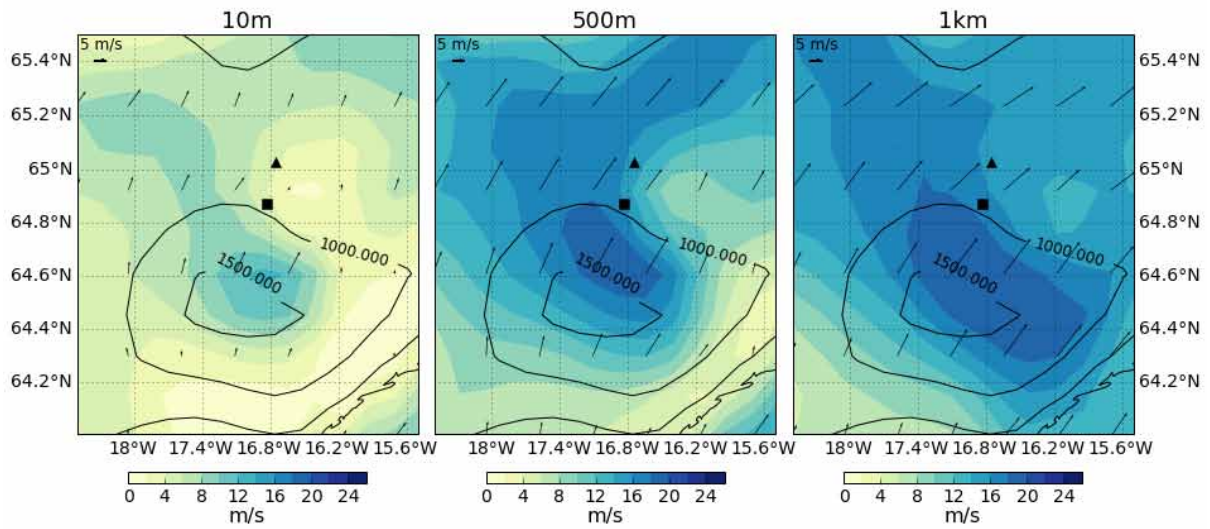
3.3.1 Case Studies

In the following case-studies we compare the model topography to the forecast horizontal wind speed and vectors using the Global versus Euro4 data-sets, and consider the impact on the NAME forecast of the transport of the gas plume from the Holuhraun fissure eruption.

3.3.1.1 2nd September 2014

Figure 3.5 shows the forecast wind speeds and wind vectors using the Global and Euro4 analysis meteorological data, in relation to the model topography, on the 2nd September 2014 at 10, 500 and 1000 m agl. Figure 3.6 shows the resulting NAME forecasts of the dispersion of the Holuhraun gas plume; for air concentrations over 0-100, 0-500 and 0-1000 m agl. The Euro4 predicts higher wind speeds, at all of the altitudes considered, over the elevated terrain of the ice cap, and calmer and lighter winds through the valley in which Holuhraun sits. Consequently using the Euro4 meteorological data with NAME the dispersion forecast predicts the plume to initially spread in all directions and, because of the low winds speeds, the gas is only slowly dispersed and high surface concentrations at the Holuhraun site are predicted. The Global data predicted higher wind speeds, the gas plume is more rapidly dispersed, and the strong south-easterly winds transport the plume immediately towards the north-east.

Global Model horizontal wind speeds and vectors on 02 September 2014 12:00 UTC



Euro4 horizontal wind speeds and vectors on 02 September 2014 12:00 UTC

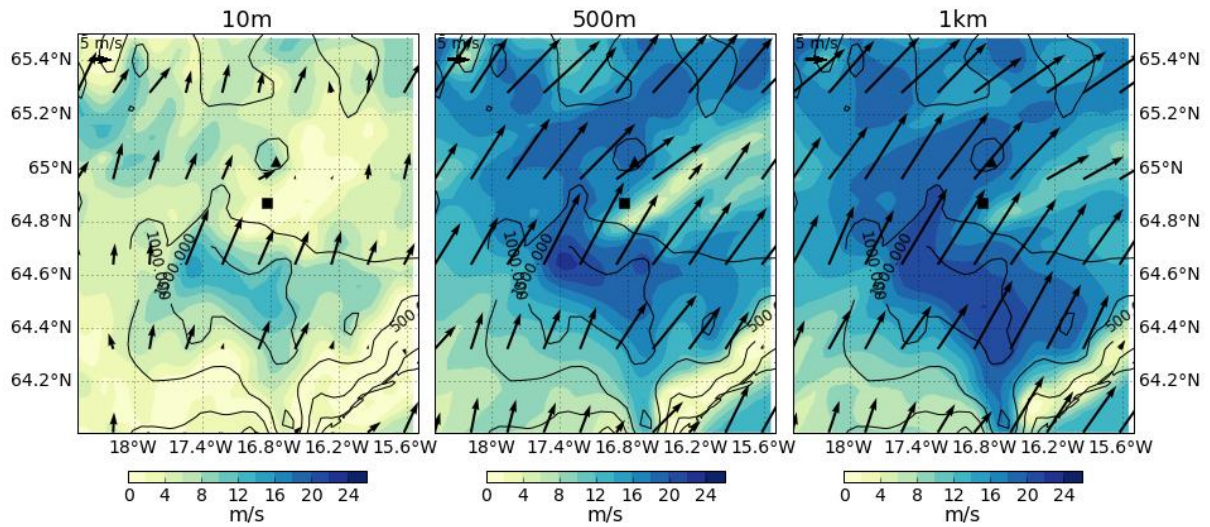


Figure 3.5. To show forecast horizontal wind speeds and wind vectors at 12:00 UTC on the 2nd September 2014 using the Global and Euro4 model configurations. The topography represented in the models is indicated by the contour lines. The black square indicates the location of the Holuhraun fissure eruption and the black triangle Askja volcano.

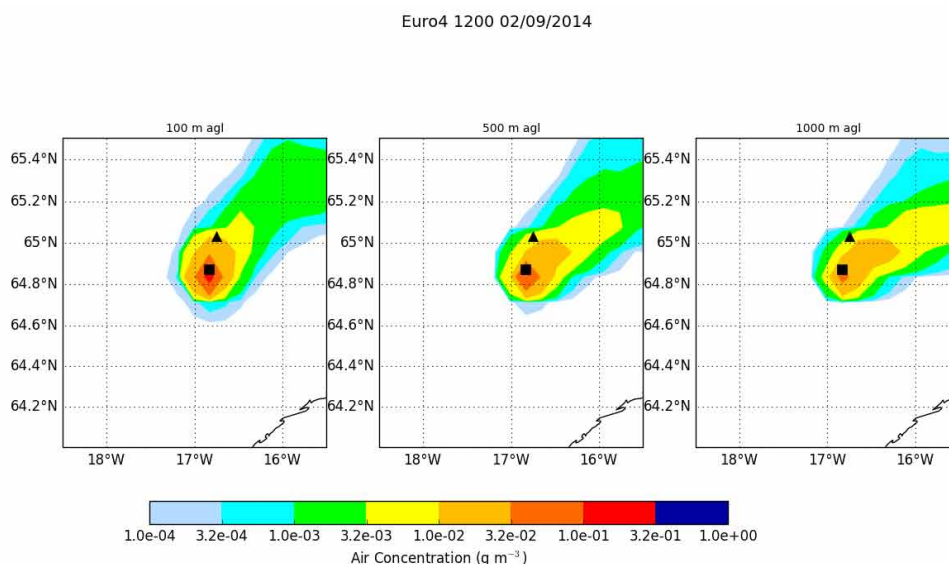
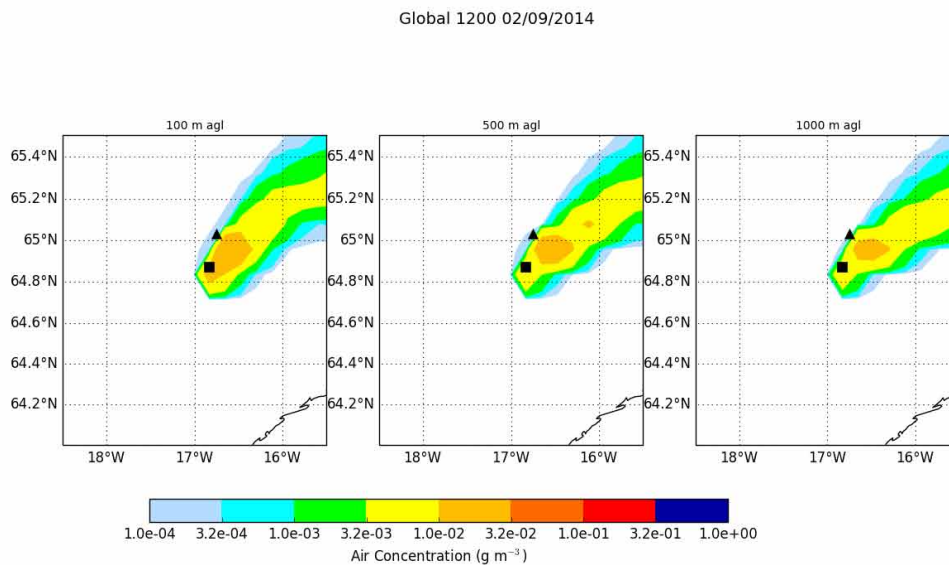
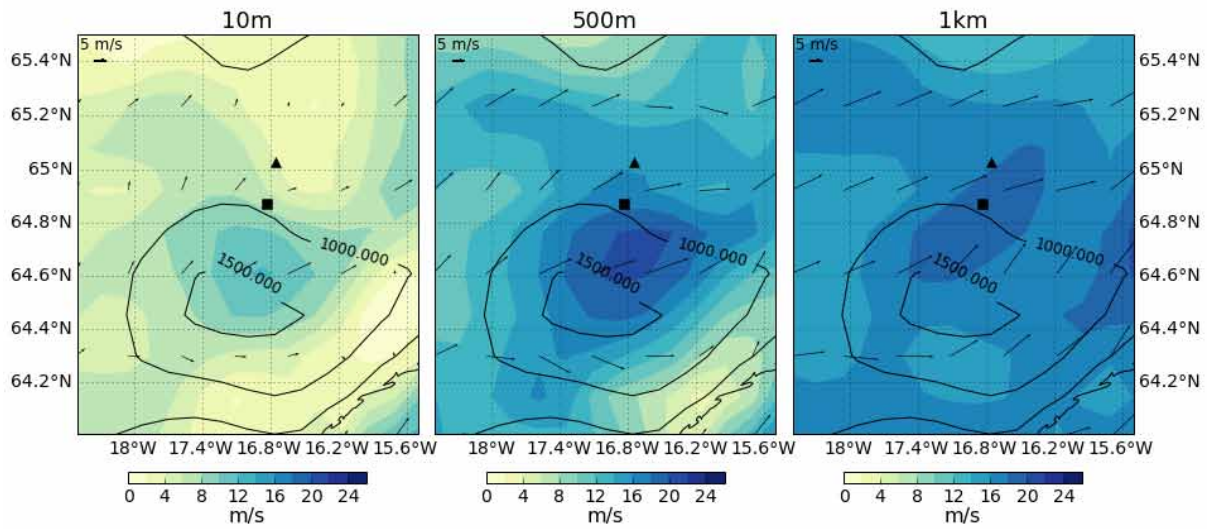


Figure 3.6. NAME forecast 1-hour averaged relative air concentrations over 0-100 m agl, 0-500 m agl and 0-1000 m agl for the Holuhraun eruption at 12:00 UTC on the 2nd September 2014 using the Global and Euro4 model configuration analysis meteorological data. Holuhraun is indicated by the black square, the triangle indicates the location of Askja.

3.3.1.2 10th September 2014

Figure 3.7 shows the forecast wind speeds and wind vectors using the Global and Euro4 analysis meteorological data on the 10th September 2014. Figure 3.8 shows the resulting NAME forecasts of the Holuhraun gas plume. The influence of the topography on the forecast wind direction is clearly reflected in the Euro4 data: winds diverge around Askja and are funnelled between the edge of the Vatnajökull ice-cap and the higher ground around the volcano, resulting in a south-east component to the wind flow south of Askja through the valley, which is not observed in the Global data. This is reflected in the simulated dispersion of the gas plume. Using the Euro4 model topography and forecast meteorology the plume is immediately dispersed eastwards from Holuhraun, whereas using the Global data the plume initially travels north.

Global Model horizontal wind speeds and vectors on 10 September 2014 12:00 UTC



Euro4 horizontal wind speeds and vectors on 10 September 2014 12:00 UTC

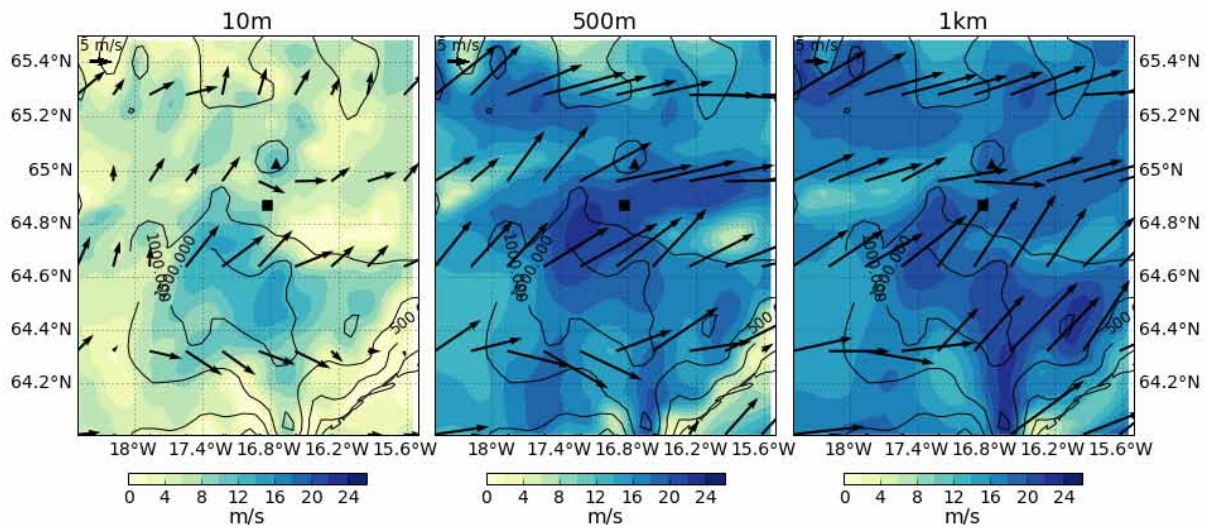
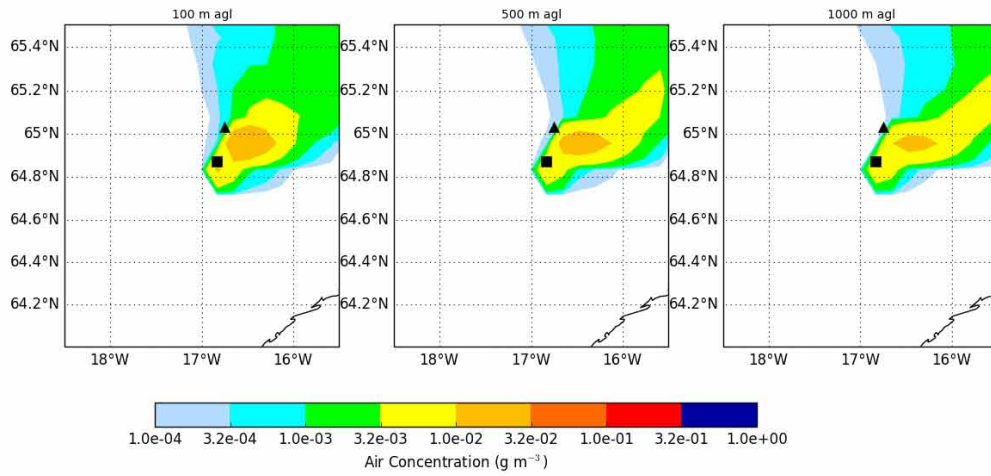


Figure 3.7. To show forecast horizontal wind speeds and wind vectors at 12:00 UTC on the 10th September 2014 using the Global and Euro4 model configurations. The topography represented in the models is indicated by the contour lines. The black square indicates the location of the Holuhraun fissure eruption and the black triangle Askja volcano.

Global 1200 10/09/2014



Euro4 1200 10/09/2014

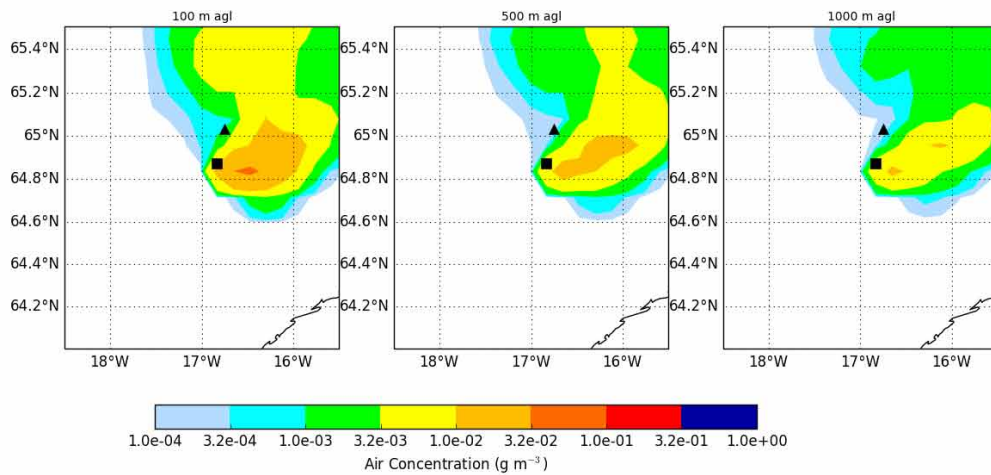
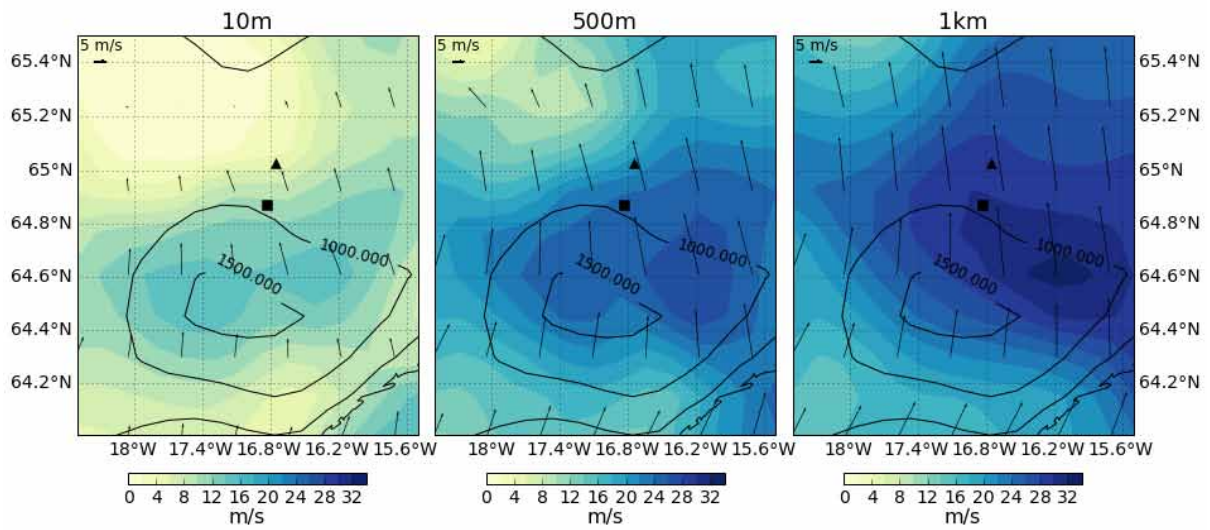


Figure 3.8. NAME forecast 1-hour averaged relative air concentrations over 0-100 m agl, 0-500 m agl and 0-1000 m agl of the Holuhraun gas plume at 12:00 UTC on the 10th September 2014 using the Global and Euro4 model configuration analysis meteorological data. Holuhraun area is indicated by the black square, the triangle indicates the location of Askja.

3.3.1.3 30th September 2014

Figure 3.9 shows the forecast horizontal wind speeds and wind vectors using the Global and Euro4 model configurations, in relation to the model topography, on the 30th September 2014 when significant differences in the forecast location of the gas plume and predicted air concentrations when using the Global versus the Euro4 met data were identified (Section 3.2). Figure 3.10 shows the resulting NAME forecasts of the Holuhraun gas plume. Here the large-scale flow pattern predicted by the Global and Euro4 model configurations are alike (Figure 3.11) and predicted wind directions are comparable over the Holuhraun site (Figure 3.10). The impact of the topography on forecast wind speed is observed in the Euro4 met data however and forecasts of the dispersion of the gas plume are still observed to vary depending on the met data used. The Euro4 predicts greater wind speeds over the higher topography of the Vatnajökull glacier, whereas calmer surface winds are forecast in the valley in which the Holuhraun site is located. This results in the initial plume dispersing in all directions and high gas concentrations close to the surface. The Global met also predicts higher wind speeds over the ice-cap but does not account for a change in wind speed over Askja or reduced wind speeds through the valley in which the Holuhraun eruption site is located. Using the Global met data the plume is simply transported to the north-west. This demonstrates that even when the large-scale meteorology is similar in the Global and Euro4 the topography used in the model can affect the small scale meteorological features close to the surface.

Global Model horizontal wind speeds and vectors on 30 September 2014 12:00 UTC



Euro4 horizontal wind speeds and vectors on 30 September 2014 12:00 UTC

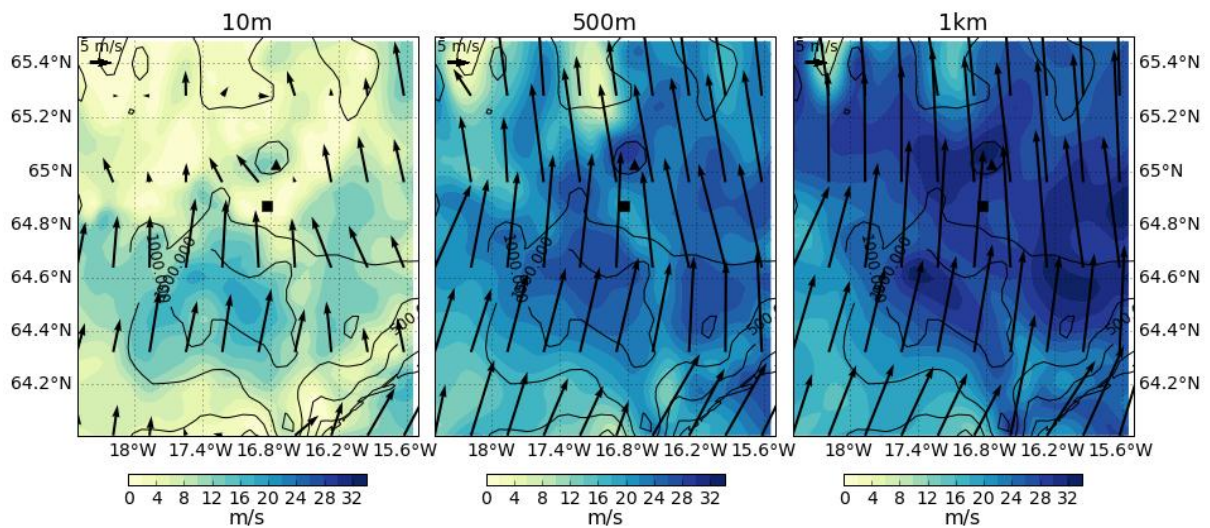


Figure 3.9. To show forecast horizontal wind speeds and wind vectors at 12:00 UTC on the 30th September 2014 using the Global and Euro4 model configurations. The topography represented in the models is indicated by the contour lines. The black square indicates the location of the Holuhraun fissure eruption and the black triangle Askja volcano.

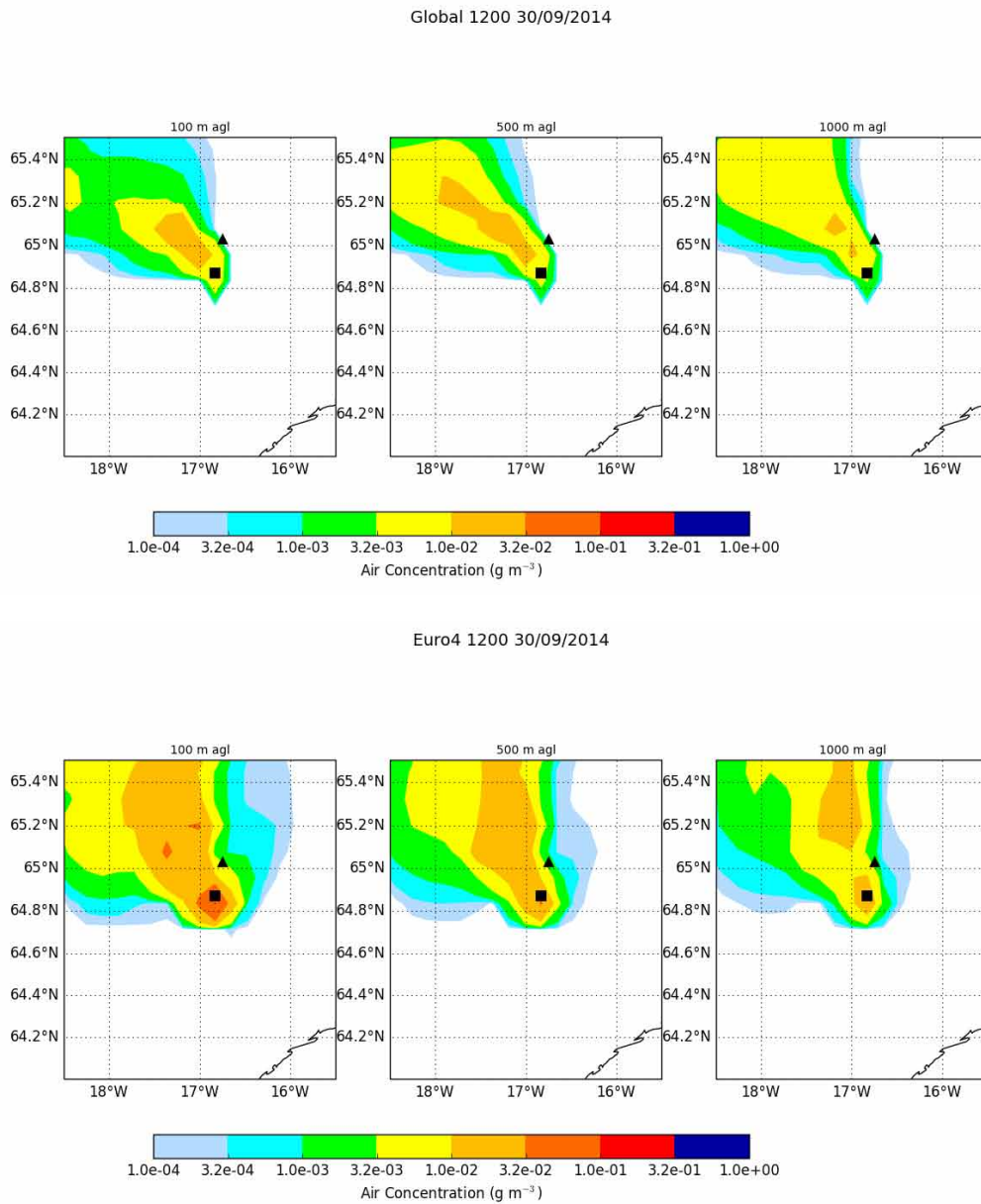
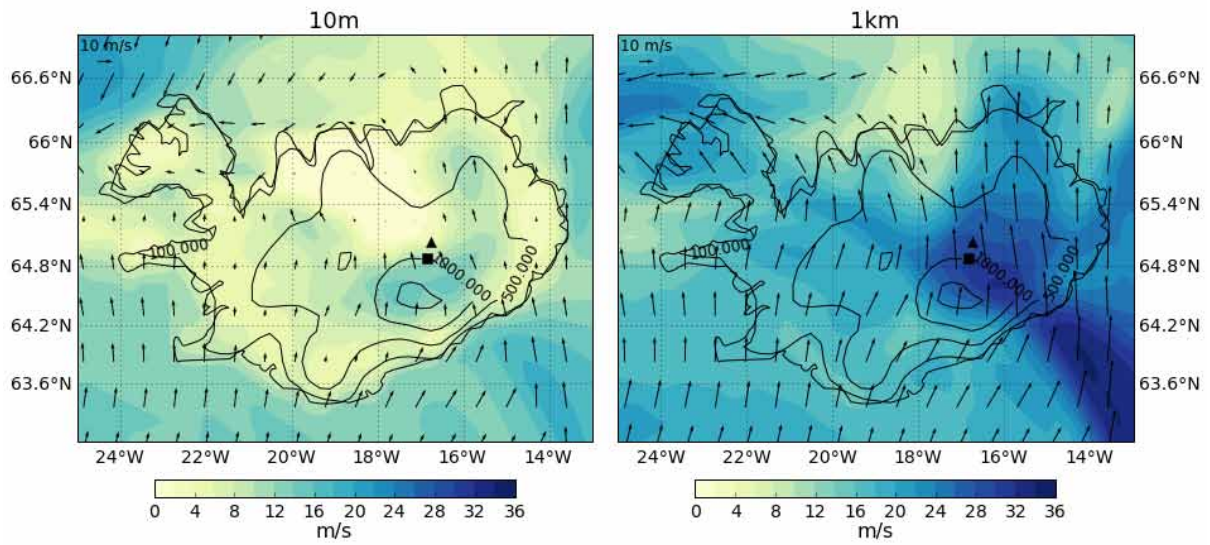


Figure 3.10. NAME forecast 1-hour averaged relative air concentrations over 0-100 m agl, 0-500 m agl and 0-1000 m agl for the Holuhraun gas plume at 12:00 UTC on the 30th September 2014 using the Global and Euro4 model configuration analysis meteorological data. Holuhraun is indicated by the black square, the triangle indicates the location of Askja.

Global Model horizontal wind speeds and vectors on 30 September 2014 12:00 UTC



Euro4 horizontal wind speeds and vectors on 30 September 2014 12:00 UTC

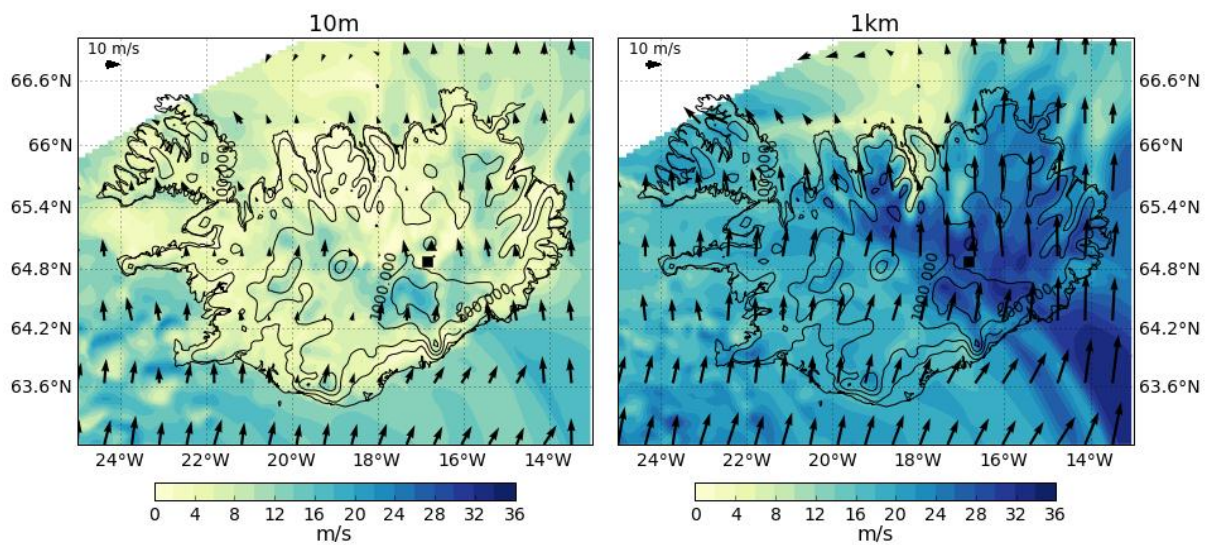


Figure 3.11. To show forecast horizontal wind speeds and wind vectors at 12:00 UTC on the 30th September 2014 using the Global and Euro4 model configurations over Iceland. The topography represented in the models is indicated by the contour lines. The black square indicates the location of the Holuhraun fissure eruption and the black triangle Askja volcano

3.4 Discussion and Conclusions

The accurate representation of topography in NWP models is important for predicting local-scale meteorological features close to the surface, especially in areas of complex terrain. As a result dispersion model forecasts of the transport of pollutants at low levels in the atmosphere are sensitive to the topographical dataset used.

The higher resolution topography used in the UM's Euro4 model configuration, compared to the Global model configuration, has a clear impact on the forecast wind speeds and directions over Iceland. The Euro4 is capable of representing more complex wind features around the **Barðarbunga** and Askja volcanic complexes and through the intervening valley in which the Holuhraun fissure eruption occurred in 2014. Euro4 wind speeds are seen to clearly vary with topography over the Vatnajökull glacier: the fastest speeds are over the top of the ice cap at all the levels considered. The influence of Askja on wind flow in the Euro4 can also be identified; there is clear flow diversion around the volcano and funneling between the edge of the glacier and the higher ground around Askja. In two of the case-studies examined here the Euro4 predicted significantly lower wind speeds over the Holuhraun eruption site, compared to the Global. As a result the NAME forecasts using the Euro4 predict higher air concentrations of gas over Holuhraun and a plume which initially travels both to the south as well as the north near the vent. In contrast using the Global met data the gas is more rapidly dispersed and the plume follows a simpler trajectory away from the eruption site. To validate the Euro4 forecast wind vectors we would need to compare the model output to surface observations. However, unfortunately there are currently no meteorological stations between the **Barðarbunga** and Askja volcanoes.

Here we have focused on the influence of orography in Iceland on the forecast winds. However, higher resolution LAMs such as the Euro4, also better represent processes influenced by the underlying surface such as the land-sea mask, surface roughness, surface heat flux and vegetation. These processes can also affect local wind features as well as the boundary layer.

It is clear that the choice of meteorological data to use with a dispersion model to forecast the transport of pollutants from volcanic eruptions depends on the type of eruption and where the plume resides in the atmosphere. In Section 2 we showed that to model the long-range transport of volcanic ash clouds at upper levels in the atmosphere the best meteorological data to use from the UM is produced by the Global model, as it is the most capable configuration at predicting upper-air winds. Here we have shown that the higher resolution Euro4 model configuration is more capable of representing more detailed wind features over complex terrain. This is because the Euro4 uses a higher resolution topography dataset. When predicting near-surface concentrations of pollutants the Euro4 is therefore more appropriate.

During the Holuhraun eruption scientists travelled to the lava field and made regular flights over the area to make measurements of the gas plume and lava flows and monitor changes in the eruption. Forecasts of the dispersion of the gas cloud were used to plan field-work and ensure scientists would not be exposed to dangerous levels of gases being released. Understanding the impact of the resolution of the topographical and meteorological data used with the dispersion model is therefore important for the safety of scientists carrying out fieldwork in the area, as well as being able to accurately predict gas concentrations downwind of the eruption site.

4. The sensitivity of dispersion model forecasts to the physical characteristics of the particles

Authors: F.M. Beckett, C.S. Witham, M.C. Hort, J.A. Stevenson, C. Bonadonna and S.C. Millington.

4.1 Introduction

Initialising a dispersion model to forecast the transport of a volcanic ash cloud requires the user to input several source parameters, typically: the source location, the mass eruption rate (MER), the plume height, the particle size distribution (PSD), the particle density and the particle shape. To assess the uncertainty on the forecasts produced we need to understand their sensitivity to the source parameters used.

Measuring the characteristics of ash particles in an ash cloud in near-real time is challenging. Therefore the London VAAC has a set of default particle characteristics which are used in the absence of further information. Particles are assumed to be spherical with a fixed density of 2300 kg m^{-3} and the PSD applied is based on Hobbs et al. (1991), see Witham et al. (2014) for a discussion on the London VAAC operational set-up. Here we examine the sensitivity of dispersion model forecasts of volcanic ash clouds to the physical characteristics assigned to the model particles.

This work has been published as a Met Office Weather Science Technical Report (Beckett et al., 2014) and submitted to JGR: Atmospheres where it is currently under review. Readers are directed to Beckett et al. (2014) for a detailed account of the study and results; here we highlight the key findings.

4.2 Key Findings

Figure 4.1a shows forecast total column mass loadings for the eruption of Eyjafjallajökull in 2010 on the 17th May at 16:00 UTC, where the source parameters are those applied by the London VAAC. In figures 4.1b-4.1d one of the source parameters is then varied. In all of the model runs **we only consider particles with diameter $\leq 125 \mu\text{m}$** and the MER applied is 5% of the total mass calculated using the Mastin relationship (Mastin et al., 2009). The difference between the forecast using the modified source parameters and the forecast produced using the operational source parameters is quantified using the following statistical measures: Pearson's Correlation Coefficient (PCC), Fractional Bias (FB), Figure of Merit in Space (FMS) and Kolmogorov-Smirnov parameter (KSP), see Appendix D for a description of each of the statistical techniques applied.

Figures 4.1b and 4.1c show the forecasts when the density distribution and the minimum sphericity attributed to the Eyjafjallajökull 2010 ash particles given by Bonadonna et al. (2011), are applied. The total grain size distribution (TGSD) attributed to the Eyjafjallajökull 2010 ash (Bonadonna et al., 2011), considered as the PSD of all the ejected particles (Mastin et al., 2009), is used in Figure 4.1d. Using the density distribution and minimum sphericity of the Eyjafjallajökull 2010 ash particles there is very little variation from the forecast of ash dispersion across Europe produced using the operational source parameters: Pearson's Correlation Coefficients (PCC) close to 1, a Fractional Bias (FB) close to zero, and a low value of the Kolmogorov-Smirnov parameter (KSP) (Table 4.1). Varying the input PSD in NAME has the most significant impact on the forecast. Using the TGSD for Eyjafjallajökull 2010 ash, considering particles up to $125 \mu\text{m}$ only, total column mass loadings are reduced compared to the forecast produced

Table 4.1. The Pearson Correlation, Fractional Bias, Figure of Merit in Space and Kolmogorov-Smirnov Parameter for NAME simulations of total column mass loading, where the input particle characteristics are varied, see Appendix D for a description of the statistical parameters used.

Operational Vs.	Pearson's Correlation Coefficient	Fraction Bias	Figure of Merit in Space	Kolmogorov-Smirnov Parameter
Minimum Sphericity	0.997	0.11	98.42	0
Density Distribution	0.999	-0.029	98.37	1
Deposit + MSG-SEVIRI PSD	0.971	-0.56	98.19	3
2% MER	1.0	-0.86	100	2

using the London VAAC operational PSD. This is because the PSD has a higher mass fraction of larger particles which fall out of the atmosphere quicker. This results in a lower Pearson's Correlation Coefficient (PCC = 0.9712), larger Fractional Bias (FB = -0.56) and the lowest value of Figure of Merit in Space (FMS = 98.19).

Dacre et al. (2013) compared NAME simulations of the 2010 Eyjafjallajökull ash cloud to the calculated total column mass loadings from measured ash concentration profiles by the FAAM research aircraft, and suggested that 2–6 % of the total emitted mass was transported by particles with diameter < 30 μm . In the London VAAC PSD 96% of the **total mass is represented by particles with diameter $\leq 30 \mu\text{m}$** . In Figure 4.1e we apply the minimum MER of 2% to the 0.1–100 μm particle size range. With respect to the simulated ash cloud using the London VAAC PSD and a 5% MER there is a perfect positive correlation (PCC = 1) and Figure of Merit in Space value (FMS = 100), as there is no spatial difference in the plumes only a change in magnitude. There is though a large Fractional Bias (FB = -0.86) when compared to the operational output due to the lower total column mass loadings.

Beckett et al. (2014) conclude that the PSD used to initialise a dispersion model has a significant impact on the forecasts. Devenish et al. (2012a) and Dacre et al. (2013) showed that model forecasts were particularly sensitive to the input MER; this study has shown that the input PSD used has a similar order impact on the forecasts. Using the TGSD for Eyjafjallajökull ash rather than the London VAAC default PSD, the impact on the forecasts of total column mass loadings is equivalent to varying the MER within its range of uncertainty

The density and shape assigned to the model particles have a lesser, although still significant, impact on the forecasts. Accounting for the density distribution and sphericity of ash from the eruption of Eyjafjallajökull in 2010, modelled particles travel up to 84% further than particles with the default particle characteristics assigned by the London VAAC. Knowledge of the density and shape of the particles is therefore also important in order to produce an accurate forecast.

In Section 7 we assess which measurement techniques developed through the FUTUREVOLC project could provide observations of volcanic ash clouds which could be used to constrain the source parameters used in dispersion models.

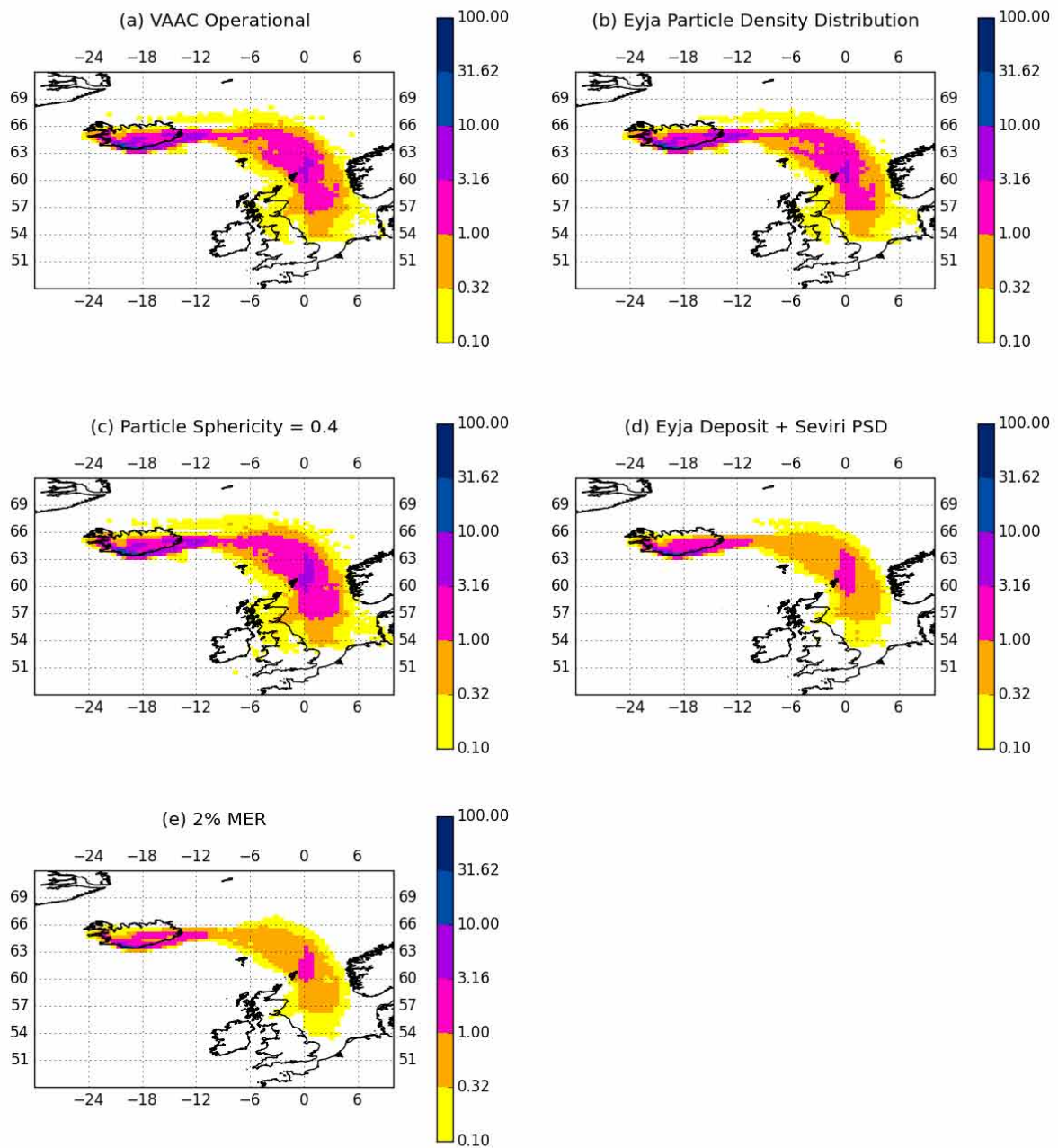


Figure 4.1. NAME simulated total column mass loadings (g m^{-2}) of the Eyjafjallajökull volcanic ash cloud on the 17th May 2010 at 16:00 UTC. The input operational source parameters used by the London VAAC (a) are compared to simulations where the source parameters are varied (b-e), see the main text for a discussion on input source parameters used. The mass eruption rate applied is 5% of the total mass calculated using the Mastin relationship (Mastin et al. 2009), except in (e) where 2% of the total mass calculated using the Mastin relationship is considered.

5. Using buoyant plume models to estimate mass eruption rates for dispersion modelling

Author: B.J. Devenish

5.1 Introduction

Quantitative forecasts of the mass loading of ash particles in the atmosphere using dispersion models are particularly sensitive to the Mass Eruption Rate (MER) used to initialise the model, see Figure 4.1 and Webster et al. (2012), Devenish et al. (2012a) and Dacre et al. (2013). One-dimensional volcanic plume-rise models offer a computationally efficient method of inferring the source mass flux from the plume rise height. Unlike empirical relationships such as those of Mastin et al. (2009) or Sparks et al. (1997), these models take into account the effect of the prevailing meteorology on the rise height of the eruption column. However, because of the difficulty in obtaining independent estimates of the source mass flux, it is difficult to assess the validity of the resulting estimates of the mass flux. A more tractable option is to compare the total emitted mass as this can be obtained from proximal deposits and remote sensing. This is done here for the eruption of Eyjafjallajökull in 2010.

The results from this project are to be presented in a special edition of the Journal of Volcanology and Geothermal Research, here we present the main findings from this study.

The duration and impact of the eruption of Eyjafjallajökull in 2010 made it one of the best observed eruptions. As a result, estimates of the total mass emitted have been possible using a mixture of ground surveys and remote sensing. In particular, Gudmundsson et al. (2012) estimated the total mass emitted to be $3.84 \pm 0.96 \times 10^{11}$ kg (excluding the mass emitted in the form of lava) using a combination of remote sensing and ground surveys and Stohl et al. (2011) used satellite column loads and an inversion model to estimate the mass contained in the fine particle fraction (2.8-28 μm diameter) that survives into the far field to be $8.3 \pm 4.2 \times 10^9$ kg. Taking these two values together gives an estimate of the distal fine ash fraction (i.e. the fraction of mass that survives into the far field) of 2%. There is, however, a lot of uncertainty regarding the distal fine ash fraction with estimates ranging from 0.1-10% (Rose et al., 2000; Dacre et al., 2011; Devenish et al., 2012a; Devenish et al., 2012b; Webster et al., 2012); this dominates any error in the estimate of the total mass from the fine particle fraction.

The volcanic plume-rise model of Devenish (2013), which includes the effects of ambient wind and moisture, was applied iteratively to a short period of the Eyjafjallajökull eruption in mid-May 2010 using realistic atmospheric profiles appropriate to the time of the eruption in order to estimate the source mass flux for a given rise height. It was shown that accounting for the prevailing meteorology can lead to significant differences in estimates of the source mass flux compared with empirical relationships between the rise height of the eruption column and the source mass flux (Mastin et al., 2009; Sparks et al., 1997). For example, if the volcanic plume is strongly bent over by the ambient wind then using one of the empirical relationships quoted above is likely to lead to an underestimate of the source mass flux. Conversely, moisture can add significantly to the energy of a volcanic plume via latent heating and so can potentially lead to an overestimate of the source mass flux. Furthermore, since the stability of the troposphere is less than that of the stratosphere, an empirical relationship of the form proposed by Mastin et al. (2009) or Sparks et al. (1997) is also likely to overestimate the source mass flux (all else being equal). Similar results were also obtained for the eruption of Eyjafjallajökull in 2010 by e.g. Woodhouse et al. (2013) and Mastin (2014).

In the next section the mass flux is calculated using the plume-rise model of Devenish (2013) for the duration of the 39-day eruption of Eyjafjallajökull in 2010. This allows the total mass emitted to be calculated which is compared with an observational estimate.

5.2 Calculation of mass emitted by Eyjafjallajökull in 2010

An initial estimate of the source mass flux is calculated from the empirical relationship between the observed rise height (above the volcano summit), z_{obs} , and the source mass flux, Q_m , proposed by Mastin et al. (2009):

$$Q_m = 141 z_{obs}^{4.15} \quad (5.1)$$

where z_{obs} is measured in km and Q_m in kg s^{-1} . The plume-rise model is applied iteratively to determine a revised source mass flux for a given rise height that accounts for the prevailing atmospheric conditions. The observed rise height appropriate to the time of interest is kept fixed and a bisection method is used to refine the value of Q_m .

An improved version of the volcanic plume-rise model of Devenish (2013) has been coupled to the Met Office's operational dispersion model NAME (Numerical Atmospheric-dispersion Modelling Environment, version 6.5, see e.g. Jones et al. (2007)) to facilitate frequent updates of the prevailing meteorology which are provided by the Met Office's numerical weather prediction model, the Unified Model (UM). The global configuration of the UM is used which at the time of the eruption had a horizontal grid spacing of about 25 km in the mid-latitudes and 70 unequally spaced vertical levels extending into the mesosphere with a typical resolution of 300-400 m in the mid-troposphere. The ambient meteorology is updated at three hourly intervals and interpolation in time and space gives appropriate profiles for Eyjafjallajökull at the time of interest. In this study, the eruption was considered to have started at 09:00 on 14th April 2010 and to have finished at 18:00 on 23rd May. The rise height of the eruption column was determined by the Icelandic Meteorological Office using a combination of methods of which radar was the most important (Arason et al., 2011); a piece-wise constant fit of their data is used here (see Fig. 3 of Webster et al., 2012). Using the same parameter values as used by Devenish (2013) (i.e. an initial temperature of 1273 K, exit velocity of 100 m s^{-1} , initial gas fraction of 3%) and neglecting any source moisture, the source mass flux was calculated at six hourly intervals. It is shown in Figure 5.1 along with the empirical formula of Mastin et al. (2009). Distinct periods of relatively vigorous volcanic activity can be identified of which the most important are the initial period, during which the largest values of Q_m occurred, and further periods in early and mid-May. As may be expected, this is consistent with the analysis of Arason et al., (2011) and Gudmundsson et al. (2012) who divide the duration of the eruption into two distinct phases, 14-18 April and 5-17 May.

Figure 5.2 shows that Q_m estimated using a plume-rise model is usually larger - sometimes more than ten times as large - than that calculated from Mastin's empirical formula using the rise height alone but can also be smaller. Of course, greater variability in Q_m (original) could also have been achieved using Equation 5.1 and a more frequently varying time series of the rise height. While it is difficult to make an a priori assessment of the magnitude of this additional variability, it is worth noting that the time-series proposed by Webster et al. (2012) and used here averages out (in some sense) many of the small fluctuations in the rise height over longer time periods than the six hourly averaged time-series in Figure 7 of Arason et al. (2011). Thus, in some cases, from 18-25 April for example where the time series of Webster et al. (2012) shows a generally higher rise height than the time series of Arason et al. (2011), one might have expected a lower mass emission rate on average interspersed with pulses of higher emission rates simply from using Equation 5.1 and the time series of Arason et al. (2011). However,

fluctuations in the observed rise height are themselves partly driven by changes in the prevailing meteorology (one could observe a fluctuating time series of rise heights for a steady state volcano) as well as changes inherent to the volcano. Disentangling these two sources of variability is clearly very difficult but in some sense the application of a volcanic plume-rise model to determining the source mass flux (as used here and elsewhere) should reveal the inherent variability of the volcano because cases in which the prevailing meteorology is close to the climatology (at least as appropriate to the data from which Equation 5.1 is constructed) will give a value of Q_m (revised)/ Q_m (original) close to unity (ignoring any errors in Equation 5.1).

Figure 5.3 shows the cumulative mass for the 39-day eruption. It shows that approximately half of the material was emitted in the early part of the eruption with significant increases in early and mid-May as may be expected given the increased volcanic activity in these periods. Both estimates of the total mass, using either Equation 5.1 or the value of Q_m obtained from the plume-rise model, lie within the error bounds of the observed mass as estimated by Gudmundsson et al. (2012).

5.3 Conclusions

As has been shown previously (e.g. Devenish, 2013, Woodhouse et al., 2013, Mastin, 2014), the iterative application of a one-dimensional volcanic plume-rise model to estimate the source mass flux can lead to significant differences with that predicted by the simple power-law relationship with rise height as given by Equation 5.1. Furthermore, it was shown that when the source mass flux was integrated over the duration of the 39-day eruption of Eyjafjallajökull in 2010, the resulting estimate for the total emitted mass agreed well with the observational estimate of Gudmundsson et al. (2012). However, it was also shown that the total emitted mass obtained from the integration of Q_m as calculated from Equation 5.1 also agreed well with this observational estimate. The question remains as to which approach is better for the operational prediction of volcanic ash concentrations in the atmosphere; this study considers only one eruption and further case studies should help to answer this question. While it is undoubtedly true that the state of the atmosphere can influence the rise height of the eruption column, the model is particularly sensitive to the parameterisation of entrainment. The sensitivity of this and other similar models primarily to entrainment parameters but also to other parameters will be discussed in depth in the special issue of the *Journal of Volcanology and Geothermal Research* devoted to volcanic plume-rise models.

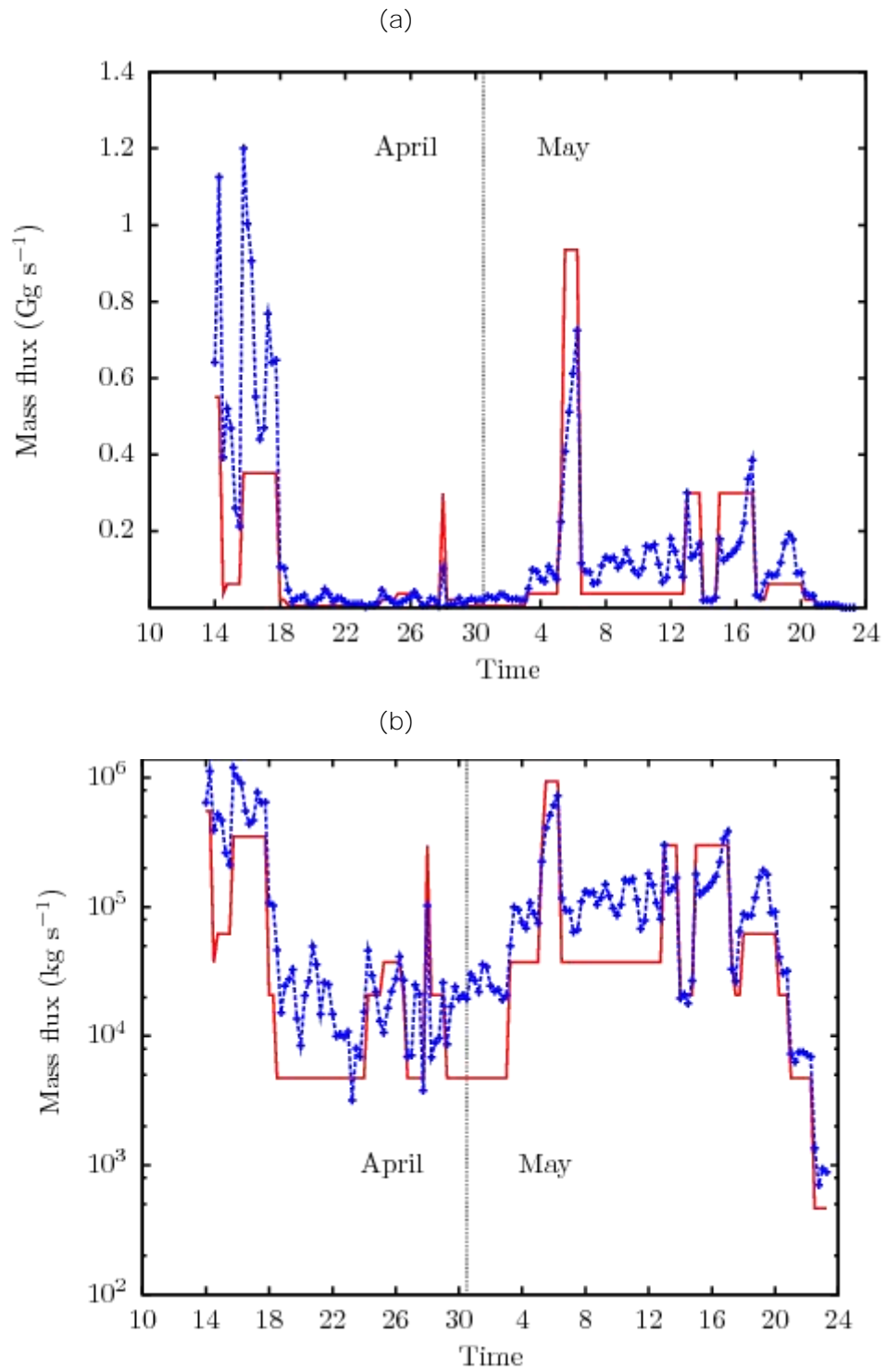


Figure 5.1. Source mass flux estimated from the plume-rise model (blue) and Mastin’s empirical formula (red): (a) linear plot and (b) logarithmic plot. The tick marks show 12:00 on the date shown.

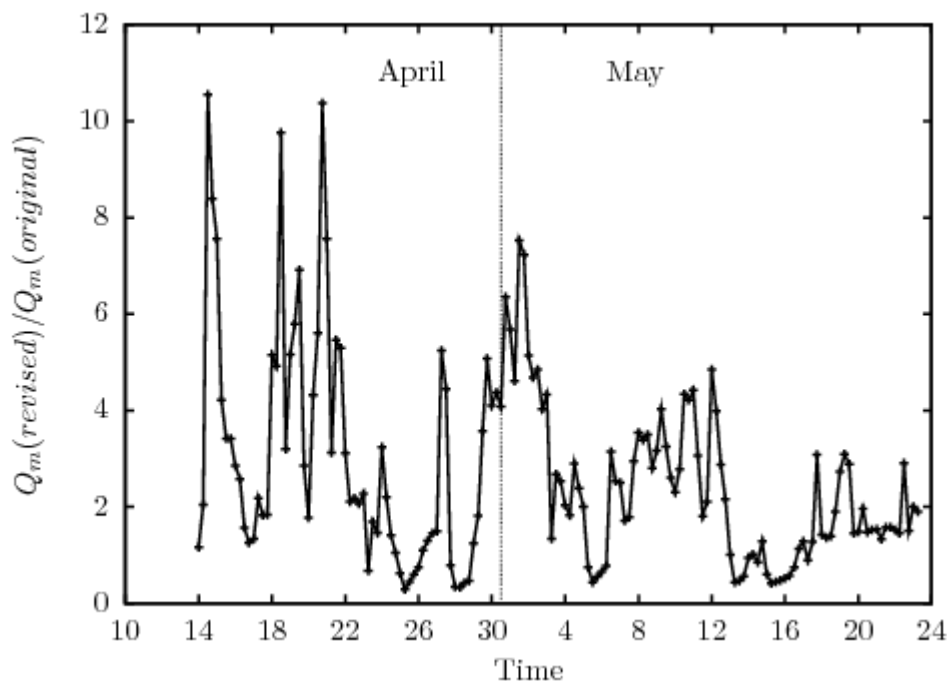


Figure 5.2. The relative increase in the source mass flux estimated from the plume-rise model (Q_m (revised)) compared with Mastin’s empirical formula (Q_m (original)). The tick marks show 12:00 on the date shown.

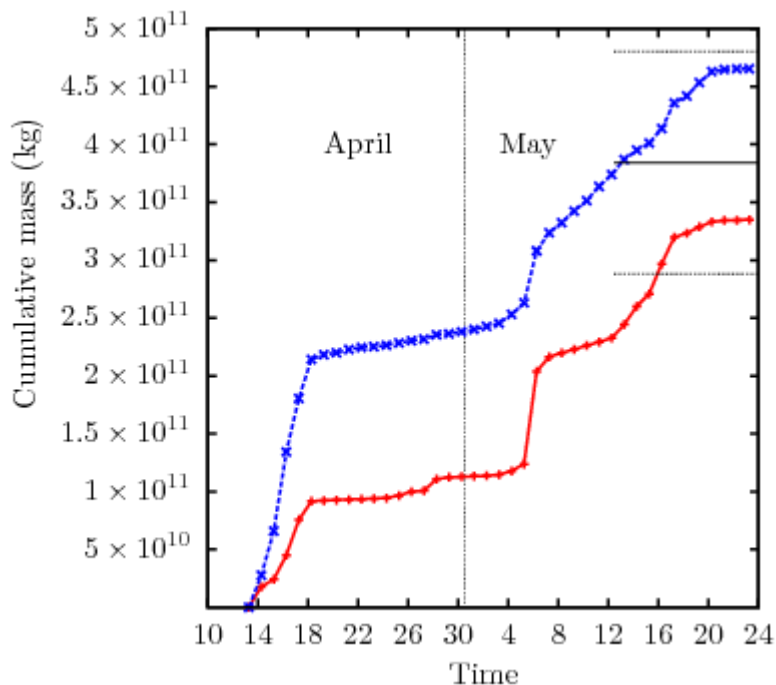


Figure 5.3. The estimated cumulative mass for the eruption Eyjafjallajökull in 2010: Mastin’s empirical formula (red); the plume-rise estimate (blue). The solid horizontal line represents the observed total emitted mass as estimated by Gudmundsson et al. (2012) with the dotted lines indicating the error in this estimate. The tick marks show 12:00 on the date shown.

6. Assessment of the impact of radar height data on model forecasts for Grímsvötn 2011

Author: C.S. Witham

6.1 Introduction

For many years C-band radar has been a key technology for determining the height of eruption columns in Iceland. More recently, X-band radar techniques have been under development with the aim of providing more quantitative data about the eruption column structure, particle size distribution and mass flux. However, the Grímsvötn 2011 eruption **demonstrates that limitations exist with the “traditional” C and X-band height detection data** which need to be better understood. Knowledge of the source and magnitude of potential errors is important because these data are being used to initialise atmospheric dispersion models of volcanic ash transport at Volcanic Ash Advisory Centres (VAAC) and elsewhere, and for plume-rise models as discussed in Section 5.

During the Eyjafjallajökull April-May 2010 and Grímsvötn May 2011 eruptions the **Icelandic Met Office’s C-band radar** situated at Keflavik airport provided key data on the evolution of the eruption column height. During an eruption a radar scan is conducted every 5 minutes. Within each scan the radar beam is increased in altitude (by increasing the elevation angle) following every full rotation. At the distance of Grímsvötn the altitude of the lowest beam is 6.2 km asl and there are only 6 scan angles between the surface and 25 km asl. This limits the vertical resolution of the data, particularly at the upper altitudes where the beams do not overlap. Even with this vertical resolution limitation, the C-band radar was the main source of information on the vertical extent of the erupted ash column in both eruptions. Full details on the radar and the resulting datasets are provided in Arason et al. (2011) and Petersen et al. (2012).

Atmospheric dispersion models are an important tool in forecasting the future location of an ash plume. Key inputs to any such model include the vertical and horizontal location of the ash at a known time and a mass eruption rate. At its simplest level, a unit mass flux can be used in order to determine potential future plume location. This provides limited information on actual ash concentrations or vertical column mass loadings, so a time-varying mass flux emission estimate is preferable. Knowing the height of plume at the vent is therefore critical for two reasons: (1) to ensure ash is emitted at the correct altitudes in the model and (2) empirical (e.g. Mastin et al, 2009) and buoyant plume rise techniques (for example as described in Section 5) for calculating the mass flux require an estimate of the plume height to determine the mass eruption rate. During both eruptions, the height information determined from the C-band radar data, in combination with data from other sources, was communicated to the London VAAC by the Icelandic Met Office to enable forecasts of the ash plume location to be made.

In May 2011 the Icelandic Met Office also had at its disposal a mobile X-band radar. Following the start of the eruption of Grímsvötn on the evening of the 21 March, the X-band was rapidly moved close to the volcano and provided complementary data for most of the eruption (Petersen et al., 2012). Figure 6.1 compares the height information from the two radars to the combined 30-minute mean height from both sensors. Overlaid is the height profile that was used in May 2011 by the London VAAC based on advice from the Icelandic Met Office. Hreinsdottir et al. (2014) provide additional height profiles that utilise data from photographs and GPS. The shapes of their profiles, particularly on the 22 and 23 May, are very similar to the radar 30-min mean. All these data show that the Grímsvötn eruption column reached heights of at least 20 km above sea level in the initial 12 hours of the eruption.

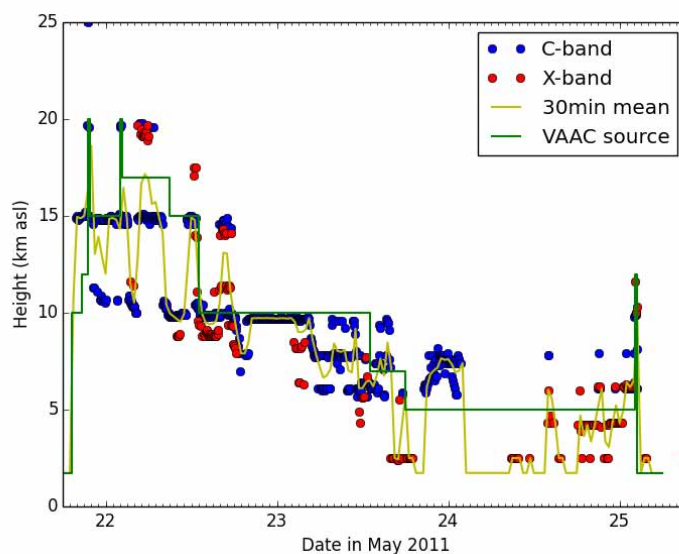


Figure 6.1. Grímsvötn plume height time-series from the C-band and X-band radar, the 30 minute mean of the two radar series, and the sequence reported to and used by the London VAAC. The vent height is at 1.725 km asl. Radar data are from Petersen et al. (2012).

6.2 Analysis

During the eruption, the height profile in Figure 6.1 was used by the London VAAC to calculate a mass eruption rate using the Mastin et al. (2009) relationship following the procedure outlined in Witham et al. (2012). Model simulations that use this VAAC source as an input to the NAME atmospheric dispersion model (Jones et al., 2007) produce a plume that matches the location of volcanic material observed in satellite retrievals (Figure 6.2). Two parts of the plume are visible in satellite images, one to the north of Iceland and one to the south. Radiosonde data from Keflavik airport shows that significant wind shear with altitude occurred over Iceland on the 22-23 May (Figure 6.3). This meant that material emitted at the top of the eruption column was transported to the north and northwest of Iceland, whilst material emitted lower down (<5.5 km) was transported to the south of Iceland. The presence of this wind shear and the good match between the modelled and observed plumes suggests that erupted material did indeed reach the heights observed by the radar.

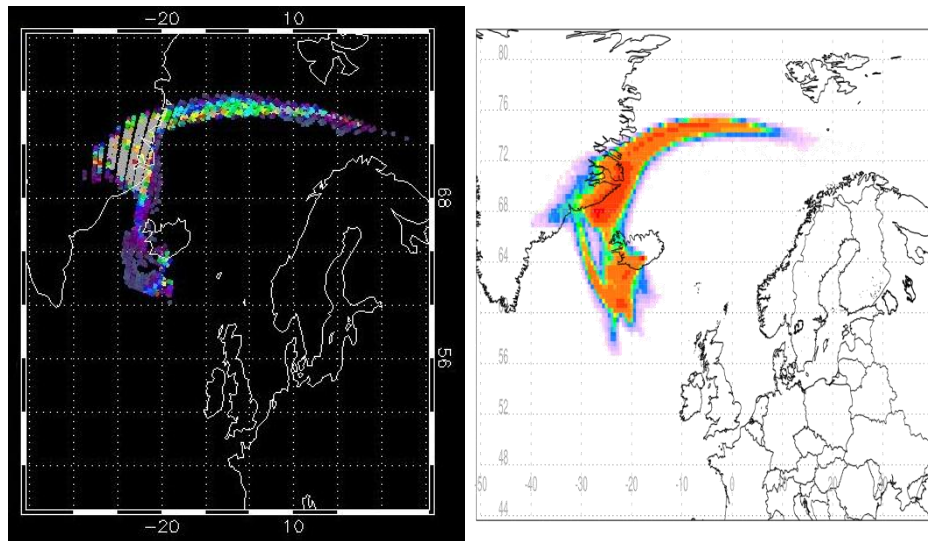


Figure 6.2. (a) Satellite observations of the volcanic plume from the IASI morning pass on 23 May at approx 10Z (provided by Elisa Carboni, University of Oxford). (b) Total column mass loading for 10Z from the NAME model simulation assuming a linear release from the vent to the maximum plume height, with time-varying mass flux calculated using the Mastin relationship (Mastin et al., 2009).

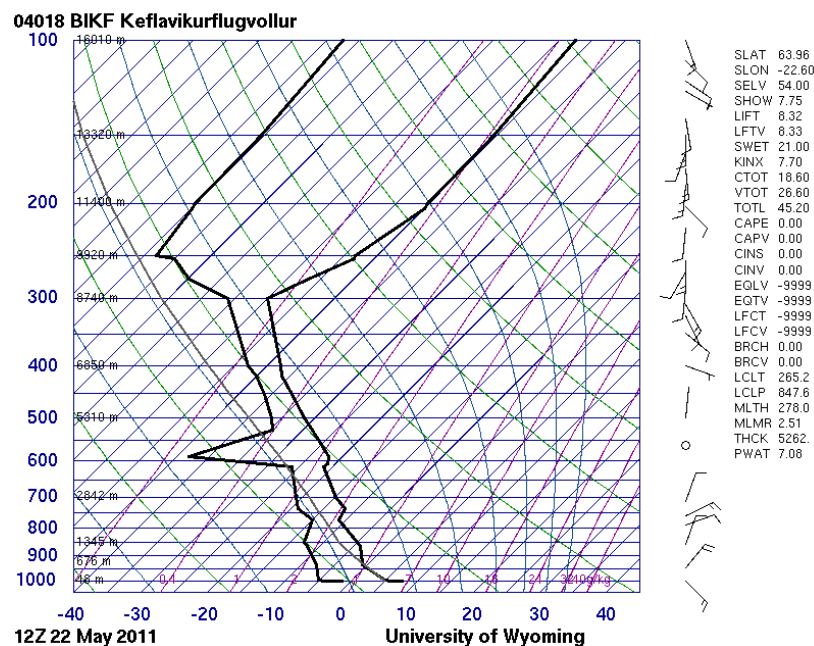


Figure 6.3. Skew-T plot of radiosonde data from Keflavik airport, Iceland from the 12Z sounding on 22 May 2011. The wind vectors to the right of the main graph show the change in wind direction with height. (Image from University of Wyoming Department of Atmospheric Science).

However, the satellite data also show a clear separation in the type of emissions, with the plume to the south composed predominantly of volcanic ash and the plume to the north predominantly sulphur dioxide (Figure 6.4 and Cooke et al., 2014). This lack of satellite evidence for volcanic ash to the north suggests that the bulk of the ash mass was not emitted at heights >10 km asl. Indeed, Cooke et al. (2014) and Stevenson et al. (2013) have demonstrated using forward model trajectories that the bulk of the ash must have been emitted between below 4-5 km asl and Moxnes et al. (2014) have derived an *a posteriori* source term in which the majority of ash emissions were below 4 km asl. Some ash must have been emitted at other heights, as seen in satellite data and suggested by inversion modelling approaches (Moxnes et al., 2014; Pelley et al., 2014), but the data reveal that sulphur dioxide was the main component emitted at the top of the eruption column. This demonstrates that the VAAC source profile used at the time is not appropriate for modelling just the ash-rich plume.

The eruption height and the mass eruption rate are major sources of uncertainty when initialising dispersion models. Simplification of the eruption height information for the VAAC source introduces discrepancies between the raw radar data and the VAAC source profile (Figure 6.1), which may contribute to the transport errors observed. However, sensitivity tests initialising the model with the raw and mean radar data height profiles do not result in very different distributions of the ash plume to the VAAC source (Figure 6.5), with all height profiles resulting in significant ash plumes to the north of Iceland. Sensitivity to the erupted mass flux has also been tested, but whilst this alters the mass column loading and concentration it does not alter the location of the plume. If a conceptual view of the vertical distribution of material in an eruption column is applied - with the bulk of the ash mass emitted in the top 25% of the height range - then the ash cloud is almost entirely transported to the north and the match to the satellite data is worsened. Use of such a vertical distribution in the operational VAAC modelling, as has been suggested by some workers, would have meant that the initial model simulations would not have forecast any of the ash to the south of Iceland. This is important as it is this part of the plume which subsequently travelled towards the UK and Europe and resulted in airspace restrictions.

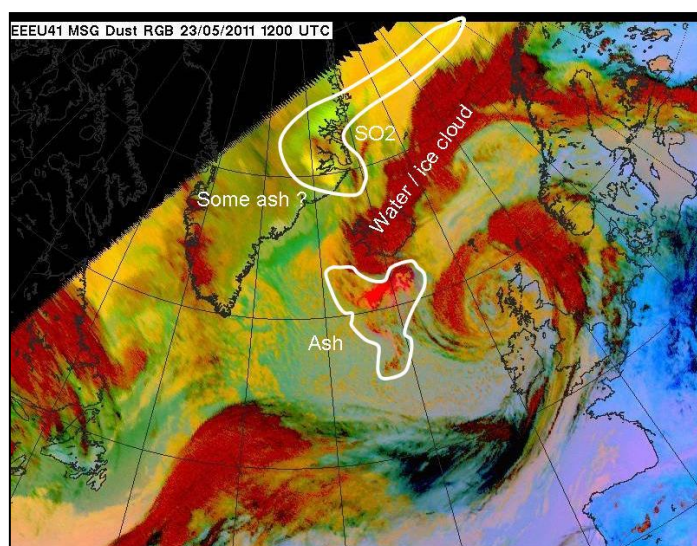


Figure 6.4. Annotated SEVIRI dust RGB image from 12Z on 23 May 2011 demonstrating the separation of ash and SO₂.

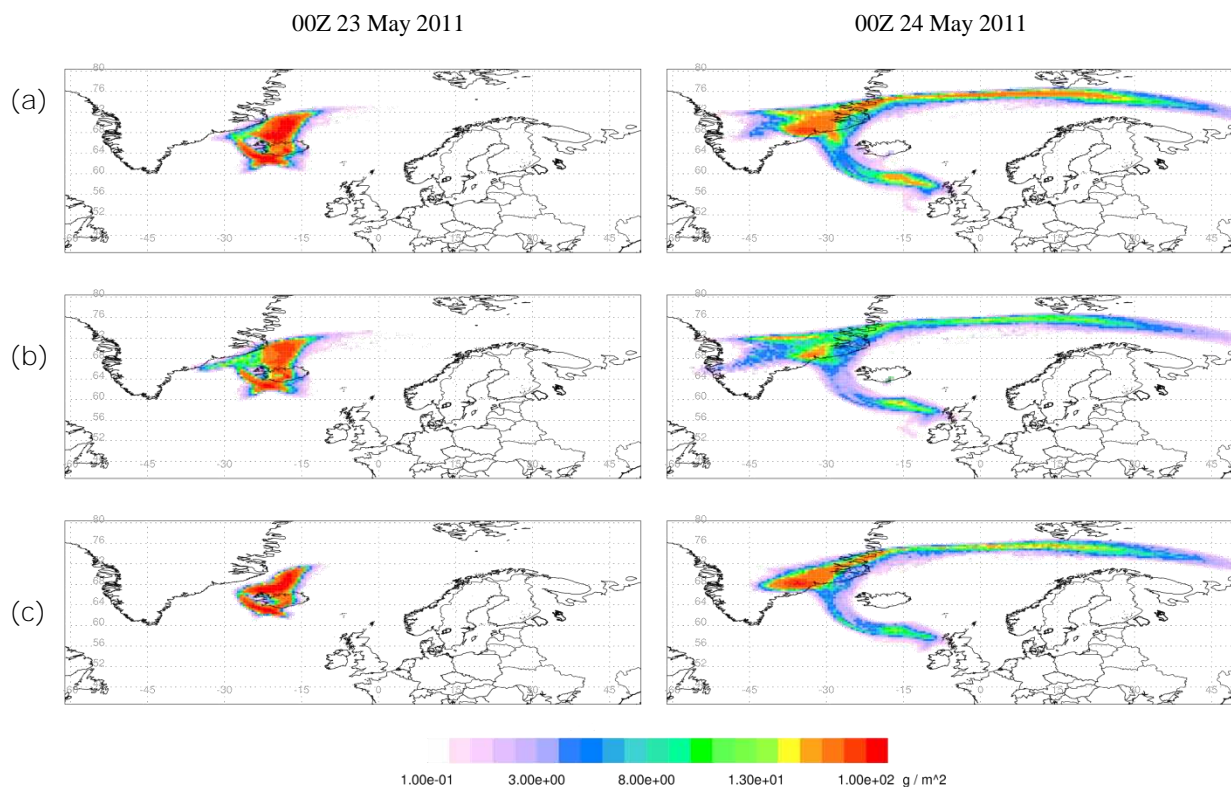


Figure 6.5. Comparison of simulated plumes at 00Z 23 May 2011 (left) and 00Z 24 May 2011 (right) using heights and mass derived from the different eruption height sequences shown in Figure 6.1: (a) the VAAC sequence, (b) the Keflavik radar sequence, (c) the mobile X-band radar sequence. The plots show 1-hour mean total column mass loading. The NAME simulation assumes a linear release from the vent to the maximum plume height, with time-varying mass flux calculated using the Mastin relationship (Mastin et al., 2009). Five percent of this mass is simulated to represent the fine ash fraction (Witham et al., 2012).

The implication is that the radar column-height data do not represent the main ash emission height for the Grímsvötn eruption. Pictures taken at the time, but which **weren't communicated to the VAAC, show apparent column collapse and the presence of an ash-rich layer much lower than the top of the eruption column** (Figure 6.6). Understanding why the ash emission occurred so much lower in the atmosphere is essential and the role of glacial melt-water in the plume formation must be considered. Buoyant plume modelling has demonstrated that a moisture rich and ash-poor plume could reach the heights observed (Mark Woodhouse, WP7, pers. comm.), but current models do not account for column collapse in the form observed.



Figure 6.6. Picture of the Grímsvötn eruption column on the 21 May, showing a low-level ash-rich plume being transported to the right of the column, which is distinctly separate from the upper level plume. Photographer: Thórdís Högnadóttir.

6.3 Conclusions

The 2011 Grímsvötn eruption shows that radar detection data of the plume top height cannot be used to conclusively determine the ash emission height. Key findings of the analysis are that:

- Emission source profiles derived from the individual and time-mean radar height data for Grímsvötn lead to most of the ash being erroneously transported to the north in model simulations.
- A top-weighted vertical emission distribution results in a considerably worse match to the satellite evidence and fails to forecast the transport of the most significant ash plume to the south.
- Column heights derived from radar data cannot be relied on for accurate height information on ash emission for use in dispersion models.

From a London VAAC perspective this presents a significant conundrum, as the previous main source of information on the height of the volcanic eruption column can no longer be relied upon to define the height of ash emission. Additional sources of information are needed. New developments under FUTUREVOLC could fulfill this requirement. In particular, the work to develop retrievals of other plume properties from radar data (FUTUREVOLC WP7) could be beneficial in future events for discriminating the location of the bulk of the ash particles from the gas phase. Plume information from visible and IR cameras may also be useful. These aspects are considered further in Section 7, but it should be noted that for the purposes of the VAAC all such data would need to be available in near real time.

7. Assessment of Critical Observations and Measurements for Dispersion Modelling

7.1 Introduction

To initialise a dispersion model to forecast the transport and dispersion of a volcanic ash cloud requires information on several critical source parameters: the location of the vent, the start and end time of the eruption, the plume height, the Mass Eruption Rate (MER), the Particle Size Distribution (PSD), the particle density and the particle shape. Forecasts are particularly sensitive to the plume height, MER (Webster et al., 2012; Devenish et al., 2012a; Dacre et al. 2013) and PSD used to initialise the model, while the particle density and particle shape assigned have lesser but still significant impacts (Beckett et al. 2014 and Section 4 above).

The FUTUREVOLC project has included the development and deployment of a range of field-based measurement techniques for monitoring and observing ash clouds in Iceland. Table 7.1 lists all the instruments which can provide data on the source parameters required to initiate dispersion models. We now assess the usefulness of each of the different measurement techniques; it is important to understand the limitations and uncertainties associated with the observations if they are to be used as source parameters in dispersion models, in order to correctly interpret the forecasts produced, and data must be provided in near-real time. It should be noted that many of the instruments deployed are already or could be used at many volcanoes across the world and the following discussion applies to any scenario where observational data are being used to initialise atmospheric dispersion models.

Table 7.1. Field instruments for observing volcanic ash clouds developed through the FUTUREVOLC project that could provide information on the source parameters required to initialise dispersion models.

Work Package	Group	Instrument	Potential Output Parameters
7	iTEM ¹ University of Geneva	Tephra Sampler	Particle Fall Velocity Particle Diameter MER
7	University of Florence	Infrasound	Eruption onset MER
7	University of Iceland	Mobile Lab	Particle Diameter Particle Shape
7	GFZ Helmholtz Centre Potsdam	Cameras (Visible)	Plume Height
7	Icelandic Met Office HIMET ² CETEMPs Universitè L'Aquila	Radar	Plume Height MER
8	Icelandic Met Office	OPCs	Particle Counts Particle Air Concentrations

1. iTEM (Integrated Technologies for Environmental Monitoring) is an SME (micro) enterprise based in Florence, Italy, who work in Earth Sciences and Geophysics
2. HIMET (High Innovation in Meteorology and Environmental Technologies) is a small enterprise which specialises in radar development.

7.2 Field instruments for observing volcanic ash clouds

Tephra Samplers

A Tephra Sampler has been developed by iTEM (Integrated Technologies for Environmental Monitoring, Florence), the University of Geneva and the University of Iceland which measures both the fall speed and diameter of volcanic ash particles. In the event of an eruption in Iceland up to 7 instruments can now be rapidly deployed into the field (Work Package Leaders 30 month Report, May 2015). In Section 4 we showed that identifying the total grain size distribution (TGSD) of the erupted tephra is critical for producing accurate forecasts of the transport of the ash cloud with atmospheric dispersion models. The Tephra Samplers will be invaluable in identifying the particle size of ash being deposited from the ash cloud, from which the TGSD can be determined. The Tephra Samplers are designed to be located close to the source, on land in Iceland, where they will be exposed to the largest particles which quickly fall out of the ash cloud. The Tephra Sampler can detect particles with diameter $> 125 \mu\text{m}$ and is therefore sensitive to a larger size range than the PLUDIX instrument previously employed to determine particle diameter, which could detect particles with diameters between $500 \mu\text{m}$ to a few centimetres (Bonadonna et al. 2011). However, to model the long range transport of volcanic ash clouds the smallest particle size fraction must be accounted for **and the London VAAC currently only considers particles with diameter $\leq 100 \mu\text{m}$.** Partners at the University of Geneva are developing a theoretical approach for determining the TGSD of the ash cloud from the measured PSDs, which will account for the smallest particle size fraction. This analysis will be implemented as part of the Tephra Sampler package and the calculated TGSD will be streamed to IMO, no further analysis will be necessary (Bonadonna, C. and Pioli, L. Pers Comm. 2014). This approach requires that the sampling strategy is effective; that the Tephra Samplers are well distributed under the plume (Bonadonna, C. and Pioli, L. Pers Comm. 2014). Three of the Tephra Samplers also include strain gauges which measure in real-time the weight and the thickness of collected material, from which a MER can be estimated. The calculated MER will be streamed to IMO and no further analysis will be required.

Infrasound

Four infrasound arrays have been installed in Iceland and infrasound data is streamed directly to IMO where it is processed on monitored servers (Work Package Leaders 30 month Report, May 2015). The data are displayed in real time to screens in IMO's monitoring room. Currently this data is used to detect the onset of eruptions. Using a combination of infrasound measurements and thermal camera imagery exit velocities of the plume from the eruption of Eyjafjallajökull in 2010 were constrained, from which MERs were determined using additional information on the vent diameter and mixture density (Ripepe et al., 2013). Although there is no operational procedure currently in place for obtaining quantitative information for estimating the MER from raw infrasound data it is hoped that this could be possible in the event of an ash-cloud forming eruption (Barsotti, S. 2014. Pers Comm.).

Mobile Lab

The Mobile Lab is designed to be deployed rapidly to the field and provide instrumentation in-situ for the measurement of tephra and ash cloud characteristics. The instruments include a particle analyser, a Scanning Electron Microscope (SEM), a mobile X-ray chemical analyser, a FLIR infrared camera, GoPro video cameras, digital cameras, sieves for grain size analysis and an automated Tephra Sampler (Work Package Leaders

30 month Report, May 2015). The instruments available will have the potential to provide information on some of the critical parameters required for dispersion models: the physical properties of the ash particles and plume heights. However, this requires scientists to be able to enter the field safely and, as with the application of the Tephra Samplers, an effective sampling strategy will be essential.

Cameras

Permanent cameras (visible) have been installed at Hekla and an automated stream is in place for sending the raw video images to IMO. In order to obtain estimates of the plume height requires manual plume feature tracking analysis which has a time overhead associated with it (Witt, T. 2014 Pers Comm.). Mobile cameras are also now available which can be deployed rapidly and were successfully tested during the **Barðarbunga** (Holuhraun) eruption (Work Package Leaders 30 month Report, May 2015).

Radar

The IMO has two fixed C-Band weather radars, located at Keflavik International Airport and at Teigsbjarg (East Iceland), and two mobile X-band radars, whose specific purpose is intended for the monitoring of volcanic eruptions, and these now provide full coverage over the whole island (Work Package Leaders 30 month Report, May 2015). Radars have traditionally been used to determine the height of the eruption plume, however limitations associated with the use of radar data have been identified in Section 6 and data should be used with care by VAACs. VARR (Volcanic Ash Radar Retrieval) algorithms have been developed by HIMET and CETEMPS to retrieve the vertical mass distribution profile, which would help constrain the height to which ash is being released into the atmosphere, and the MER of ash from radar images produced from the fixed and mobile radars. Work is in progress to automate this process to ensure that there is a reliable data stream in the event of an ash cloud producing eruption (Barsotti, S. 2014 Pers. Comm.).

OPCs

Two Optical Particle Counters (OPCs) have been set up as part of the FUTUREVOLC project, they are both mobile and can be installed at short notice. Data is collected remotely via a modem and are processed in near real time (Work Package Leaders 30 month Report, May 2015). The results are streamed to the FUTUREVOLC database and presented as total particle counts and particle concentrations as a function of time (Work Package Leaders 30 Report, May 2015). The OPCs are sensitive to airborne particles with diameters from 0.3 μm to 10 μm (Work Package Leaders 30 month Report, May 2015). In deliverable 8.6 we assess the use of OPC data collected at a single location, in Mariubakki in the south of Iceland, for calibrating NAME resuspended ash forecasts. However, comparing dispersed model output with data collected at one or two single point locations is challenging and non-ideal for a model calibration. We show that there is an offset in the peaks between the modelled air concentrations and those calculated from OPC count data, this could be due to not correctly capturing the topography and the micro-meteorology of the area in the model, or due to uncertainty in the source area. **Further, typically particles with diameter $\leq 10 \mu\text{m}$** travel significant distances from the eruption vent (Beckett et al. 2014; Stevenson et al. 2015), and it is unclear how well OPC data will represent ash concentrations near to source. In conclusion OPC data is

unlikely to provide information on ash cloud forming eruptions and will not be able to provide source parameter information for atmospheric dispersion models.

REFIR

In addition to the field-based techniques discussed above a multi-parameter system, REFIR (Real time Eruption source parameters FUTUREVOLC Intelligence and Reconnaissance), which assesses the MER of an eruption given all the possible data sources, including plume rise models, is being developed by partners at the University of Iceland. **This has the potential to provide an informed 'best-guess' of the time-varying MER that could be directly used by dispersion models.** The uncertainty associated with the estimated MER could also be inferred from the range of calculated MERs from all the data sources and would also be valuable for interpreting dispersion model forecasts.

7.3 Summary

The range of field instruments which have been implemented through the FUTUREVOLC project for observing volcanic ash clouds in Iceland have the potential to improve scientists ability to constrain all of the source parameters required to initialise dispersion models: the location of the vent, the timing of the eruption, the plume height, MER and the physical characteristics of the ash particles. Dispersion model forecasts are particularly sensitive to the plume height, MER and PSD used to initialise the model. To use observations of these parameters effectively we need to understand the limitations and uncertainties associated with data retrieved, in order to be able to meaningfully interpret the dispersion forecasts produced. Further, it should be noted that the new techniques introduced have yet to be implemented during a volcanic ash cloud forming event and therefore how the data will be combined, used and communicated by IMO remains untested.

8. Conclusions

Atmospheric dispersion models are used by VAACs to forecast the long-range transport and dispersion of volcanic ash clouds. The analyses presented in this study on the sensitivities of model forecasts have improved our understanding of the behaviour of dispersion models and the uncertainties associated with the forecasts they produce. This knowledge can help VAACs improve their application of dispersion models and interpretation of forecasts of volcanic ash clouds.

We have shown that the choice of meteorological dataset used for driving an atmospheric dispersion model should depend on the application. Ash cloud transport from explosive eruptions is largely driven by upper air winds whereas the dispersion of pollutants closer to the surface is influenced by the boundary layer meteorology which is sensitive to the local topography. When NAME is used by the London VAAC it is driven by **meteorological data from the Met Office's Unified Model (UM)**. We have shown that the **UM's Global configuration is the most appropriate dataset to use when forecasting ash cloud transport over the area of responsibility covered by the London VAAC**. Considering the Holuhraun effusive eruption in Iceland during September 2014 we find that the higher resolution Euro4 model configuration is more capable of representing the complex topographical features and resulting surface wind speeds and directions in the area surrounding the Holuhraun lava field.

Other key inputs into a dispersion model for volcanic ash cloud forecasting are:

- Location of the eruption vent
- Eruption timings (start and end times of ash emission)
- Plume height(s)
- Mass eruption rates
- Particle size distribution
- Particle density
- Particle shape

It is known that dispersion model forecasts of the mass loading of ash in the atmosphere are particularly sensitive to the MER and plume height used, but we have identified that forecasts are also sensitive to the input PSD used. Measurements of the TGSD of the tephra, MERs and plume heights in near real time could be hugely beneficial for VAAC services. However, it is important for the uncertainties on measurements to also be communicated so that dispersion forecasts can be correctly interpreted. The development and deployment of the Tephra Samplers, infrasound arrays, the mobile lab and visible cameras in Iceland, as part of the FUTURVOLC project, all have the potential to provide valuable information to VAACs on these input parameters in the event of an ash cloud forming eruption. Near vent buoyant plume models also represent a useful tool for estimating MERs. The use of multiple models combined in an ensemble (e.g. REFIR) would have the potential to be able to better constrain time-varying 'best-guess' MERs and their associated uncertainties. Radar data has been extensively used to estimate plume heights, including during the recent Icelandic eruptions of Eyjafjallajökull in 2010 and Grímsvötn in 2011. However, we show that the use of X and C-Band radar data for inferring plume heights during the eruption of Grímsvötn in 2011 poorly represented the height at which the ash was released into the atmosphere. The development of new retrieval algorithms as part of the FUTURVOLC project may help to resolve these uncertainties in future eruptions.

Acknowledgments

FMB would like to thank Philip Gill, Laurence Beard and Clare Bysouth (Verification Team, Met Office) for their assistance with VerPy, used to produce the verification plots presented in Section 2, and Helen Champion, Helen Webster and Andrew Jones (ADAQ, Met Office) for their guidance on running NAME with forecast meteorology. FMB would also like to thank Susan Leadbetter, Laura Burgin and Rachel Pelley (ADAQ, Met Office) for their assistance with Python. Finally, FMB would also like to thank Alison Rust, Kathy Cashman and Emma Liu (University of Bristol, UK) for a stimulating discussion on the shape of volcanic ash particles.

References

- Arakawa, A. and Lamb, V. R. Computational design of the basic dynamic processes of the UCLA general circulation model, *Methods Comput. Phys.*, 17, 173–265, 1977.
- Arason, P., Petersen, G.N. and Bjornsson, H. Observations of the altitude of the volcanic plume during the eruption of Eyjafjallajökull, April-May 2010, *Earth System Science Data*, 4, 1-25, 2011.
- Beckett, F.M., Witham, C.S., Hort, M.C., Stevenson, J.A., Bonadonna, C., Millington, S.C. The sensitivity of NAME forecasts of the transport of volcanic ash clouds to the physical characteristics assigned to the particles. *Forecasting Research Technical Report*, 592, 2014. <http://www.metoffice.gov.uk/media/pdf/4/3/FRTR592.pdf>
- Bonadonna, C., Genco, R., Gouhier, M., Pistolesi, M., Cioni, R., Alfano, F., Hoskuldsson, A., Ripepe, M. Tephra sedimentation during the 2010 Eyjafjallajökull eruption (Iceland) from deposit, radar, and satellite observations. *JGR*, 116:B12202, 2011.
- Bush, M., Bell, S., Christidis, N., Renshaw, R., MacPherson, B., Wilson, C. Development of the North Atlantic European Model (NAE), into an operational model. *Forecasting Research Technical Report.*, 470, 2006.
- Chai, T. and Draxler, R.R. Root mean square error (RMSE) or mean absolute error (MAE)? - Arguments against avoiding RMSE in the literature. *Geosci. Model Dev.*, 7:1247–1250, 2014.
- Charney, J.G. and Phillips, N.A.: Numerical integration of the quasi-geostrophic equations for barotropic and simple baroclinic flows, *J. Meteor.*, 10, 71–99, doi:10.1175/1520-0469(1953)010<0071:NIOTQG>2.0.CO;2, 1953.
- Clayton, A.M., Lorenc, A.C., Barker, D.M. Operational implementation of a hybrid ensemble/4D-Var global data assimilation system at the Met Office. *Q.J.R. Meteorol. Soc.*, 139:1445–1461, 2013.
- Cooke, M.C., Francis, P.N., Millington, S., Saunders, R. and Witham, C. Detection of the Grímsvötn 2011 volcanic eruption plumes using infrared satellite measurements, *Atmospheric Science Letters*, DOI: 10.1002/asl2.506, 2014.
- Dacre, H. F., Grant, A.L.M., Hogan, R.J., Belcher, S.E., Thomson, D.J., aish, B.J., Marenco, F., Haywood, J.M., Ansmann, A., Mattis, I. Evaluating the structure and magnitude of the ash plume during the initial phase of the Eyjafjallajökull eruption using lidar observations and NAME simulations. *Journal of Geophysical Research*, 116, D00U03, 2011.
- Dacre, H.F., Grant, A.L.M., Johnson, B.T. Aircraft observations and model simulations of concentration and particle size distribution in the Eyjafjallajökull volcanic ash cloud. *Atmos. Chem. Phys.*, 13:1277–1291, 2013.
- Davies, T., Cullen, M.J.P., Malcolm, A.J., Mawson, M.H., Staniforth, A., White, A.A., Wood, N. A new dynamical core for the Met Office's global and regional modelling of the atmosphere. *Q.J.R. Meteorol. Soc.*, 131:1759–1782, 2005.
- Davies, T. Lateral boundary conditions for limited area models. *Journal of the Royal Meteorological Society*, 140:185–196, 2014.
- Devenish, B.J., Francis, P.N., Johnson, B.T., Sparks, R.S.J., Thomson, D.J.. Sensitivity analysis of dispersion modelling of volcanic ash from Eyjafjallajökull in May 2010. *JGR*, 117:D00U21, 2012a.

- Devenish, B. J., Thomson, D.J., Marenco, F., Leadbetter, S.J., Ricketts, H., Dacre, H.F. A study of the arrival over the United Kingdom in April 2010 of the Eyjafjallajökull ash cloud using ground-based lidar and numerical simulations. *Atmospheric Environment*, 48, 152–164, 2012b.
- Devenish, B.J. Using simple plume models to refine the source mass flux of volcanic eruptions according to atmospheric conditions. *Journal of Volcanology and Geothermal Research* 256, 118-127, 2013.
- Gudmundsson, M.T., Hognadóttir, T. Volcanic systems and calderas in the Vatnajokull region, central Iceland, constraints on crustal structure from gravity data. *J. Geodyn.* 43, 153–169, 2007.
- Gudmundsson, M.T., Thordarson, T., Hoskuldsson, A., Larsen, G., Bjornsson, H., Prata, F.J., Oddsson, B., Magnússon, E., Hognadóttir, T., Petersen, G.N., Hayward, C.L., Stevenson, J.A., Jonsdóttir, I. Ash generation and distribution from the April-May 2010 eruption of Eyjafjallajökull, Iceland. *Scientific Reports* 2, 572, 2012.
- Hobbs, P.V. Radke, L.F., Lyons, J.H., Ferek, R.J., Coffman, D.J. Airborne measurements of particle and gas emissions from the 1990 volcanic eruptions of Mount Redoubt. *JGR*, 96:572 18,735–18,752, 1991.
- Hreinsdóttir, S., et al. Volcanic plume height correlated with magma-pressure change at Grímsvötn Volcano, Iceland, *Nature Geoscience*, 7, 214-218, DOI: 10.1038/NGEO2044, 2014.
- Jolliffe, I.T. and Stephenson, D.B. In *Forecast Verification: A Practitioner's Guide in Atmospheric Science*, 2nd Edition. Wiley, 2011
- Jones, A.R., Thomson, D.J., Hort, M.C., and Devenish, B.J. The UK Met Office's next-generation atmospheric dispersion model, NAME III. In C. Borrego and A.-L Norman, editors, *Air Pollution Modelling and its Application*, 580–589, Springer, 2007.
- Mastin, L.G., Guffanti, M., Guffanti, M., Servranckx, R., Webley, P., Barsotti, S., Dean, K., Durant, A., Ewert, J.W., Neri, A., Rose, W.I., Schneider, D., Siebert, L., Stunder, B., Swanson, G., Tupper, A., Volentik, A., Waythomas, C.F. A multidisciplinary effort to assign realistic source parameters to models of volcanic ash-cloud transport and dispersion during eruptions. *JVGR*, 186:10–21, 2009.
- Mastin, L.G., 2014. Testing the accuracy of a 1-D volcanic plume model in estimating mass eruption rate. *Journal of Geophysical Research* 119, 2474-2495.
- Mittermaier, M.P. A strategy for verifying near-convection-resolving model forecasts at observing sites. *Weather and Forecasting*, 29:185–204, 2014.
- Moxnes, E.D., Kristiansen, N.I., Stohl, A., Clarisse, L., Durant, A., Weber, K., Vogel, A. Separation of ash and sulfur dioxide during the 2011 Grímsvötn eruption. *JGR: Atmospheres*, 119, DOI:10.1002/2013JD021129, 2014.
- Nawri, N., Bjornsson, H., Petersen, G.N., Jonasson, K. Surface wind and air temperature over Iceland based on station records and ECMWF operational analyses. *IMO Report VI 2012-008*, 2012.
- Oke, T.R. *Boundary layer climates*. Routledge. Second Edition, 1987.

- Pelley, R., Cooke, M., Manning, A., Thomson, D., Witham, C., and Hort, M. Inversion technique for estimating emissions of volcanic ash from satellite imagery, Geophysical Research Abstracts, 16, EGU 2014-12950, 2014.
- Peterson, G.N., Bjornsson, H., Arason, P., and von Löwis, S. Two weather radar time series of the altitude of the volcanic plume during the May 2011 eruption of Grímsvötn, Iceland, Earth System Science Data, 4, 121-127, 2012.
- Ripepe, M., Bonadonna, C., Folch, A., Delle Donne, D., Lacanna, G., Marchetti, E., Hoskuldsson, A. Ash-plume dynamics and eruption source parameters by infrasound and thermal imagery: The 2010 Eyjafjallajökull eruption. EPSL: 366, 112-121, 2013.
- Rose, W.I., Bluth, G.J.S., Ernst, G.G.J. Integrating retrievals of volcanic cloud characteristics from satellite remote sensors: a summary. Philosophical Transactions of the Royal Society A 358, 1585-1606, 2000.
- Sigmundsson et al. **Segmented lateral dyke growth in a rifting event at Barðarbunga volcanic system, Iceland.** Nature, 517:191-195, 2015.
- Smith, R.B. **The influence of mountains on the atmosphere.** Advances in Geophysics, 21:87-230, 1979.
- Sparks, R.S.J., Bursik, M.I., Carey, S.N., Gilbert, J.S., Glaze, L.S., Sigurdsson, H., Woods, A.W. Volcanic plumes. John Wiley & Sons, Chichester. 574 pp, 1997.
- Stevenson, J.A., Loughlin, S.C., Font, A., Fuller, G.W., MacLeod, A., Oliver, I.W., Jackson, B., Horwell, C.J., Thordarson, T. and Dawson, I. UK monitoring and deposition of tephra from the May 2011 eruption of Grímsvötn, Iceland. Journal of Applied Volcanology, 2(3), doi:10.1186/2191-5040-2-3, 2013.
- Stevenson, J.A., Millington, S.C., Beckett, F.M., Swindles, G.T., Thordarson, T. Big grains go far: understanding the discrepancy between tephrochronology and satellite infrared measurements of volcanic ash. Atmos. Meas. Tech, 8:2069-2091, 2015.
- Stohl, A., Prata, A.J., Eckhardt, S., Clarisse, L., Durant, A., Henne, S., Kristiansen, N.I., Minikin, A., Schumann, U., Seibert, P., Stebel, K., Thomas, H.E., Thorsteinsson, T., Tørseth, K., Weinzierl, B. Determination of time- and height-resolved volcanic ash emissions and their use for quantitative ash dispersion modeling: the 2010 Eyjafjallajökull eruption. Atmospheric Chemistry and Physics 11, 4333-4351, 2011.
- Walters, D., Wood, N., Vosper, S., Milton, S. ENDGame Overview Report. Available at: <http://www.metoffice.gov.uk/media/pdf/s/h/ENDGameGOVSciv2.0.pdf>, 2014.
- Webster, H.N., Thomson, D.J., Johnson, B.T., Heard, I.P.C., Turnbull, k. Marengo, F. Kristiansen, N.I., Dorsey, J., Minikin, A., Weinzierl, B., Schumann, U., Sparks, R.S.J., Loughlin, S.C., Hort, M.C., Leadbetter, S.J., Devenish, B.J., Manning, A.J., Witham, C.S., Haywood, J.M., Golding, B.W. Operational prediction of ash concentrations in the distal volcanic cloud from the 2010 Eyjafjallajökull eruption. JGR, 117:D00U08, 2012.
- Witham, C., Hort, M., Thomson, D., Leadbetter, S., Devenish, B. and Webster, H. 2012. The current volcanic ash modelling set-up at the London VAAC, Technical Summary v1.1, Met Office,

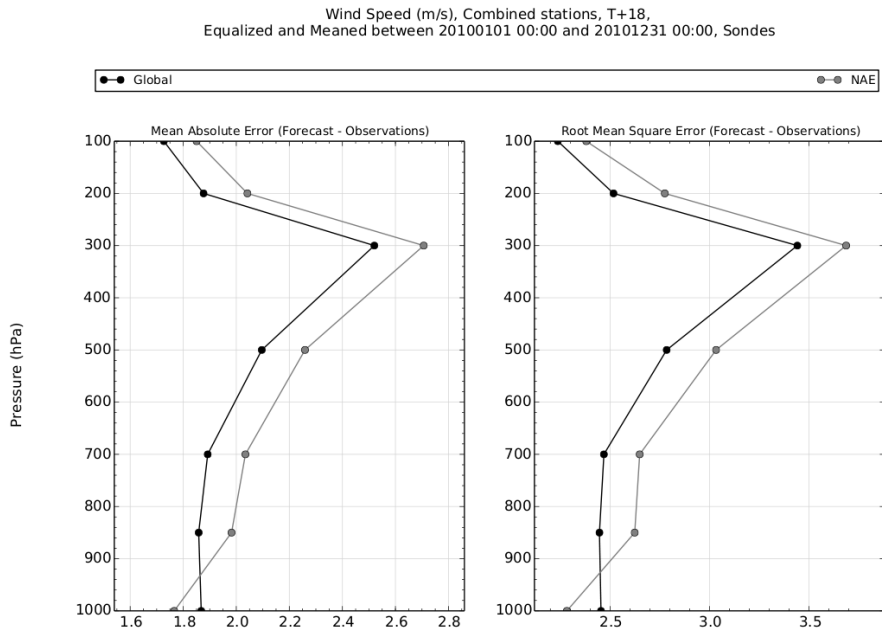
http://www.metoffice.gov.uk/media/pdf/p/7/London_VAAC_Current_Modelling_SetUp_v01-1_05042012.pdf

- WMO. Guide to meteorological instruments and methods of observation, Geneva, World Meteorological Organisation (2008 edition, updated in 2010). Available at <http://www.wmo.int/pages/prog/www/IMOP/CIMO-Guide.html>, 2010.
- WMO. WMO Publication No. 306 - Manual on codes. Volume I.1 and Volume I.2. Available at <http://www.wmo.int/pages/prog/www/WMOCodes.html>, 2011.
- Wood, N., Staniforth, A., White, A., Allen, T., Diamantakis, M., Gross, M., Melvin, T., Smith, C., Vosper, S., Zerroukat, M., Thuburn, J. An inherently mass-conserving semi-implicit semi-Lagrangian discretization of the deep-atmosphere global non-hydrostatic equations. *Q.J.R.Meteorol. Soc.*, 2014.
- Woodhouse, M.J., Hogg, A.J., Phillips, J.C., Sparks, R.S.J. Interaction between volcanic plumes and wind during the 2010 Eyjafjallajökull eruption, Iceland. *Journal of Geophysical Research* 118, 92-109, 2013.

Appendix A. Comparing 0Z and 12Z data

A.1 Global vs. NAE

(a)



(b)

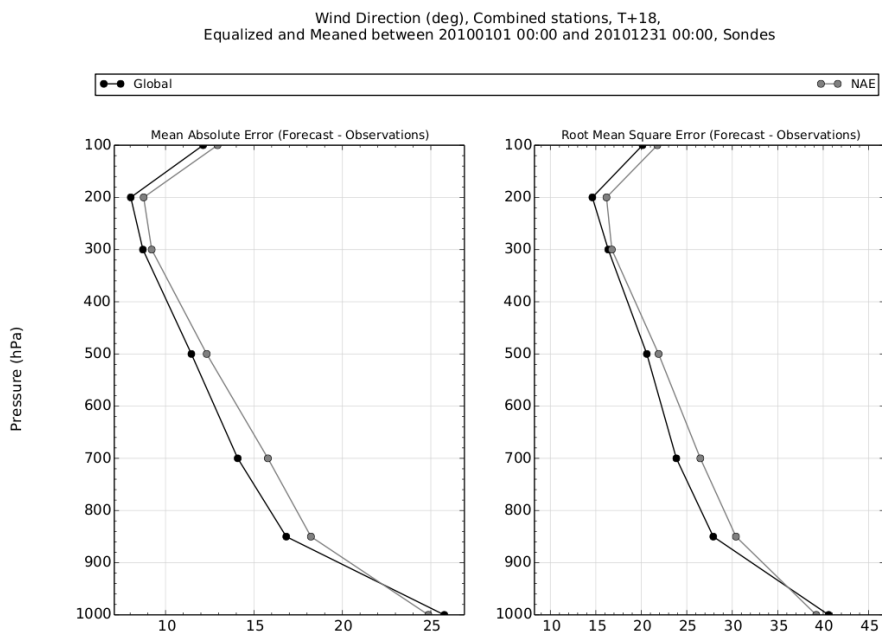
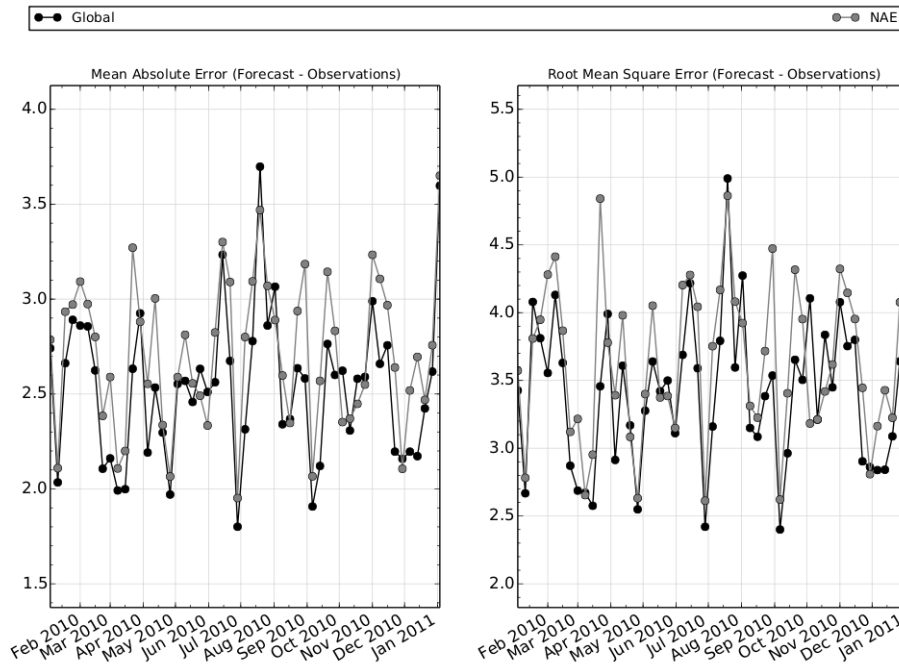


Figure A.1.1. Vertical profiles of MAE and RMSE, comparing Global model and NAE model forecast wind speed and wind direction data to radiosonde data at 0Z during 2010.

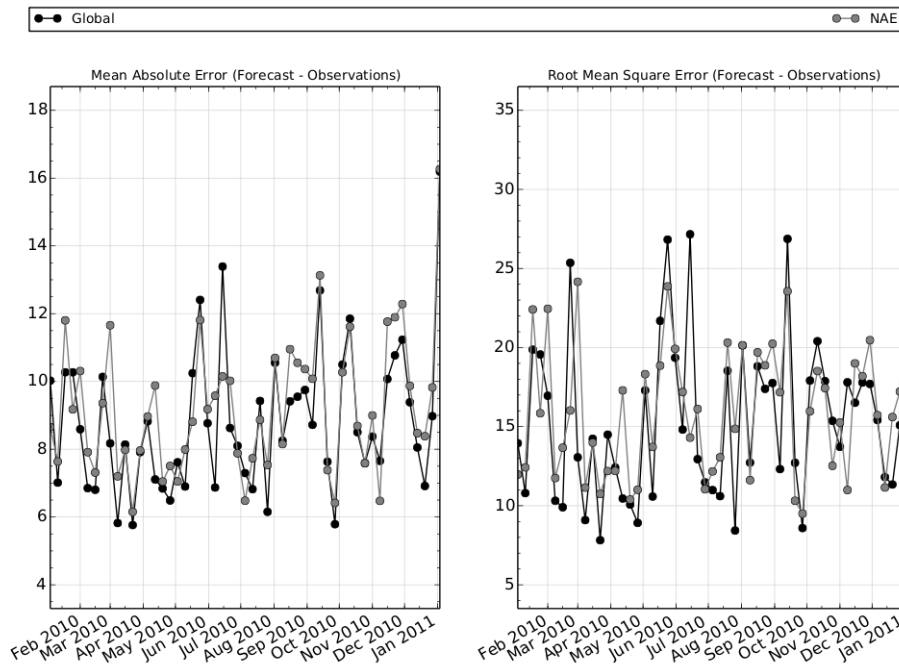
(a)

Wind Speed (m/s) @ 300hPa, Combined stations, T+18, Sondes, Equalized



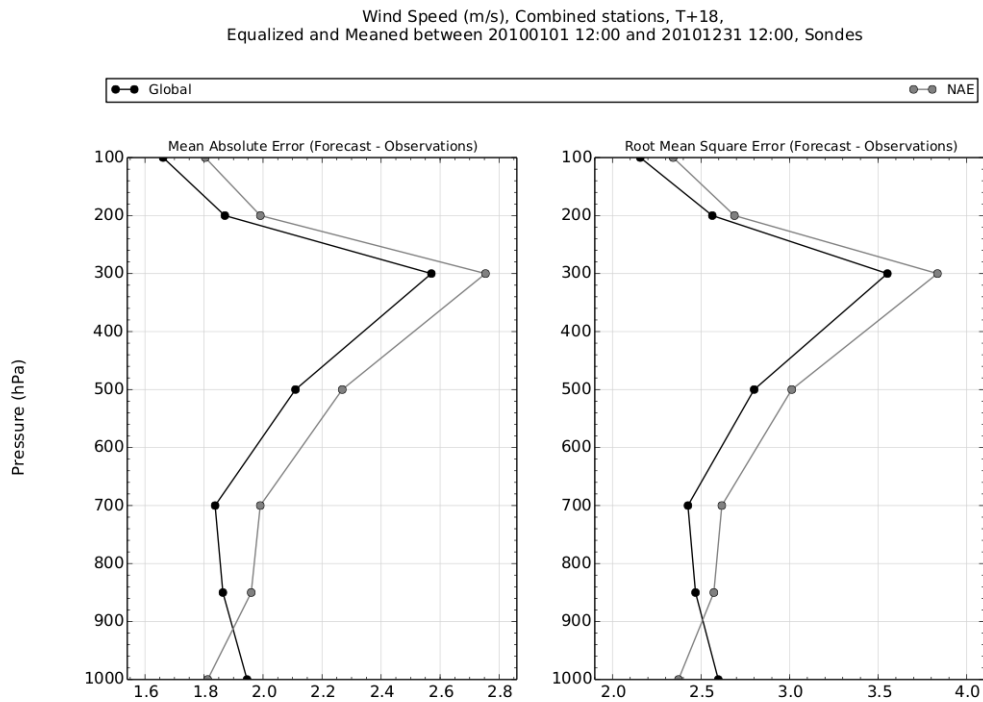
(b)

Wind Direction (deg) @ 300hPa, Combined stations, T+18, Sondes, Equalized

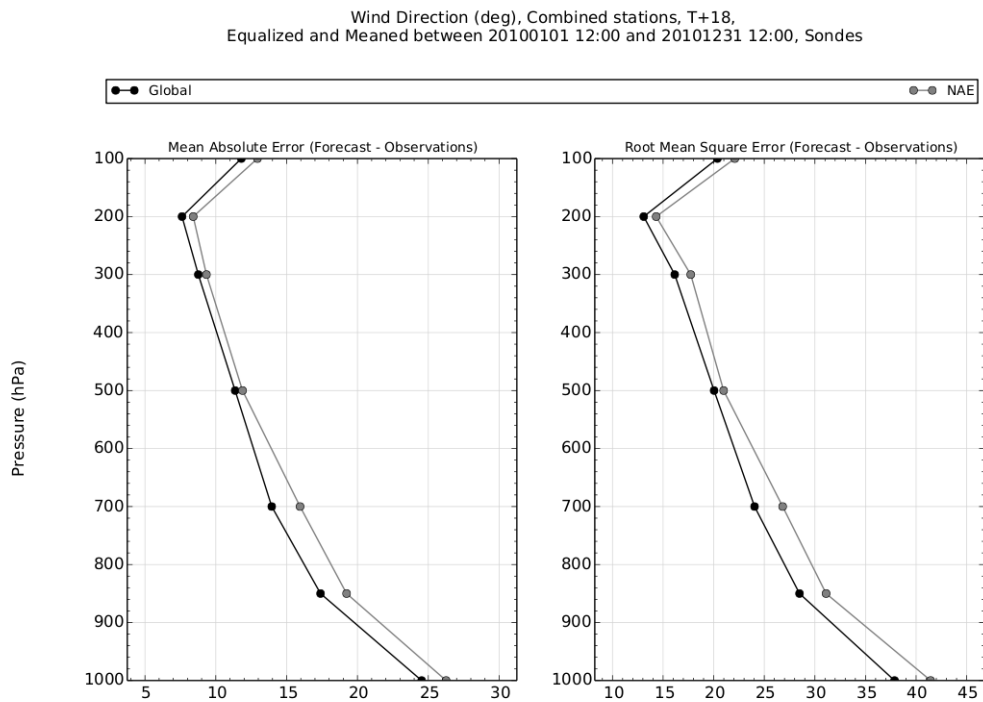


(a)

Figure A.1.2. Time series of MAE and RMSE, comparing Global model and NAE model forecast wind speed and wind direction data to radiosonde data at 0Z during 2010.



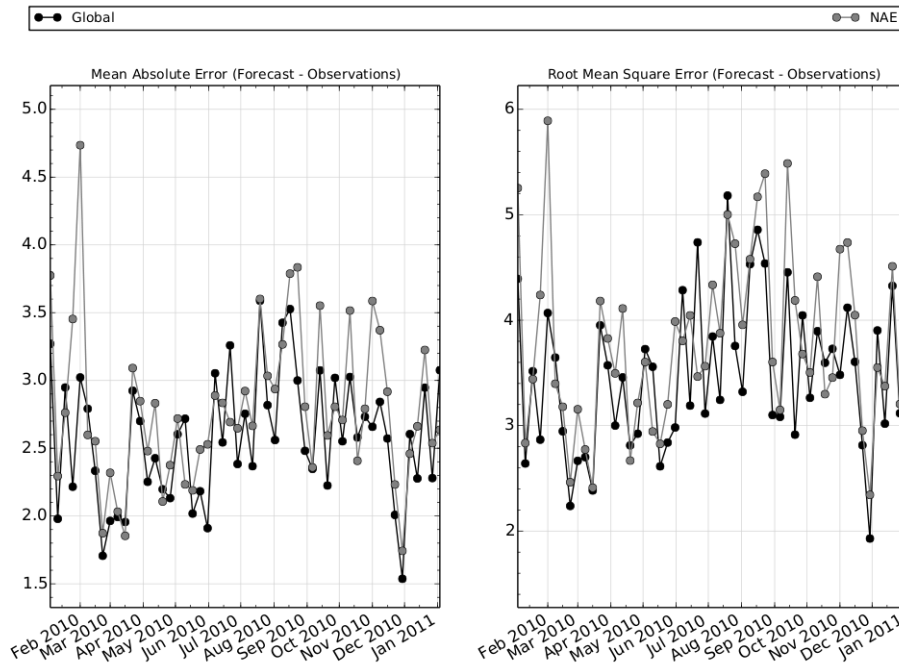
(b)



(a)

Figure A.1.3. Vertical profiles of MAE and RMSE, comparing Global model and NAE model forecast wind speed and wind direction data to radiosonde data at 12Z during 2010.

Wind Speed (m/s) @ 300hPa, Combined stations, T+18, Sondes, Equalized



(b)

Wind Direction (deg) @ 300hPa, Combined stations, T+18, Sondes, Equalized

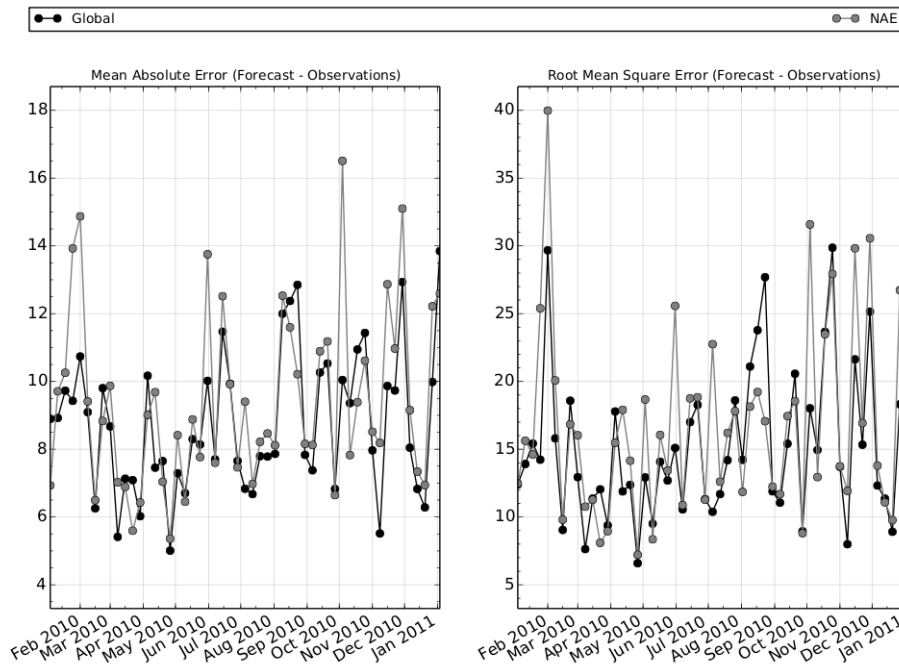
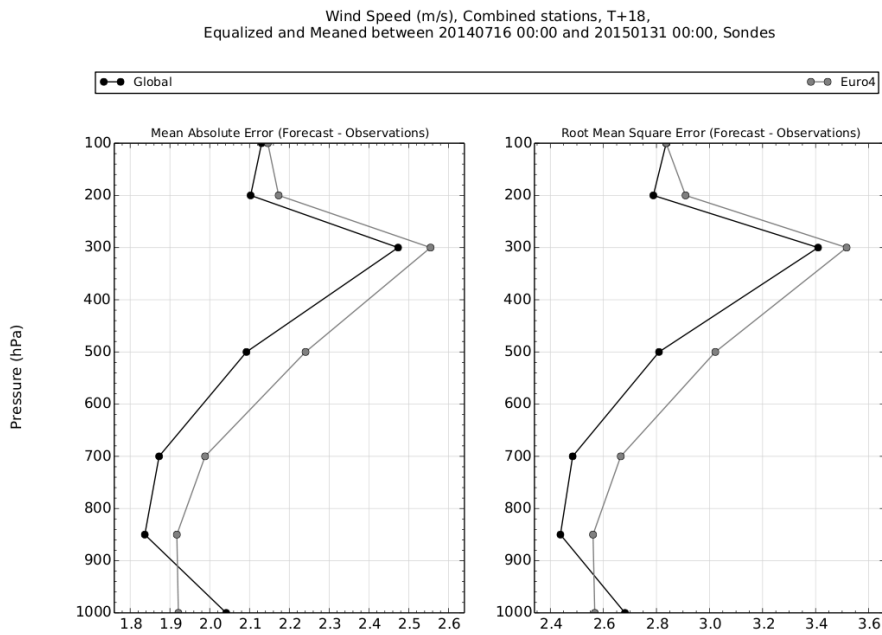


Figure A.1.4. Time series of MAE and RMSE, comparing Global model and NAE model forecast wind speed and wind direction data to radiosonde data at 12Z during 2010.

A.2 Global with ENDGame dynamics vs Euro4

(a)



(b)

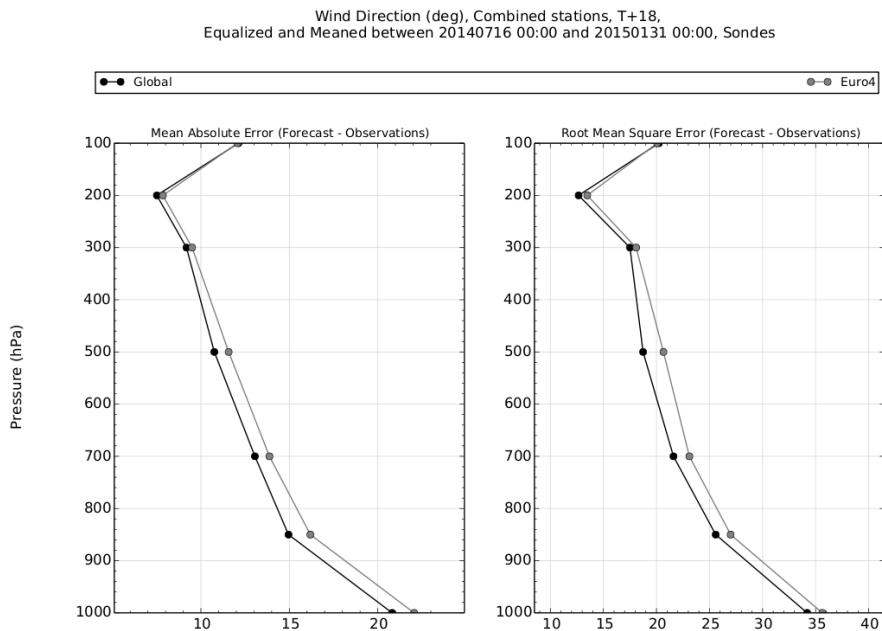
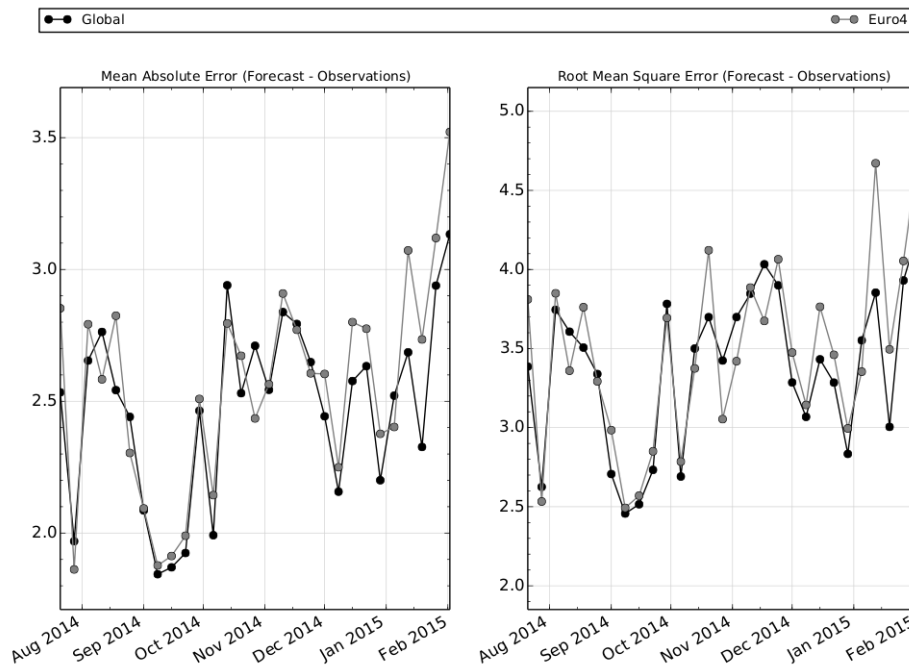


Figure A.2.1. Vertical Profiles of MAE and RMSE, comparing Global model with ENDGame dynamics and Euro4 model forecast wind speed and wind direction to radiosonde data at 0Z over the period 16/07/2014 – 31/01/2015.

(a)

Wind Speed (m/s) @ 300hPa, Combined stations, T+18, Sondes, Equalized



(b)

Wind Direction (deg) @ 300hPa, Combined stations, T+18, Sondes, Equalized

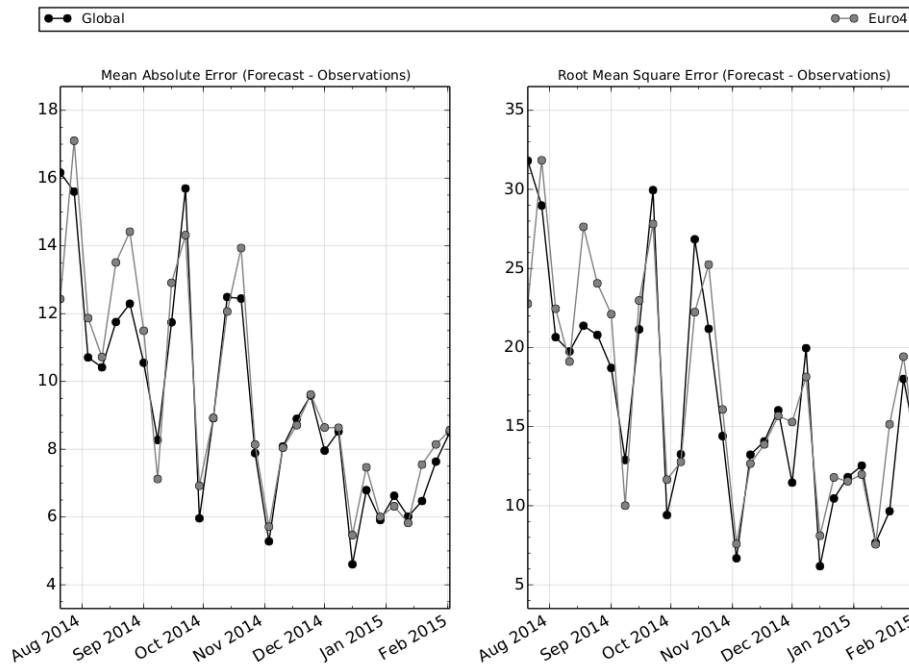
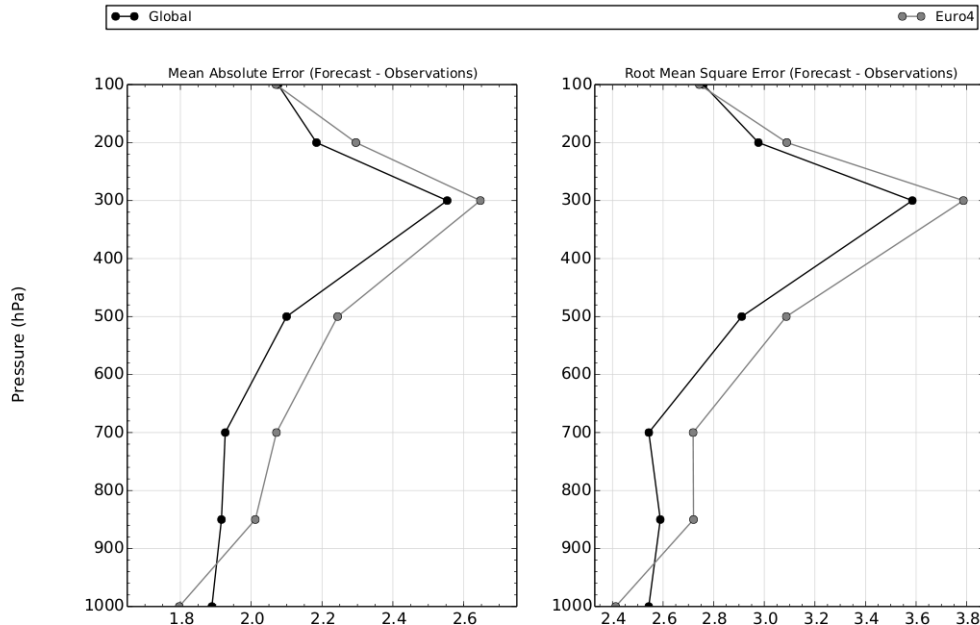


Figure A.2.1. Time series of MAE and RMSE, comparing Global model with ENDGame dynamics and Euro4 model forecast wind speed and wind direction to radiosonde data at OZ over the period 16/07/2014 – 31/01/2015.

(a)

Wind Speed (m/s), Combined stations, T+18,
Equalized and Meaned between 20140716 12:00 and 20150131 12:00, Sondes



(b)

Wind Direction (deg), Combined stations, T+18,
Equalized and Meaned between 20140716 12:00 and 20150131 12:00, Sondes

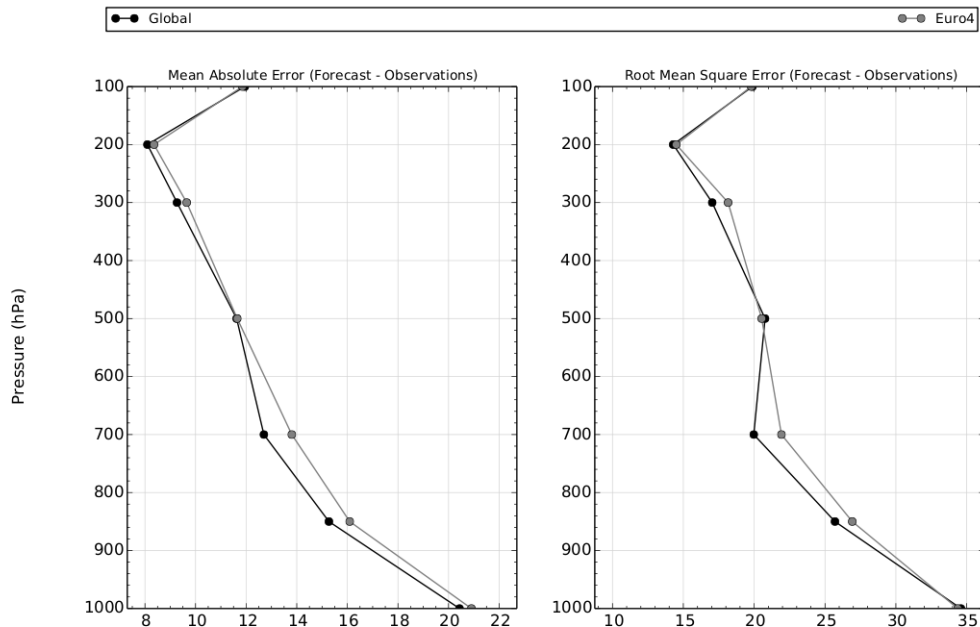
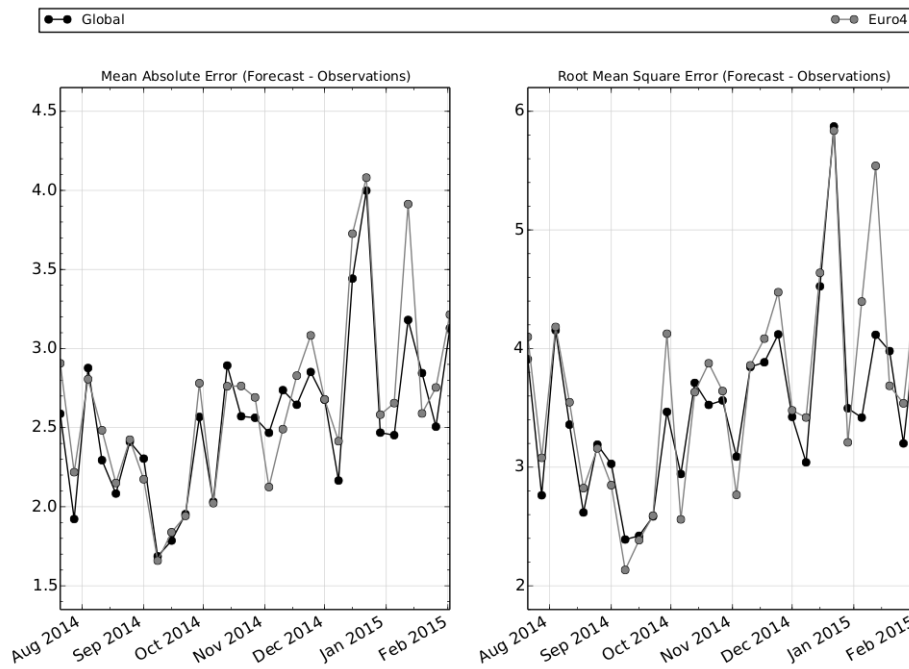


Figure A.2.3. Vertical Profiles of MAE and RMSE, comparing Global model with ENDGame dynamics and Euro4 model forecast wind speed and wind directions to radiosonde data at 12Z during 16/07/2014 – 31/01/2015.

(a)

Wind Speed (m/s) @ 300hPa, Combined stations, T+18, Sondes, Equalized



(b)

Wind Direction (deg) @ 300hPa, Combined stations, T+18, Sondes, Equalized

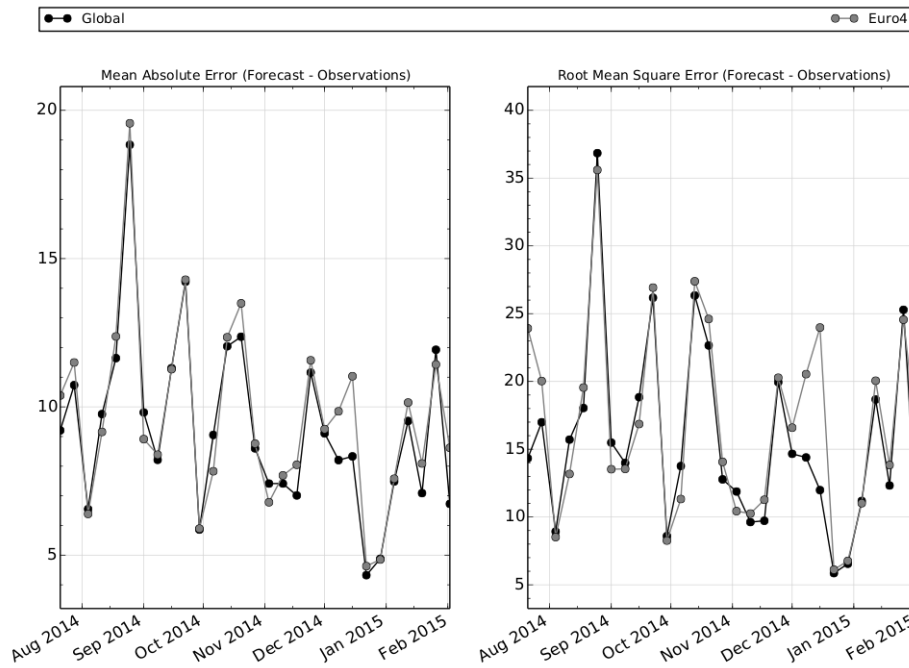
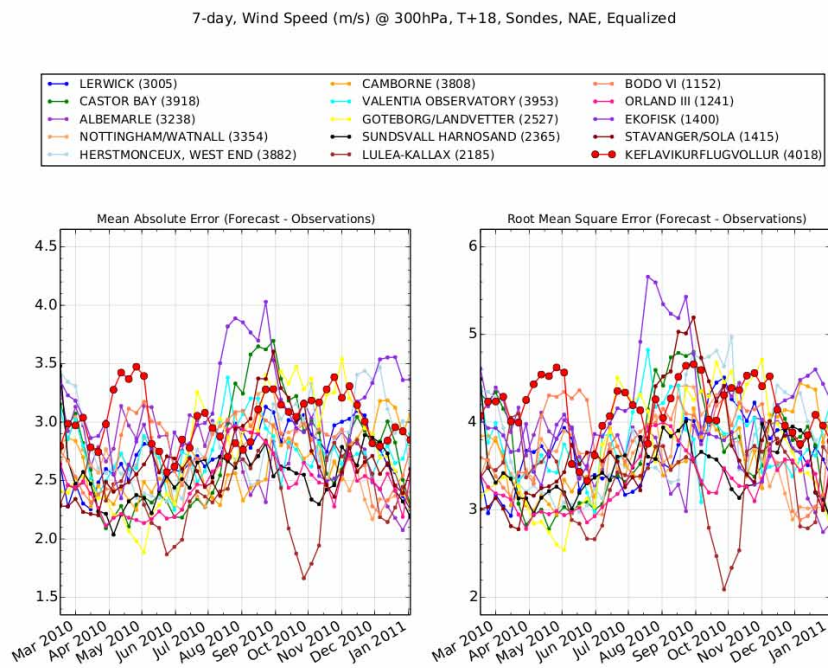


Figure A.2.4. Time series of MAE and RMSE, comparing Global model with ENDGame dynamics and Euro4 model forecast wind speed and wind direction to radiosonde data at 12Z during 16/07/2014 – 31/01/2015.

Appendix B NAE Station Time Series

(a)



(b)

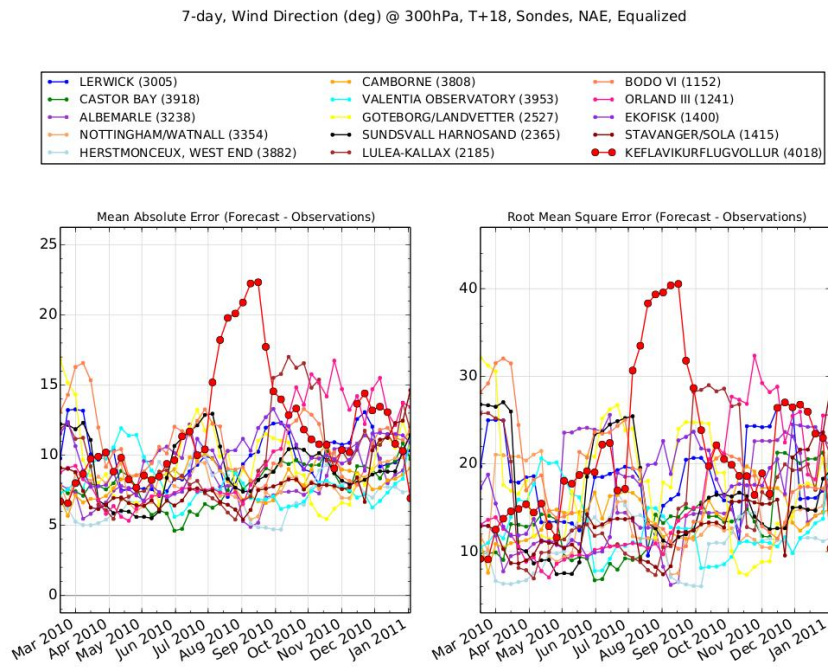
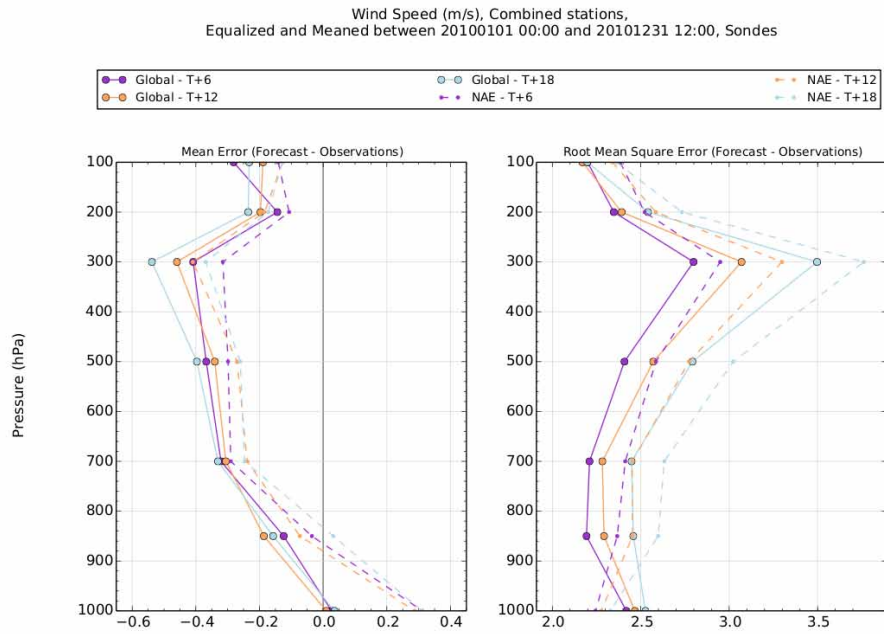


Figure B.1: Time series of MAE and RMSE of the NAE forecast at T+18 of wind speed and wind direction, calculated for each of the individual radiosonde station datasets during 2010.

Appendix C Using Mean Error

C.1 Global vs NAE

(a)



(b)

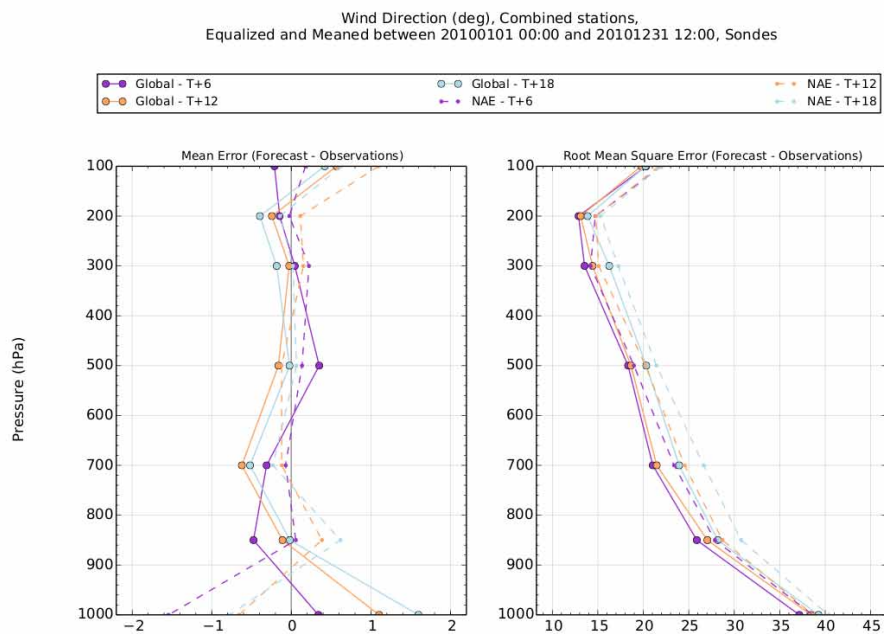
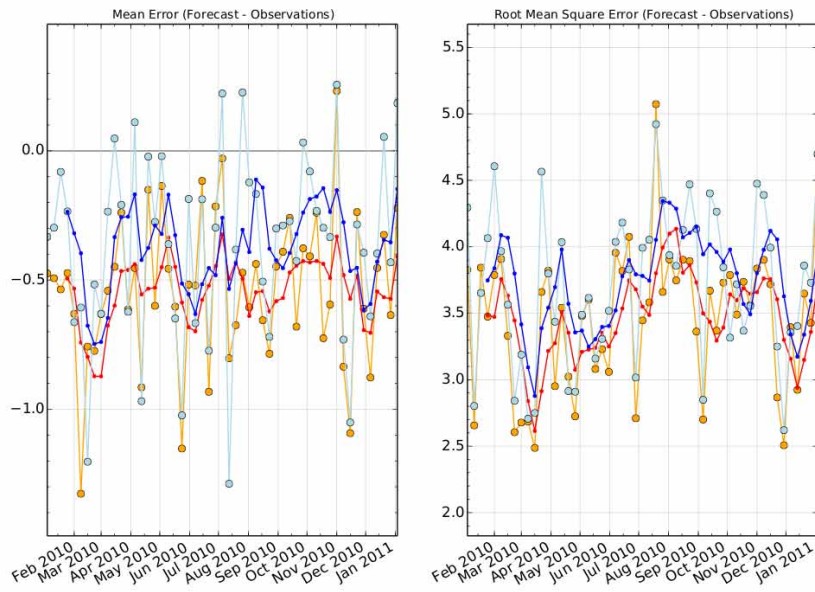


Figure C.1.1: Vertical profiles of ME and RMSE, comparing Global model and NAE model forecast wind speed and wind direction to radiosonde data during 2010.

(a)

Wind Speed (m/s) @ 300hPa, Combined stations, T+18, Sondes, Equalized



(b)

Wind Direction (deg) @ 300hPa, Combined stations, T+18, Sondes, Equalized

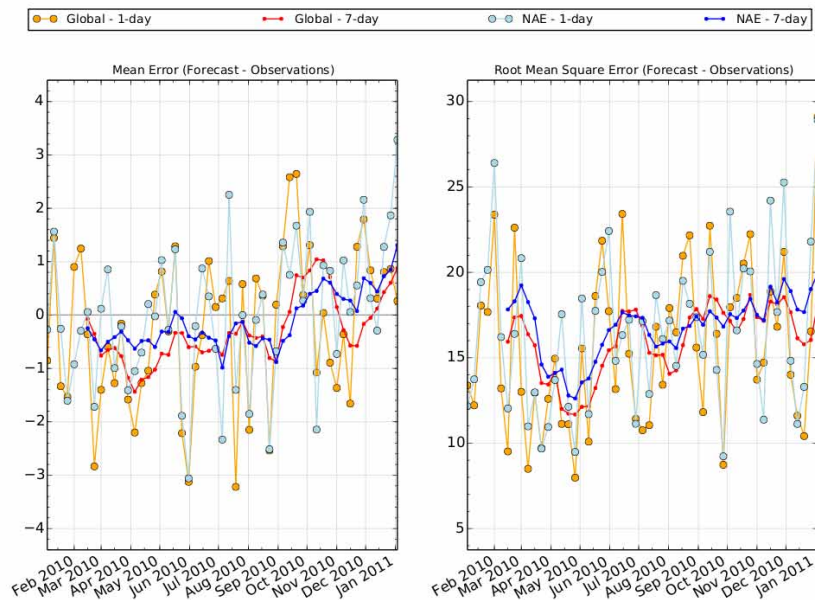
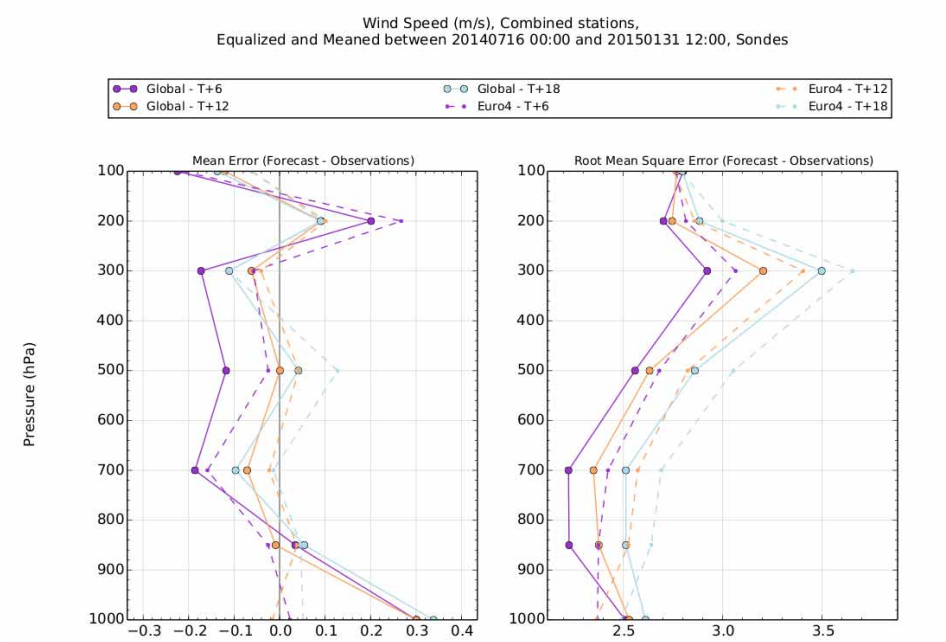


Figure C.1.2: Timeseries of ME and RMSE of the Global and NAE modelled wind speed and wind direction with respect to radiosonde data, at 300 hPa for forecast T+18 during 2010. The light blue and orange lines show the weekly mean, using daily aggregated data, of the Global and NAE forecast meteorology respectively. The dark blue and red lines show the 4-weekly running mean, using weekly aggregated data for the Global and NAE forecast meteorology respectively.

C.2 ENDGame Global vs. Euro4

(a)



(b)

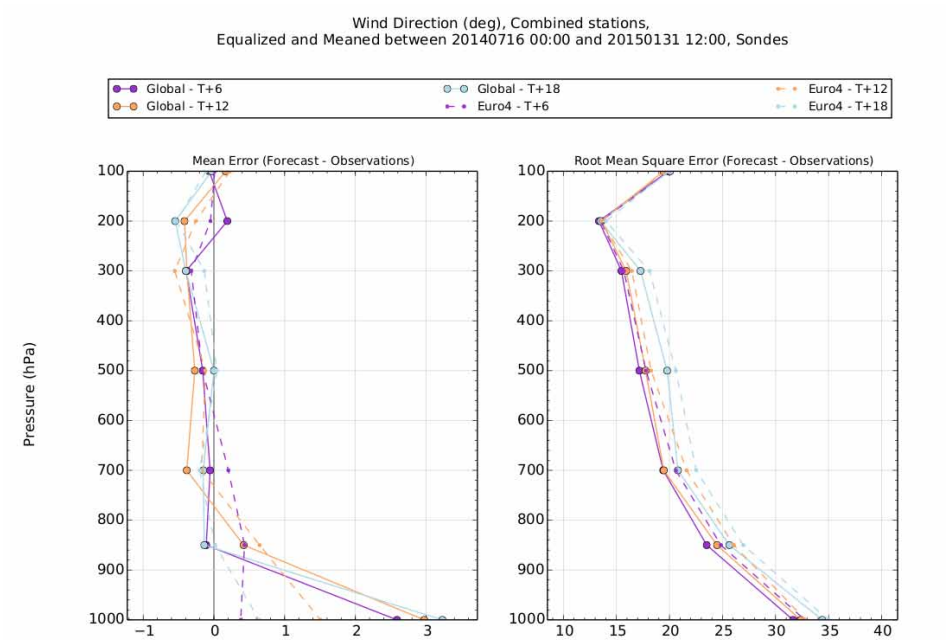
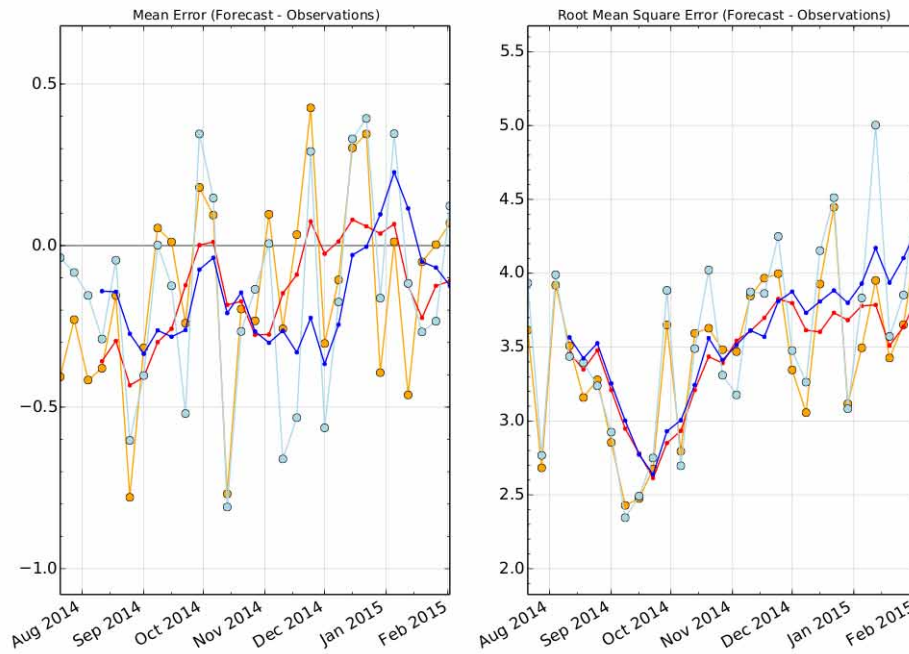


Figure C.2.3: Vertical profiles of ME and RMSE, comparing Global model with ENDGame dynamics and Euro4 model wind speed and wind direction to radiosonde data between July 2014 and January 2015, the period for which these model configurations were operational.

(a)

Wind Speed (m/s) @ 300hPa, Combined stations, T+18, Sondes, Equalized



(b)

Wind Direction (deg) @ 300hPa, Combined stations, T+18, Sondes, Equalized

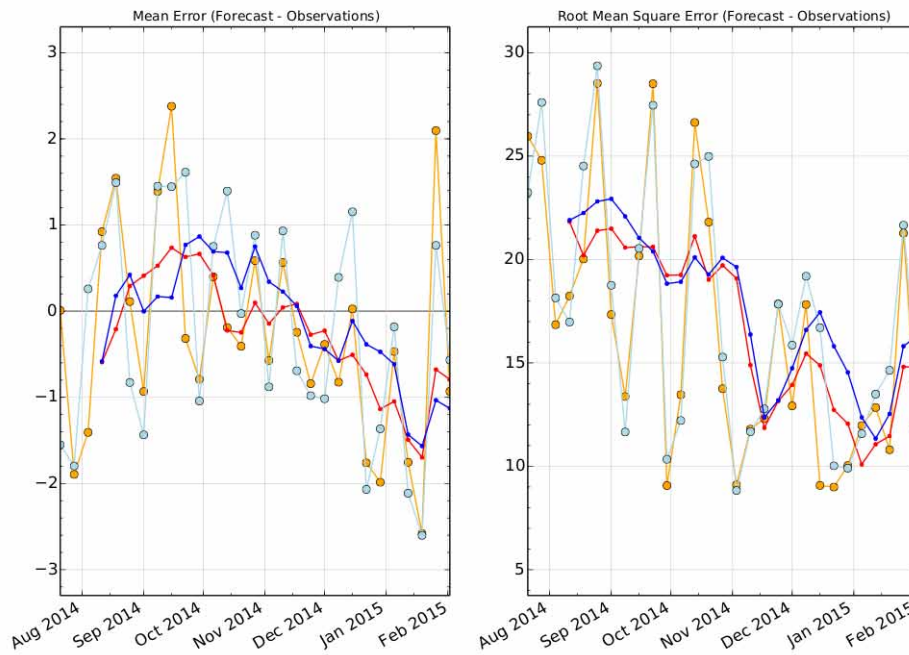


Figure C.2.4: Timeseries of ME and RMSE, comparing Global model with ENDGame dynamics and Euro4 model wind speed and wind direction to radiosonde data between July 2014 and January 2015.

Appendix D. Statistical Measures

The Pearson's Correlation Coefficient (PCC) represents the scatter between paired (i.e. at the same location) data points, and ranges in value between -1 and +1. A value of +1/-1 represents a perfect positive or negative linear association between the two variables. In our examples this accounts for the difference in both the position of the plume and the given total column mass loading values at a grid point.

The Fractional Bias represents the difference in magnitude between paired data points at the same location, it does not account for any spatial differences in the plume. Values range between -2 and +2 where positive values represent over-prediction and negative values under-prediction. A value of 0 represents a perfect match. It therefore represents the systematic bias which leads to an under/over-estimate compared to the alternative model output.

The Figure of Merit in Space represents the percentage of overlap of data in space, it does not consider the magnitude of the values, in the studies presented here it represents the overlap between the positions of the two different forecast plumes (e.g. plumes generated with different meteorology or varying source parameters). A high value of Figure of Merit in Space represents a high degree of similarity between model outputs, a low value does not necessarily represent poor model performance, just that the plumes are shifted in space.

The Kolmogorov-Smirnov Parameter (KSP) represents the maximum absolute difference between two cumulative distributions, it is the probability of occurrence of predicted and measured values not greater than a given threshold. It is a measure of how well the model reproduces the output concentrations regardless of when or where it occurred. A high value suggests that the model outputs have very different output concentrations. The maximum difference between the two distributions can not be greater than 100%.

Appendix E. Daily Forecasts of the Holuhraun eruption during September 2014

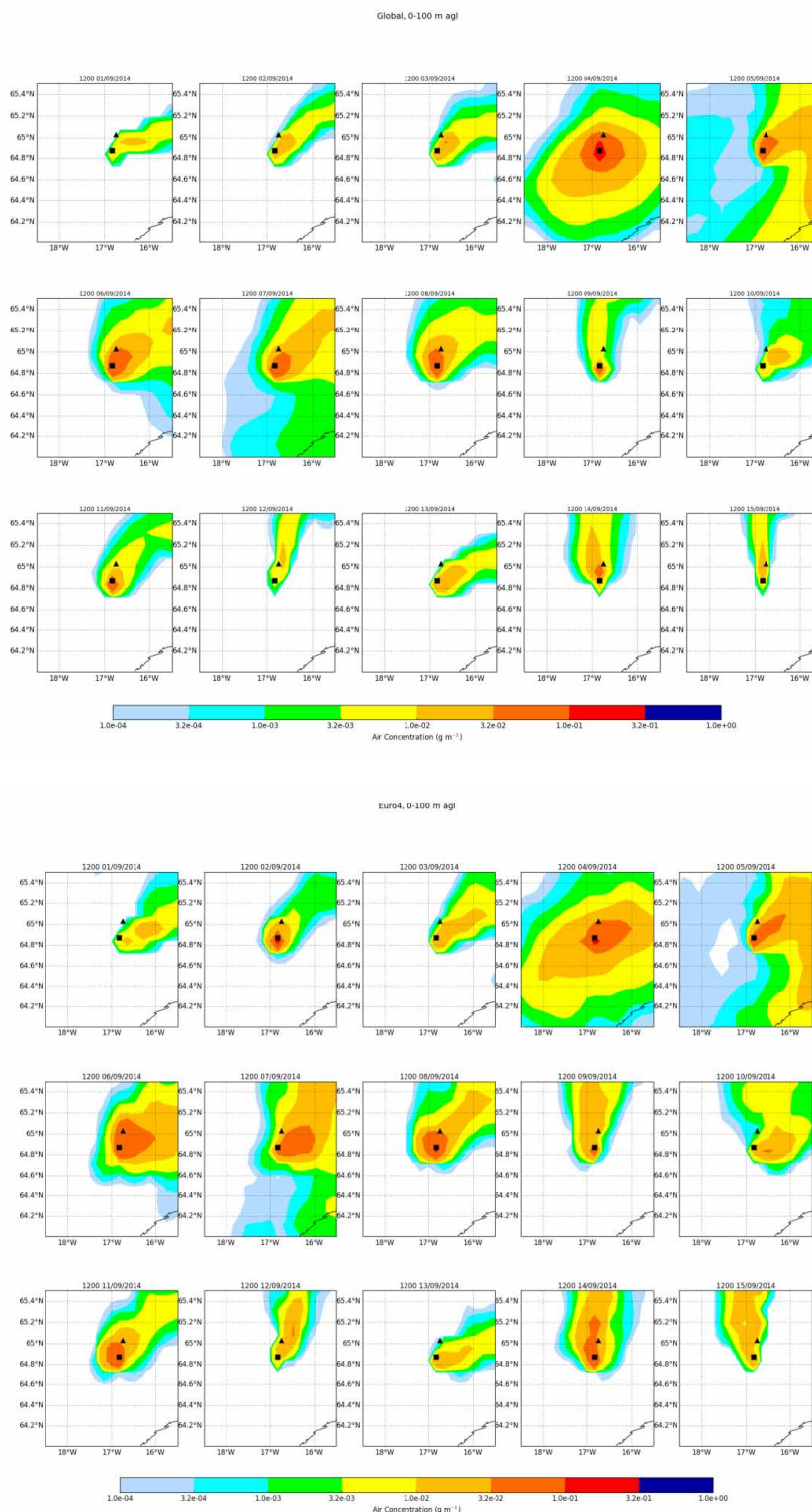


Figure E.1. NAME forecast air concentration over 0–100 m agl for the Holuhraun eruption during the 1st – 15th September 2014 using the Global and Euro4 model configuration topography and analysis meteorological data, zoomed-in over the Holuhraun area, which is indicated by the black square, the triangle indicates the location of Askja.

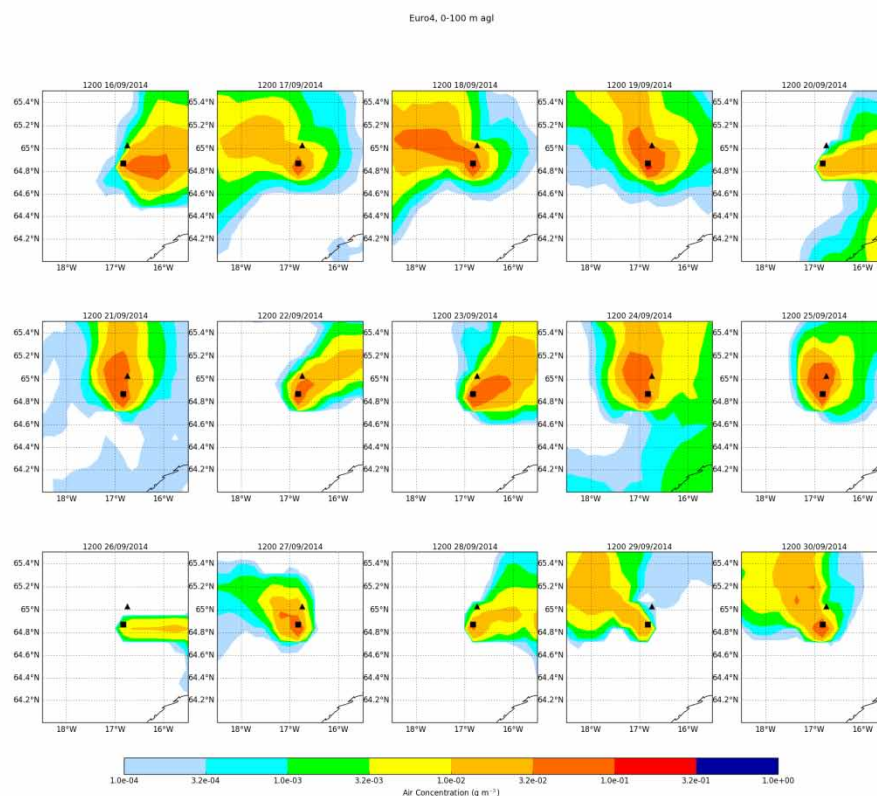
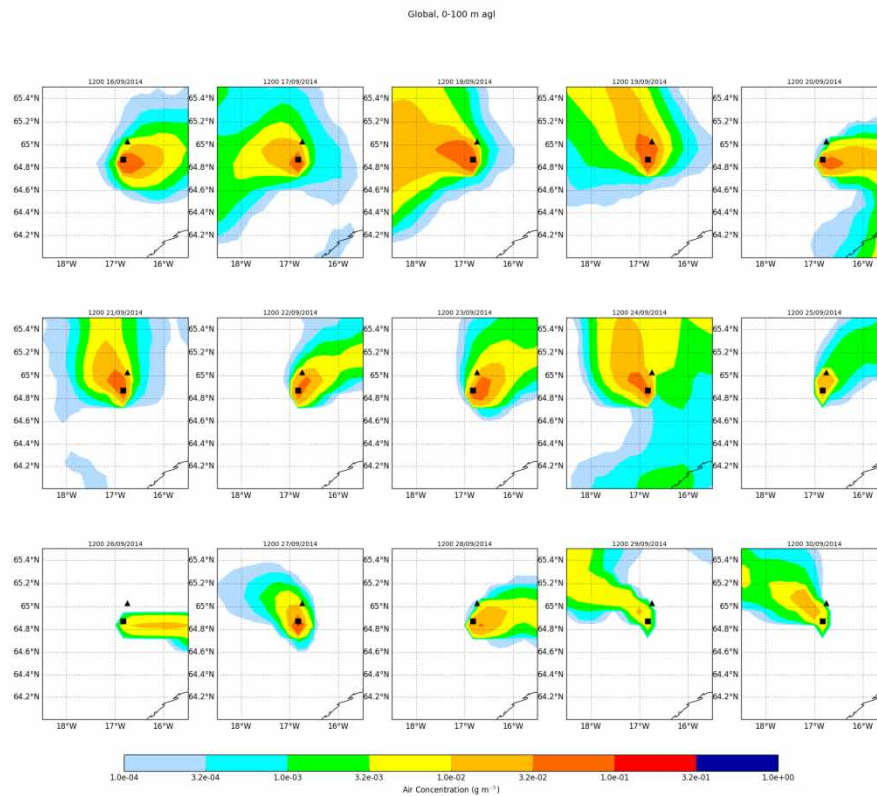


Figure E.2. NAME forecast air concentration over 0–100 m agl for the Holuhraun eruption during the 16th – 30th September 2014 using the Global and Euro4 model configuration topography and analysis meteorological data, zoomed-in over the Holuhraun area, which is indicated by the black square, the triangle indicates the location of Askja.

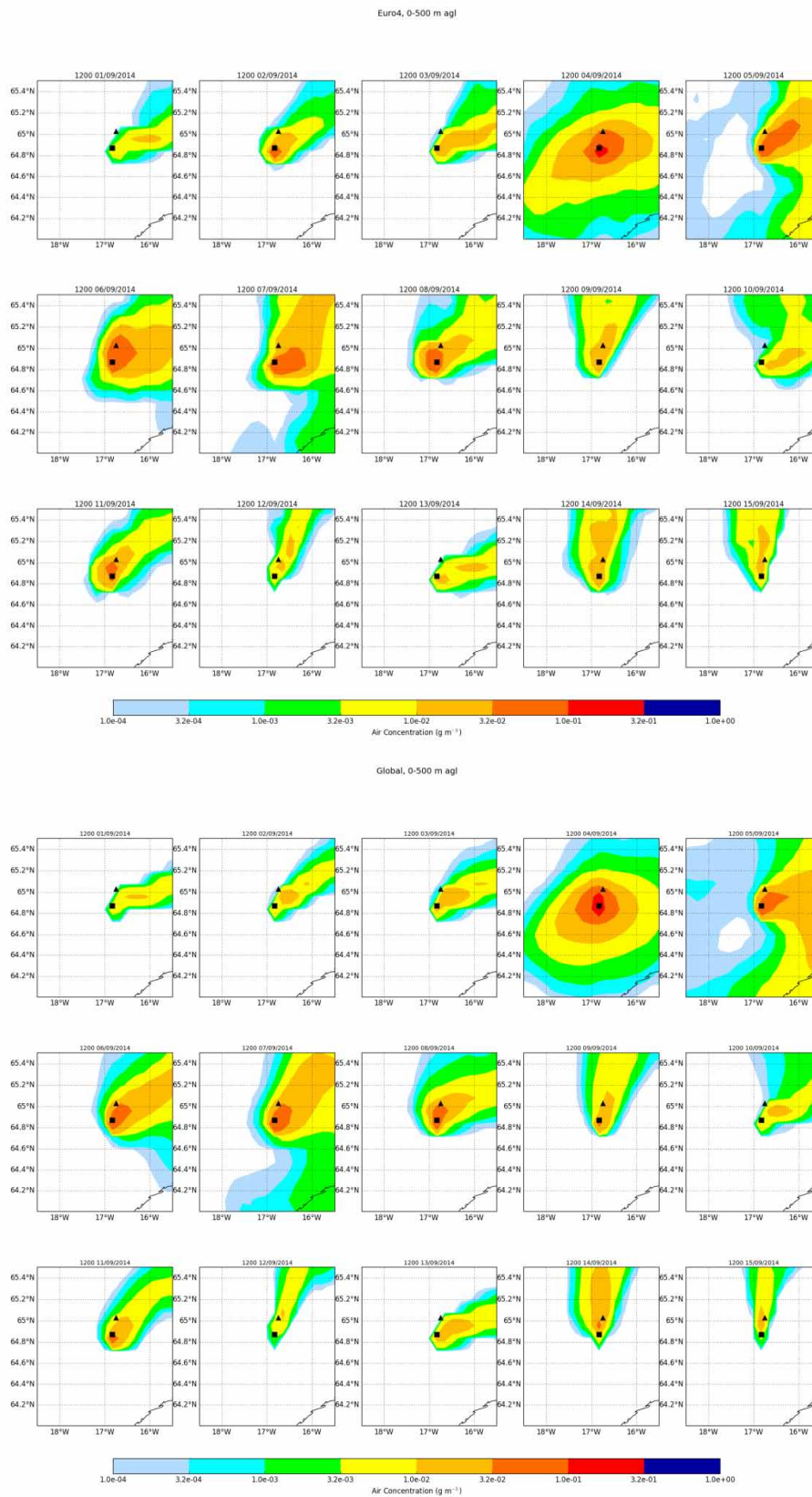


Figure E.3. NAME forecast air concentration over 0–500 m agl for the Holuhraun eruption during the 1st – 15th September 2014 using the Global and Euro4 model configuration topography and analysis meteorological data, zoomed-in over the Holuhraun area, which is indicated by the black square, the triangle indicates the location of Askja.

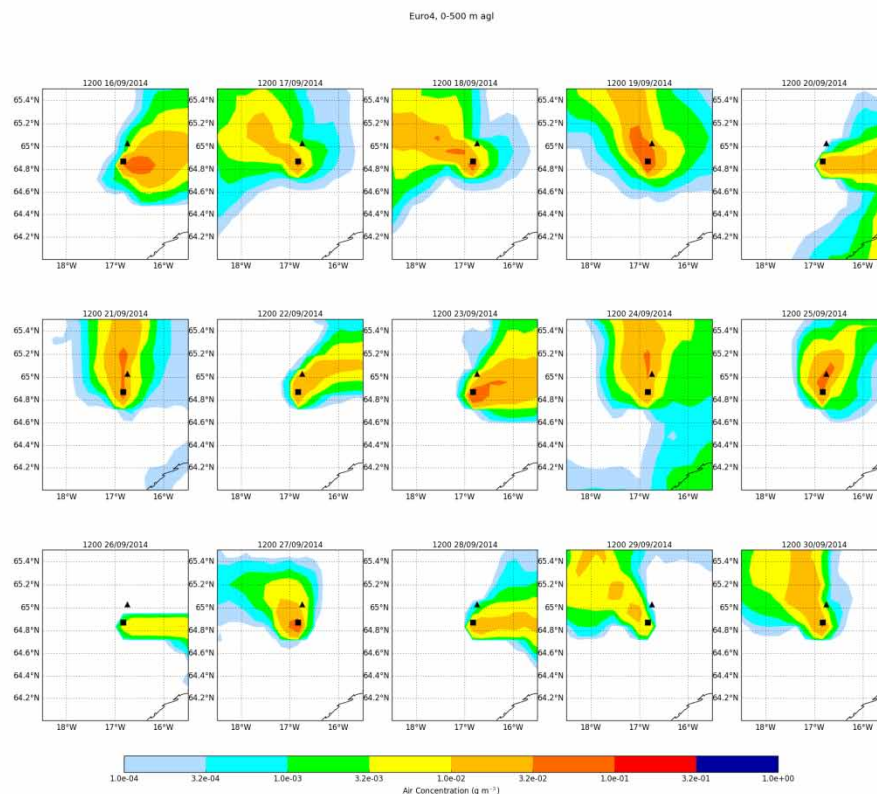
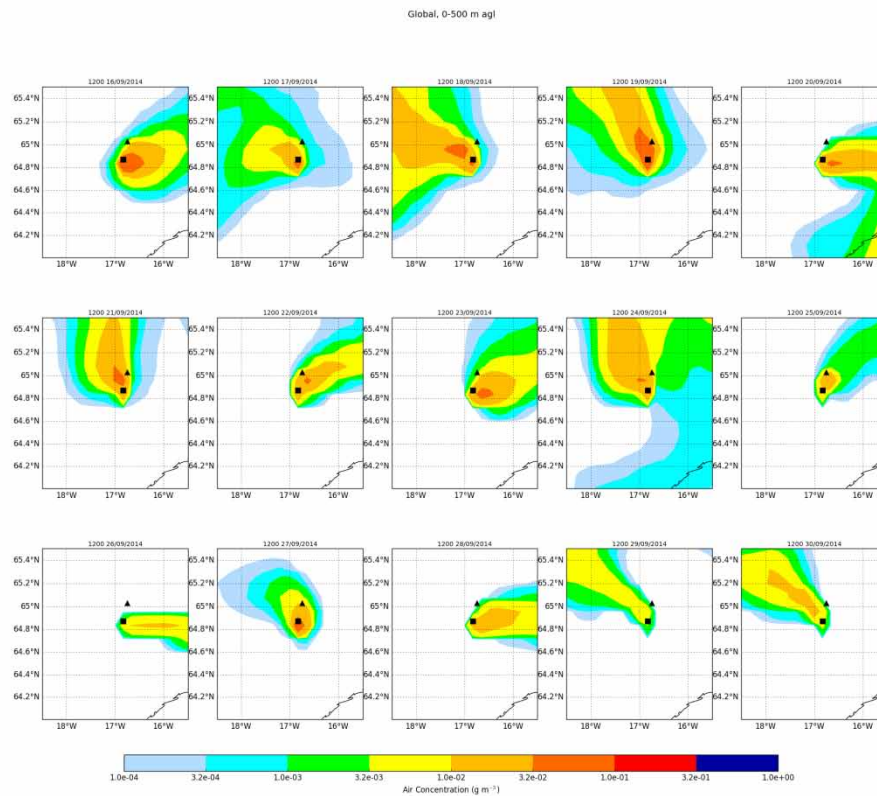


Figure E.4. NAME forecast air concentration over 0–500 m agl for the Holuhraun eruption during the 16th – 30th September 2014 using the Global and Euro4 model configuration topography and analysis meteorological data, zoomed-in over the Holuhraun area, which is indicated by the black square, the triangle indicates the location of Askja.

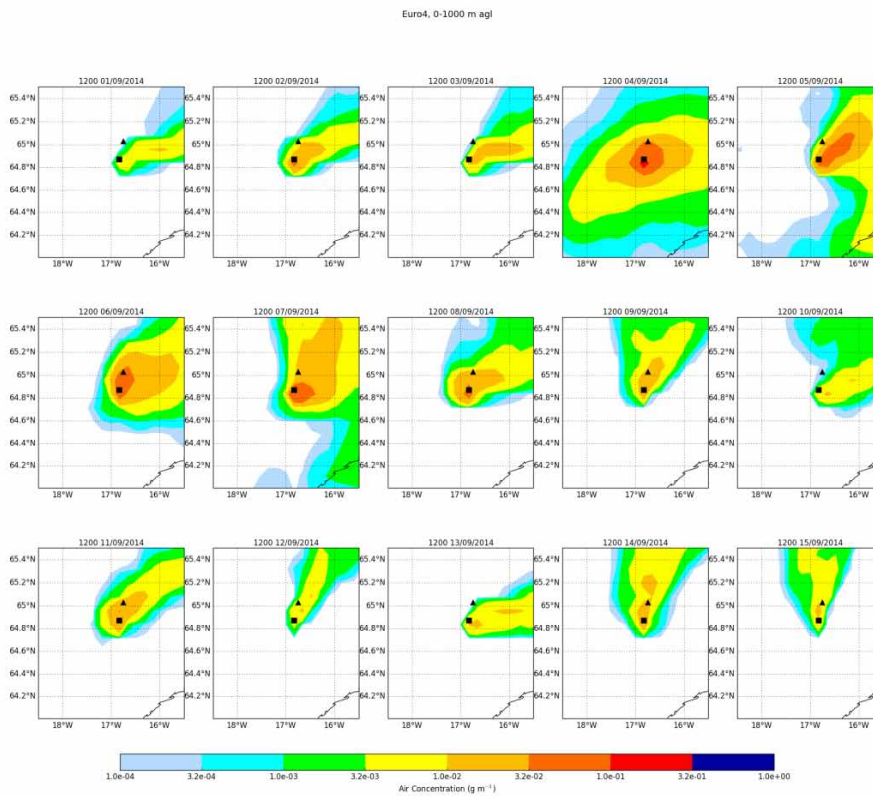
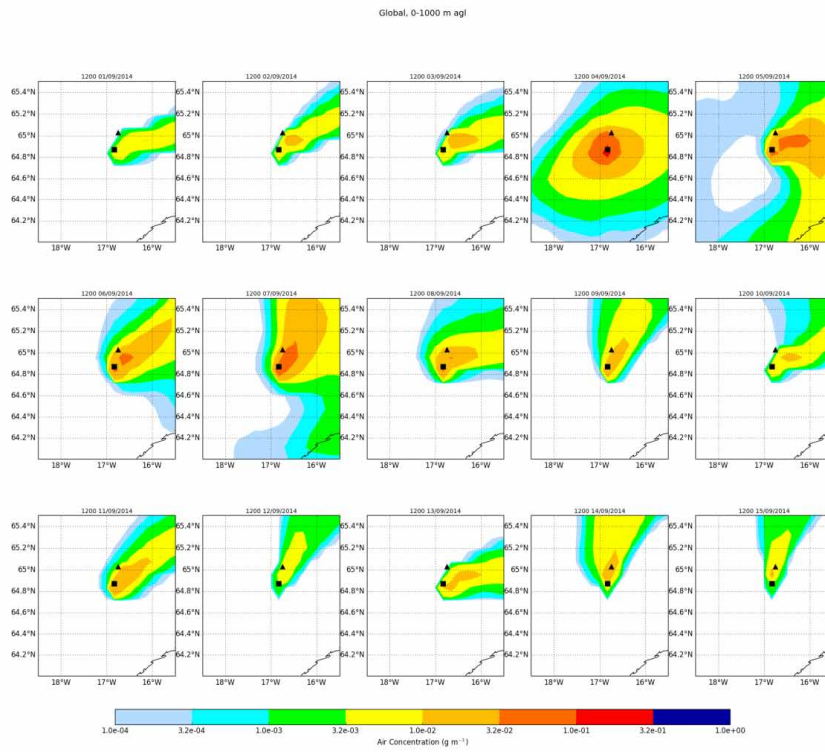


Figure E.5. NAME forecast air concentration over 0–1000 m agl for the Holuhraun eruption during the 1st – 15th September 2014 using the Global and Euro4 model configuration topography and analysis meteorological data, zoomed-in over the Holuhraun area, which is indicated by the black square, the triangle indicates the location of Askja.

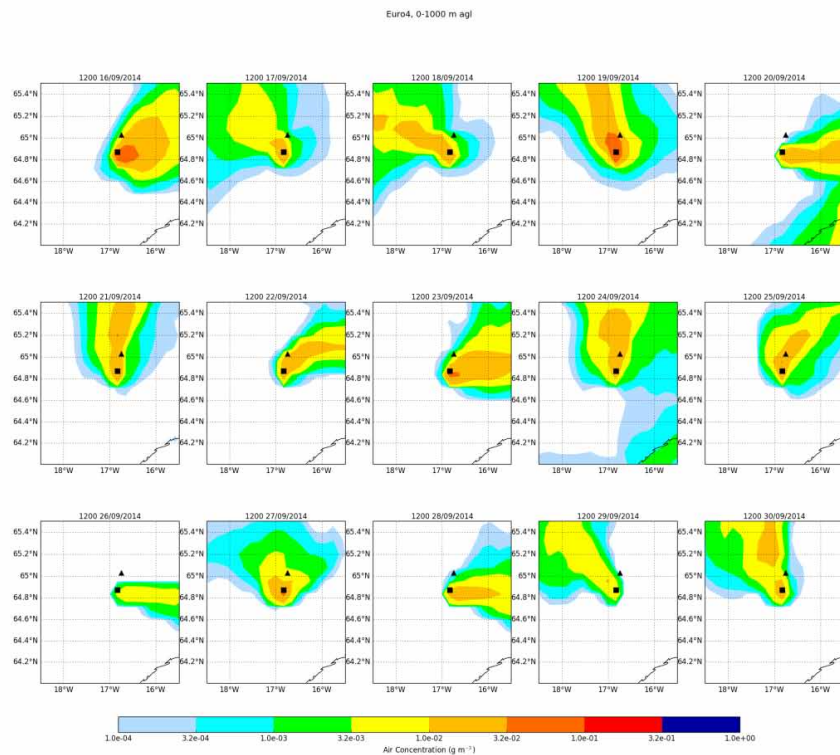
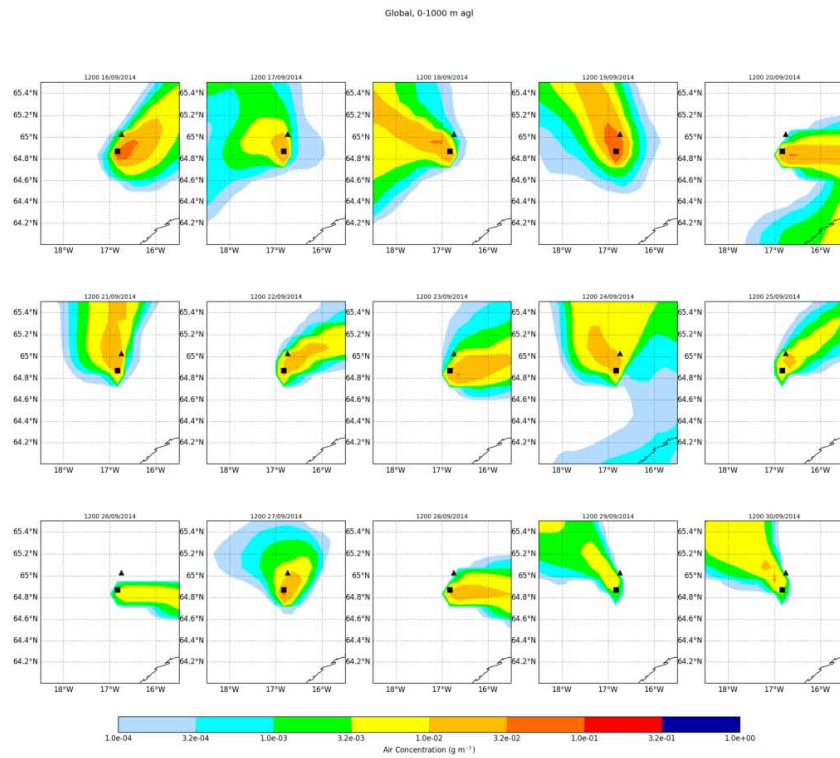


Figure E.6. NAME forecast air concentration over 0–1000 m agl for the Holuhraun eruption during the 16th – 30th September 2014 using the Global and Euro4 model configuration topography and analysis meteorological data, zoomed-in over the Holuhraun area, which is indicated by the black square, the triangle indicates the location of Askja.

Appendix F. Calculated Statistical Coefficient for the Daily Holuhraun Forecasts

Table F.1. Calculated Figure of Merit in Space (FMS) and Pearson’s Correlation Coefficient (PCC) between the NAME forecast using the Global met data versus the Euro4 met data for the Holuhraun eruption during September 2014, at 0-100 m agl, 0-500 m agl and 0-1000 m agl.

Time (UTC) + Date	0-100 m agl		0-500 m agl		0-1000 m agl	
	FMS	PCC	FMS	PCC	FMS	PCC
1200 01/09/2014	59.63	0.85	60.5	0.9	68.7	0.95
1200 02/09/2014	60.22	0.5	60	0.59	45.04	0.8
1200 03/09/2014	66.13	0.9	70.83	0.89	80.23	0.92
1200 04/09/2014	73.48	0.93	78.71	0.92	86.29	0.95
1200 05/09/2014	72.2	0.94	74.91	0.92	76.11	0.91
1200 06/09/2014	72.83	0.91	79.8	0.89	80.32	0.87
1200 07/09/2014	75.18	0.83	68.74	0.9	72.1	0.84
1200 08/09/2014	51.22	0.94	62.5	0.9	65.89	0.94
1200 09/09/2014	66.85	0.79	75.16	0.84	70.6	0.92
1200 10/09/2014	53.27	0.5	64.95	0.73	61.54	0.77
1200 11/09/2014	58.06	0.77	57.93	0.65	44.19	0.77
1200 12/09/2014	27.78	0.72	34.51	0.85	32.17	0.87
1200 13/09/2014	62.17	0.86	74.09	0.87	74.44	0.93
1200 14/09/2014	60.15	0.73	66.44	0.87	64.21	0.9
1200 15/09/2014	31.55	0.66	40.62	0.78	40.64	0.83
1200 16/09/2014	33.98	0.66	42.27	0.83	64.65	0.94
1200 17/09/2014	34.16	0.83	47.35	0.82	62.06	0.87
1200 18/09/2014	60.74	0.87	67.4	0.92	69.47	0.93
1200 19/09/2014	60.05	0.89	69.82	0.96	78.18	0.98
1200 20/09/2014	69.59	0.84	74.23	0.89	74.64	0.92
1200 21/09/2014	50.49	0.82	63.37	0.78	65.08	0.85
1200 22/09/2014	37.39	0.94	41.11	0.89	47.5	0.91
1200 23/09/2014	40.78	0.89	54.66	0.89	72.9	0.95
1200 24/09/2014	54.39	0.86	57.45	0.83	71.34	0.86
1200 25/09/2014	60.41	0.68	56.39	0.61	52.74	0.6
1200 26/09/2014	68.44	0.92	68.33	0.91	61.96	0.91
1200 27/09/2014	47.06	0.87	55.17	0.8	64.86	0.85
1200 28/09/2014	59.76	0.83	64.74	0.91	65.75	0.96
1200 29/09/2014	67.09	0.71	63.75	0.75	63.41	0.84
1200 30/09/2014	26.51	0.52	31.71	0.5	54.73	0.66